NASA TN D-1838

NASA TN D-1838

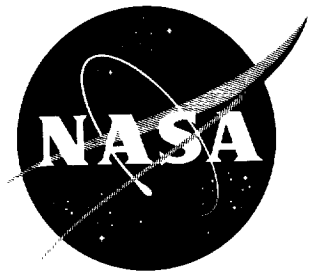

TECHNICAL NOTE

D-1838

TRAJECTORY SIMULATION APPLICABLE TO STABILITY AND CONTROL STUDIES OF LARGE MULTI-ENGINE VEHICLES

By Ronald J. Harris

George C. Marshall Space Flight Center
Huntsville, Alabama

NATIONAL AERONAUTICS AND SPACE ADMINISTRATION
WASHINGTON

August 1963

NATIONAL AERONAUTICS AND SPACE ADMINISTRATION

TECHNICAL NOTE D-1838

TRAJECTORY SIMULATION APPLICABLE TO STABILITY AND CONTROL STUDIES OF LARGE MULTI-ENGINE VEHICLES

By

Ronald J. Harris

ADVANCED FLIGHT SYSTEMS BRANCH
PROPULSION AND VEHICLE ENGINEERING DIVISION

ACKNOWLEDGEMENT

The author wishes to express sincere appreciation to H. F. Thomae and Dr. H. G. L. Krause for their suggestions, to F. D. Montgomery for programming the equations on the IBM 7090 digital computer, and to L. R. Cohen for the two-dimensional results shown in the numerical example.

TABLE OF CONTENTS

		Page
SUMMARY		1
SECTION I.	INTRODUCTION	2
SECTION II.	COORDINATE SYSTEMS	4
	A. Coordinate Description	4
	B. Coordinate Resolution	6
SECTION III.	EQUATIONS OF MOTION	12
	A. Basic Equations	12
	B. Gravity Forces	18
	C. Aerodynamic Forces and Moments	19
	D. Thrust Forces and Moments	25
	E. Miscellaneous Forces and Moments	40
	F. General Equations of Motion	41
SECTION IV.	CONTROL EQUATIONS	45
SECTION V.	SOLUTION OF THE EQUATIONS	55
SECTION VI.	NUMERICAL EXAMPLE	55

LIST OF ILLUSTRATIONS

Figure	Title	Page
1.	Illustration of Vehicle Body Axes	5
2.	Arbitrary Orientation of Body and Earth-Fixed Axes	8
3.	Details of Euler Sequence	9
4.	Illustration of Aerodynamic Angles	20
5.	Wind Resolution in the $X_g - Y_g$ Plane	23
6.	Typical Arrangement of Eight-Engine Booster as Seen From Rear	26
7.	Illustration of Angles Associated with Initial and Gimbaled Positions of Engine Number One	28
8.	Comparison of Exact and Approximate Methods for Calculating $F_{T_{Z_1}}$ -	33
9.	Attitudes of Aerodynamically Unstable Vehicle in Response to Wind with Attitude and Angle of Attack Control	48
10.	Mass, Center of Gravity, and Thrust Moment Arm Data	58
11.	Mass Moments and Product of Inertia Characteristics	59
12.	Center of Pressure and Axial Force Coefficient	60
13.	Rate of Change of Normal Force Coefficients with Angle of Attack	61
14.	Pitching Moment and Yawing Moment Stability Derivatives	62
15.	Rolling Moment Stability Derivatives	63
16.	Wind Velocity Profile	64
17.	Drift-Minimum Yaw and Pitch Attitude Control Gains	67
18.	Drift-Minimum Yaw and Pitch Angle of Attack Control Gains	68
19.	Load-Minimum Yaw and Pitch Angle of Attack Control Gains	69

LIST OF ILLUSTRATIONS (Concluded)

Figure	Title	Page
20.	Yaw and Pitch Attitude Rate Control Gains	70
	(a) Damping Ratios ζ_Y and ζ_P Equal 0.5	70
	(b) Damping Ratios ζ_Y and ζ_P Equal 0.75	70
	(c) Damping Ratios ζ_Y and ζ_P Equal 1.0	71
21.	Time History of Gimbal Angle and Lateral Acceleration in Response to Wind Disturbance (Drift-Minimum Principle)	73
22.	Time History of Angle of Attack and Yaw Angle in Response to Wind Disturbance (Drift-Minimum Principle)	74
23.	Time History of Lateral Acceleration and Gimbal Angle in Response to Wind Disturbance (Load-Minimum Principle)	75
24.	Time History of Yaw Angle and Angle of Attack in Response to Wind Disturbance (Load-Minimum Principle)	76
25.	Time History of Dispersion of Longitudinal Acceleration and Flight Path Angle	77
26.	Effect of Natural Frequency on Maximum Values of Lateral Acceleration, Yaw Angle, Angle of Attack and Gimbal Angle (Drift-Minimum Principle)	78
27.	Effect of Natural Frequency on Maximum Values of Gimbal Angle and Angle of Attack (Load-Minimum Principle)	79
28.	Effect of Wind Direction on Maximum Acceleration	81
29.	Effect of Wind Direction on Maximum Values of Gimbal Angle and Angle of Attack	82

LIST OF TABLES

1.	Program Inputs	43, 44
2.	Nominal Trajectory for Numerical Example	65

LIST OF SYMBOLS

A_e	nozzle exit area of engine, sq. ft.
A_1, A_2	dimensionless constants defined in the text
a_{OY}, a_{OP}	yaw and pitch attitude control gains, dimensionless
a_{1Y}, a_{1P}	yaw and pitch attitude rate control gains, sec.
B_1, B_2	dimensionless constants defined in the text
b_{OY}, b_{OP}	yaw and pitch angle of attack control gains, dimensionless
C_ℓ	rolling moment coefficient, dimensionless
$C_{\ell_{\alpha_Y}}$	rate of change of rolling moment coefficient yaw angle of attack, $\frac{\partial C_\ell}{\partial \alpha_Y}$, 1/rad
C_{ℓ_P}	rate of change of rolling moment coefficient with rolling velocity, $\left(\frac{\partial C_\ell}{\partial \frac{pD}{2V_R}}\right)$, 1/rad
C_{ℓ_r}	rate of change of rolling moment coefficient with yawing velocity $\frac{\partial C_\ell}{\partial \left(\frac{rD}{2V_R}\right)}$, 1/rad
C_m	pitching moment coefficinet, dimensionless
$C_{m_{\dot{\alpha}_P}}$	rate of change pitching moment coefficient with the time derivative of pitch angle of attack $\frac{\partial C_m}{\partial \left(\frac{\dot{\alpha}\, pD}{2V_R}\right)}$, 1/rad

C_{m_q} rate of change of pitching moment coefficient with pitching velocity, $\frac{\partial C_m}{\partial\left(\frac{qD}{2V_R}\right)}$, 1/rad

C_n yawing moment coefficient, dimensionless

$C_{n_{\dot{\alpha}_Y}}$ rate of change of yawing moment coefficient with time derivative of yaw angle of attack, $\frac{\partial C_n}{\partial\left(\frac{\dot{\alpha}_Y D}{2V_R}\right)}$ 1/rad

C_{n_r} rate of change of yawing moment coefficient with yawing velocity, $\frac{\partial C_n}{\partial\left(\frac{rD}{2V_R}\right)}$, 1/rad

C_X axial force coefficient, dimensionless

C_{X_o} axial force coefficient at zero angle of attack, dimensionless

$C_{X_{\alpha_P}}$ rate of change of axial force coefficient with pitch angle of attack, $\frac{\partial C_X}{\partial \alpha_P}$, 1/rad

C_Y lateral force coefficient, dimensionless

$C_{Y_{\alpha_Y}}$ rate of change of lateral force coefficient with yaw angle of attack, $\frac{\partial C_Y}{\partial \alpha_Y}$, 1/rad

C_Z normal force coefficient

LIST OF SYMBOLS (Cont'd)

$C_{Z_{\alpha_P}}$	rate of change of normal force coefficient with pitch angle of attack, $\frac{\partial C_Z}{\partial \alpha_P}$, 1/rad
CG	distance of center of gravity from reference plane passing through engine gimbal points, feet
C_1, C_2	dimensionless go-no-go constants in rolling moment equation (have value of 0 or 1)
CP	distance of center of pressure from reference plane passing through engine gimbal points, feet
C_{1Y}, C_{1P}	specific aerodynamic restoring torque in yaw and pitch, $\frac{1}{\text{rad - sec}^2}$
C_{2Y}, C_{2P}	specific yaw and pitch control torques, $\frac{1}{\text{rad - sec}^2}$
D	reference length for aerodynamic coefficients, feet
f_{nY}, f_{nP}	yaw and pitch undamped natural frequency, cycles per second
F_A	general aerodynamic forces, pounds
F_G	general gravitational force, pounds
F_M	miscellaneous forces and moments, pounds
F_T	general thrust forces, pounds
F_X, F_Y, F_Z	total force components along the X, Y, Z axes, respectively, pounds

LIST OF SYMBOLS (Cont'd)

g	acceleration of gravity, ft/sec^2
h_{0Y}, h_{0P}	roll control gains, dimensionless
H_T	total angular momentum, lb - ft - sec
$\bar{i}$, $\bar{j}$, $\bar{k}$	unit vectors along the X, Y, Z axes, respectively
I_X, I_Y, I_Z	mass moments of inertia about the X, Y, and Z axes, respectively, lb- ft - sec^2
I_{XY}, I_{XZ}, I_{YZ}	mass products of inertia referred to the body axis system, lb - ft - sec^2
$K_{L_{1n}}$, $K_{L_{3n}}$, $K_{M_{1n}}$, $K_{M_{2n}}$, $K_{N_{1n}}$, $K_{N_{2n}}$, $K_{X_{1n}}$, $K_{Y_{1n}}$, $K_{Z_{1n}}$,	dimensionless constants defined in text
$K_{L_{2n_c}}$, $K_{L_{4n_c}}$, $K_{M_{3n_c}}$, $K_{M_{4n_c}}$, $K_{N_{3n_c}}$, $K_{N_{4n_c}}$, $K_{Y_{2n_c}}$, $K_{Z_{2n_c}}$	constants defined in text, 1/rad
$K_{R_{n_c}}$	dimensionless roll proportionality constant
k_{1Y}, k_{2Y}, k_{3Y}, k_{1P}, k_{2P}, k_{3P}	parameters defined in text, ft/sec^2
L, M, N	total moment components about the X, Y, and Z axes, ft - lbs.
L_M, M_M, M_N	miscellaneous moments about the X, Y, and Z axes, ft - lbs.

LIST OF SYMBOLS (Cont'd)

L_T	total linear momentum, lb - sec
M	Mach number, dimensionless
m	mass, $\frac{\text{lb - sec}^2}{\text{ft}}$
p, q, r	roll, pitch, and yaw rotational velocity components, respectively, rad/sec
P_o	free-stream static pressure used as reference for T_{on}, lb/ft^2
P	free-stream static pressure at any altitude, lb/ft^2
q'	dynamic pressure, lb/ft^2
r_e	distance from instantaneous center of gravity to center of nozzle exit plane, ft
r_{ex}, r_{ey}, r_{ez}	components of r_e parallel to the X, Y, and Z axes, ft
R	radial distance from vehicle center line to engine gimbal point, ft
S	reference area for aerodynamic coefficients, sq ft
T_o	measured thrust at free-stream static pressure equal to P_o, lb
T	thrust corrected for altitude, lb
t	time, sec

LIST OF SYMBOLS (Cont'd)

u, v, w	vehicle translational velocity components relative to earth, along the X, Y, and Z axes, respectively, ft/sec
u_R, v_R, w_R	vehicle translational velocity components, relative to wind, along the X, Y, and Z axes, respectively, ft/sec
V	resultant translational velocity of vehicle relative to earth, ft/sec
V_e	exit velocity of gases from nozzle, ft/sec
V_R	resultant translational velocity of vehicle relative to wind, ft/sec
V_W	resultant wind velocity parallel to Xg - Yg plane, ft/sec
V_S	speed of sound, ft/sec
X, Y, Z	body-fixed axes
Xg, Yg, Zg	geodetic earth-fixed axes and distance along these axes, ft
$\dot{X}_{wg}, \dot{Y}_{wg}, \dot{Z}_{wg}$	components of wind velocity parallel to Xg, Yg, and Zg axes, respectively, ft/sec
α	total angle of attack, rad
α_w	wind angle, rad

LIST OF SYMBOLS (Cont'd)

α_Y, α_P	projections of total angle of attack into yaw and pitch planes, respectively, rad
β	total gimbal angle referenced to line parallel to the vehicle center line, rad
β'	total gimbal angle referenced to initial canted axis, rad
β_o	initial cant angle of engine, rad
β_{Y_o}, β_{P_o}	yaw and pitch components of β_o, rad
β_Y, β_P	yaw and pitch gimbal angles relative to projections of the initial cant axis in the yaw and pitch planes, respectively, rad
β_{Y_T}, β_{P_T}	yaw and pitch components of β, rad
β_ρ	angle defining thrust direction, rad
γ_w	angle between horizontal wind component and vehicle center line, deg
ζ_Y, ζ_P	ratio of damping to critical damping of yaw and pitch rotary motion, dimensionless
θ, ψ, Φ	Euler angles relating attitude of body-fixed axes to earth-fixed axes, rad
θ_c, ψ_c, Φ_c	nominal or desired values of θ, ψ, and Φ, rad
θ_W	wind direction referenced to true north, deg

λ	launch azimuth referenced to true north, deg
ρ_∞	free-stream density, $\frac{lb - sec^2}{ft^4}$
Ω	total angular velocity of vehicle, rad/sec

Subscripts:

n(n = 1, 2, 3, ---)	used to distinguish engines in a multi-engine booster
n_c (n_c = 1, 3, 5,---)	used to distinguish control engines
o	indicates initial values unless otherwise specified

Other notations:

dots (.) over symbols denote differentiation with respect to time.

a bar (−) over a symbol indicates a vector.

NATIONAL AERONAUTICS AND SPACE ADMINISTRATION

TECHNICAL NOTE D-1838

TRAJECTORY SIMULATION APPLICABLE TO STABILITY AND CONTROL STUDIES OF LARGE MULTI-ENGINE VEHICLES

By Ronald J. Harris

SUMMARY

A three-dimensional six-degree-of-freedom trajectory simulation applicable to preliminary stability and control studies of vehicles having large multi-engine boosters is formulated. The simulation employs rigid body equations of motion referenced to a special set of body axes known as Euler axes, an orthogonal right-handed triad having its origin at the instantaneous center of gravity of the vehicle. Fuel sloshing and elasticity effects are ignored. Simplifications are kept to a minimum in the derivation of the basic equations; consequently, the complexity of the simulation can be varied by assigning zero values to certain parameters. The aerodynamic characteristics of the vehicle are assumed to be a function of both Mach number and angle of attack. Vehicle mass and inertia characteristics are assumed to be time variant. Winds of arbitrary velocity and direction are incorporated into the simulation.

Artificial stabilization is assumed to be provided by thrust vector control and application of the drift-minimum or load-minimum principle, although other control modes can be applied. Thrust forces are resolved in a manner which allows arbitrary location of the engines, except for the restrictions that the engine array must be symmetrical with respect to the vehicle center line and gimbal points must lie in a plane perpendicular to the center line.

The simulation will provide basic systems design information concerning the dynamic behavior of specific configurations with emphasis being placed primarily on the boost phase of flight. The basic information desired is the engine gimbal angles necessary for stabilization and the responsive motion of the vehicle to a specified disturbance. A numerical example is included which illustrates the application and flexibility of the simulation. Results are compared where possible with a typical two-dimensional simulation.

SECTION I. INTRODUCTION

Conventional body of revolution type vehicles are generally aerodynamically unstable since the center of pressure of the body alone is near the shoulder of the nose fairing, while the center of gravity is nearer the base. In the past, many vehicles have been stabilized by the addition of fins to the body, or by a combination of fins and spinning the vehicle in flight (Ref. 1). The provision of complete fin stabilization becomes less attractive with increasing size of the vehicle, for example those employed in manned space flight missions, because of large weight penalties and because the increasing fin span interferes with launching equipment. However, in some cases, relatively small fins may be used advantageously as a means of decreasing instability and reducing the load imposed on the main control system. Spin stabilization is rarely even considered for large vehicles, especially those using liquid propellants because of the resulting fuel sloshing and centrifugal force problems.

Artificial stabilization by means of a control system, rather than the provision of a stable airframe, appears to be the best approach for large vehicles (Ref. 2). Such a control system requires control torques which may be produced by air vanes, jet vanes, engine gimbaling, and several other means or combinations of these. Control by engine gimbaling, sometimes referred to as thrust vector control, has been successfully employed in several large vehicles and appears to be attractive for those of the future. Consequently, only gimbal control is considered in this report. The limiting of maximum required control deflections to reasonably small values is important in view of the increasing complexity of gimbal bearings, adequate closure of the vehicle's base for protection from base heating, and structural requirements for engine mounts and airframe (Ref. 2).

Since the success of a mission often depends on proper attitude stabilization of the vehicle, control requirements and restrictions need to be considered during the preliminary design phase when the basic vehicle configuration is established. Such studies should be as simplified as the desired degree of accuracy allows. Furthermore the methods used should be quite flexible to cope with the variety of configurations usually encountered.

A unique method of artificial stabilization of aerodynamically unstable vehicles known as the "drift minimum principle" (Ref. 3) has been widely used in preliminary control investigations and is of considerable current interest (Refs. 4 and 5). Application of this scheme renders the vehicle path almost insensitive to wind forces, which are the primary source of disturbance during the early stages of flight. This principle utilizes linear control equations in which the so-called control gains are predetermined in a specified manner for each vehicle. A variation of the principle, in which temporary path instability is allowed in order to reduce the loads on the vehicle, is referred to as

the "load-minimum principle." Both the load-minimum and drift-minimum control modes are discussed more recently in Reference 6, with two other possible control schemes. A more generalized discussion of the problems of attitude stabilization for large guided missiles can be found in Reference 2.

Preliminary vehicle design applications of the above principles have been almost entirely restricted to two-dimensional, planar analyses. Consequently, these studies are limited to independent investigations of pitch, yaw, and roll motions, with roll motion frequently neglected entirely. Analyses of this type are partially justified for symmetrical configurations. For non-symmetrical vehicles, which could be the case for configurations carrying winged payloads for manned space flight, a three-dimensional analysis of the dynamic motion is necessary to study the aerodynamic and coupling effects properly (Ref. 7). In a three-dimensional simulation, pitch, yaw, and roll motions are examined simultaneously. For multi-engine boosters, three dimensions are often necessary to resolve the thrust forces and moments properly.

In the two-dimensional analyses, flight conditions must be assumed constant in all planes of motion except the plane being considered. Often the vehicle aerodynamic characteristics are assumed to be constant (Ref. 2) although the Mach number and angle of attack may be changing. Furthermore, wind disturbances in the two-dimensional analyses are necessarily restricted to constant direction and it is assumed that a direct side wind results in the maximum yaw disturbance. In Reference 8, however, it was found that in most cases, the maximum yaw dispersion does not coincide with a direct side wind. Winds of arbitrary velocity and direction are easily incorporated in a three-dimensional simulation (Ref. 9).

Restricted three-dimensional equations, with linear thrust vector control, are formulated in Reference 10, but are not suitable for studies involving multi-engine vehicles. Previous studies involving multi-engine vehicles have been limited to a particular engine arrangement (Ref. 4). The literature reviewed indicates that there is a need for a three-dimensional trajectory simulation, applicable to stability and control studies, incorporating variable wind, variable aerodynamics, and arbitrary engine arrangement.

This study formulates a general three-dimensional six-degree-of-freedom trajectory simulation applicable to stability and control studies of vehicles having large multi-engine boosters. The simulation is formulated in a manner allowing arbitrary location of the engines with respect to the center line of the vehicle, except for the restrictions that the engine array must be symmetrical, and gimbal points must lie in a plane perpendicular to the center line. The vehicle is assumed to be a rigid body relying on artificial stabilization by thrust vector control. Elasticity and fuel sloshing effects are ignored.

The simulation will provide basic systems design information concerning the dynamic behavior of specific configurations with emphasis primarily on the boost phase of flight. The basic information desired is the engine gimbal angles necessary for stabilization and the responsive motion of the vehicle to a specified disturbance. A linear control system is assumed and two control modes, namely, the drift-minimum and load-minimum principles (Ref. 6), are considered.

A ficticious, but realistic, vehicle is postulated as an illustrative example and typical results are presented. The results are compared, where possible, with typical two-dimensional results. Indications are that the simulation derived in this study satisfies the intended purpose and is adequate for preliminary stability and control studies of large multi-engine vehicles.

SECTION II. COORDINATE SYSTEMS

A. COORDINATE DESCRIPTION

The choice of coordinate systems and the methods of coordinate resolution are extremely important in the formulation and solution of any system of equations. Several coordinate systems used in solving the three-dimensional flight equations have been investigated in Reference 11. The conclusion is reached that the best axis system from the standpoint of simplicity is one employing wind axes for translational equations and body axes for rotational equations. Such a procedure is rarely employed, however, because confusion is inevitable when different axis systems are used for the two sets of equations.

Wind axes have long been used in analytical stability and control studies (Ref. 12) to take advantage of the resulting simplifications in the equations of motion. However, since wind axes are not fixed with respect to the body, it is necessary either to assume that the time rate of change of the moments and products of inertia is negligible, formulate an auxiliary expression for their time dependency; consequently, a special set of body axes known as Euler axes is used in this study.

The Euler axis system (Ref. 13) is associated with an orthogonal right-handed triad having its origin at the instantaneous center of gravity of the vehicle as shown in Figure 1.

The X-direction is positive along the longitudinal axis pointing forward. The Y and Z directions are the pitch and yaw axes, respectively, with the Y-axis positive to the right looking in the flight direction. With respect to the Euler axis system, the vehicle has linear and angular velocities and accelerations but no displacements. This system is especially adaptable to studies of rigid body flight dynamics since the velocities

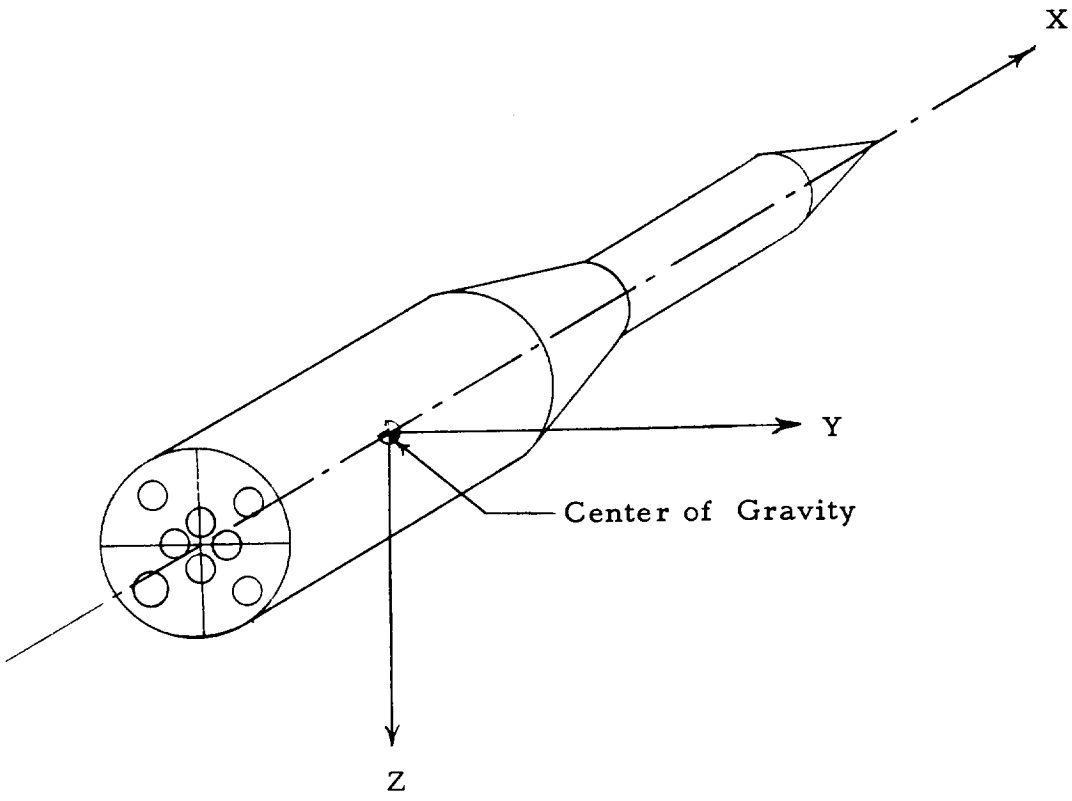

FIGURE 1. ILLUSTRATION OF VEHICLE BODY AXES

measured with respect to these axes are the same as the velocities that are measured by instruments mounted in the vehicle. Another advantage of this system, as opposed to wind axes, is that the moments and products of inertia are independent of time, except for changes in the vehicle's mass.

Another set of axes used in establishing the equations of motion is referred to as earth-fixed axes. A flat, non-rotating earth is assumed for this study so that the earth-fixed axis system is actually an inertial system which is needed when applying Newton's Laws. For a flat earth, these axes are at all times parallel to the axes of the vehicle's stabilized platform.

In the earth-fixed system (Xg, Yg, Zg), the Zg axis is the vertical axis being positive in the opposite direction of gravity. The Xg axis is defined by the desired flight azimuth with the Yg axis completing the right-handed orthogonal system.

A third system, often needed in connection with aerodynamic parameters, is the stability or experimental axis system. This system is commonly used in wind tunnel facilities and the like for referencing aerodynamic data. However, depending upon model instrumentation, such data can also be referenced to body axes. For this study, it is assumed that all aerodynamic parameters are referenced to the body or Euler axis system.

B. COORDINATE RESOLUTION

Before going into a derivation of the equations of motion, it is desirable to develop the transformations relating the body and earth-fixed coordinate systems. As yet, no parameters have been defined for relating the two. For this purpose, the Euler angles θ, ψ, and ϕ are introduced and will be referred to as the pitch, yaw, and roll angles, respectively. Euler devised a method of rotating an axis system successively about its own axes so that at the end of the third rotation the system is parallel to a second specified axis system. Care must be taken in using Euler angles since they do not obey the commutative law thereby requiring that a specified sequence of rotation be maintained throughout a particular analysis.

A standardized Euler sequence has been used in formulating the three-dimensional flight equations for aircraft and unguided vehicles (Refs. 7, 9, and 11). This particular sequence has the order yaw, pitch, and roll with the pitch angle referenced to the horizontal plane. By a twist of fate, all Euler sequences have a singularity when the second rotation is exactly $\pm 90°$. The singularity is a zero in the denominator of one of the equations relating the angular velocity components of the vehicle to the time rate of change of the Euler angles (Ref. 11). Consequently, the conventional sequence used for studies involving aircraft and unguided vehicles has a singularity at $\theta = \pm 90°$, and is obviously unsuitable for vertically launched vehicles. As a result of this situation, a different Euler sequence is used in the present study. The rotational order for this study is θ, ψ, and ϕ (pitch, yaw, roll) with θ being referenced to the vertical Zg axis.

It is pointed out in the development of the transformation equations that this system has a a singularity at $\psi = \pm 90°$, a condition that is not likely to occur.

An arbitrary orientation of body and earth-fixed axes is shown in Figure 2 with the Euler angles indicated. Also shown are the axes about which the time rates of change of the Euler angles are measured. It should be noted that these axes are not mutually orthogonal, thus explaining why the Euler sequence is not commutable. In their original positions, X coincides with Zg and Z coincides with Xg while Y and Yg are 180° out of phase. Any arbitrary orientation of the body and earth-fixed axes is obtained as follows:

1. Rotate about the Yg-axis through the angle θ to define the X_1, Y_1, Z_1 system (Fig. 3).

2. Rotate about X_1 through the angle ψ to form the X_2, Y_2, Z_2 system.

3. Rotate about Z_2 through the angle Φ to establish X_3, Y_3, Z_3. The X_3, Y_3, and Z_3 axes correspond to the body axes Z, -Y, and X, respectively.

The angles are positive when, in performing the rotations described, the right-hand rule is applied.

From Figure 2, keeping in mind that initially Y and Yg are 180° out of phase, it can be seen that:

$$\left.\begin{aligned} X_1 &= X_g \cos\theta - Z_g \sin\theta \\ Y_1 &= Y_g \\ Z_1 &= Z_g \cos\theta + X_g \sin\theta \end{aligned}\right\} \quad (1a, b, c)$$

$$\left.\begin{aligned} X_2 &= X_1 \\ Y_2 &= Y_1 \cos\psi + Z_1 \sin\psi \\ Z_2 &= Z_1 \cos\psi - Y_1 \sin\psi \end{aligned}\right\} \quad (2a, b, c)$$

$$\left.\begin{aligned} X_3 &= Z = X_2 \cos\Phi + Y_2 \sin\Phi \\ Y_3 &= -Y = Y_2 \cos\Phi - X_2 \sin\Phi \\ Z_3 &= X = Z_2 \end{aligned}\right\} \quad (3a, b, c)$$

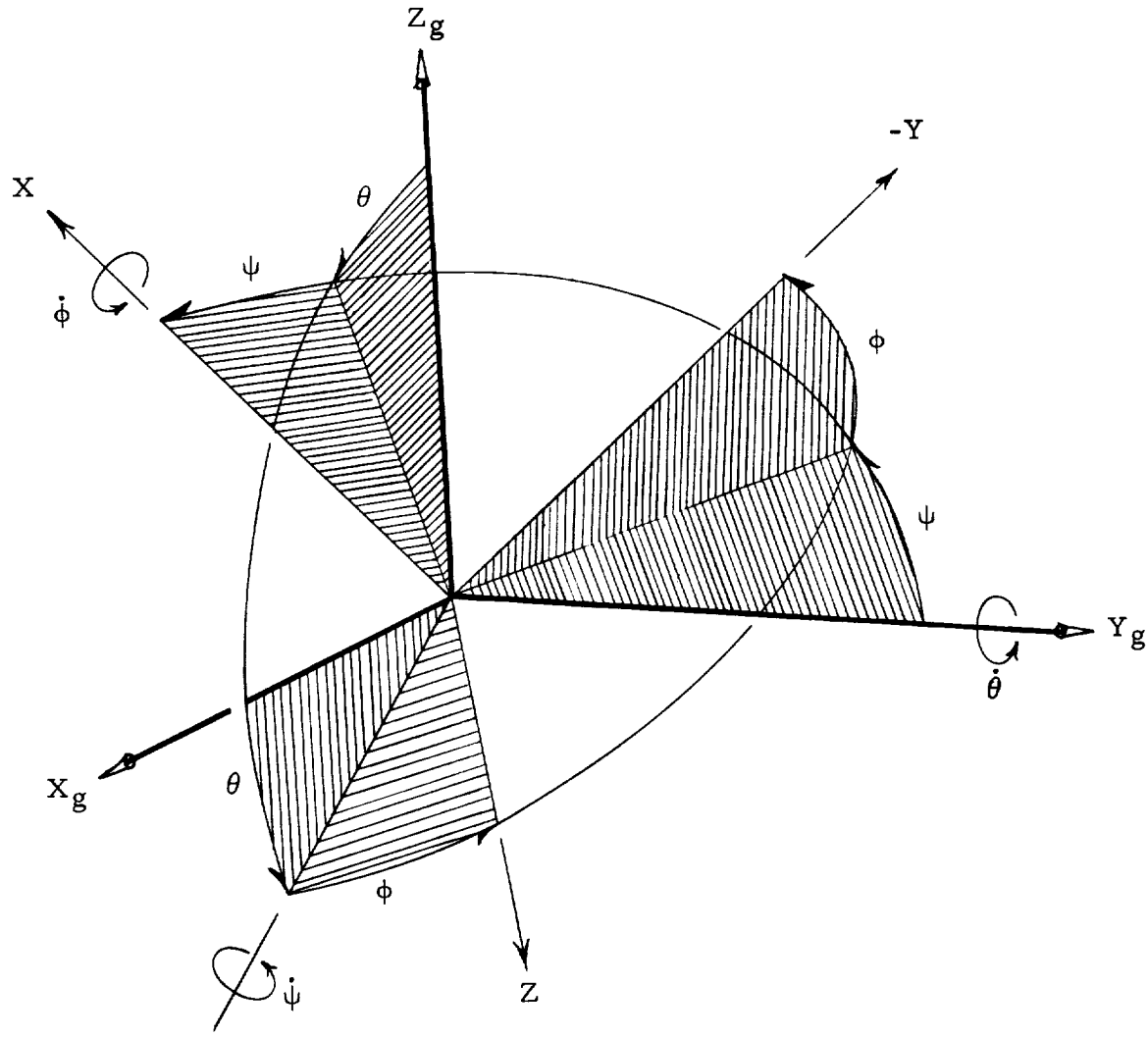

FIGURE 2. ARBITRARY ORIENTATION OF BODY AND EARTH-FIXED AXES

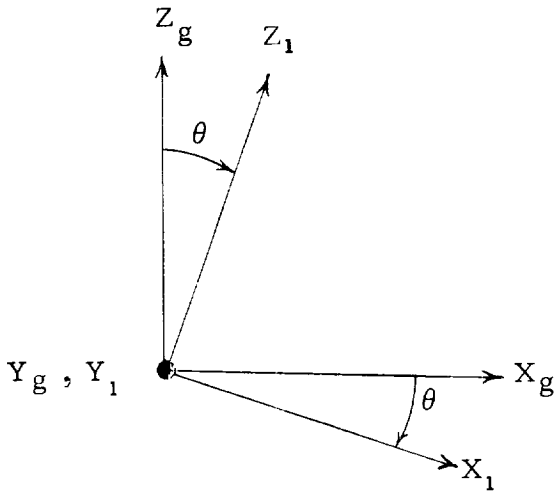

Step 1

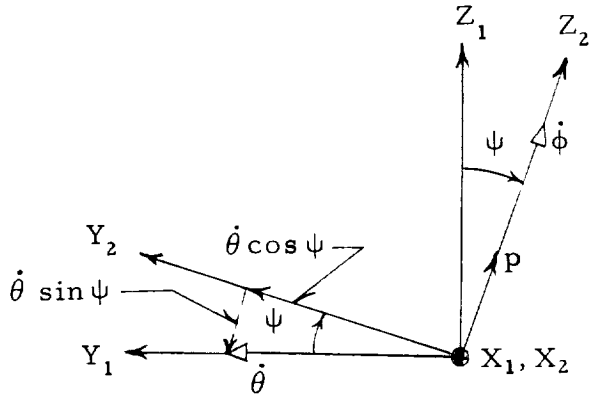

Step 2

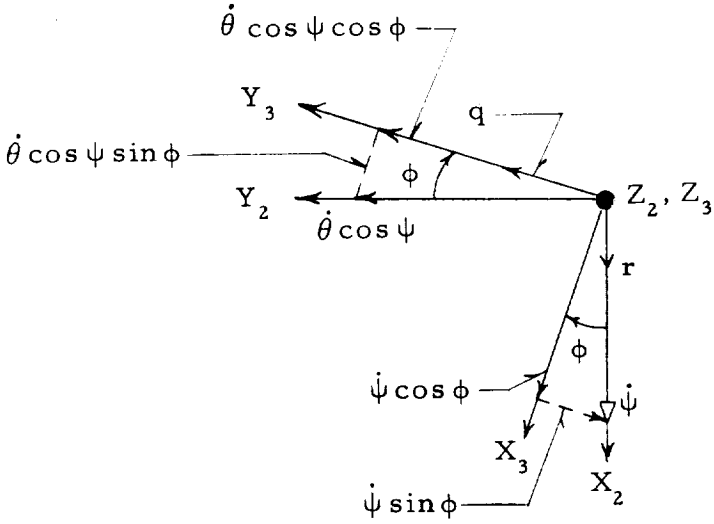

Step 3

X_3, Y_3, Z_3 Correspond to Z, -Y, X Respectively

FIGURE 3. DETAILS OF EULER SEQUENCE

Combining Equations 1, 2, and 3 gives

$$
\left.
\begin{aligned}
X &= Xg \sin\theta \cos\psi - Yg \sin\psi + Zg \cos\theta \cos\psi \\
Y &= Xg (\cos\theta \sin\Phi - \sin\theta \sin\psi \cos\Phi) - Yg \cos\psi \cos\Phi \\
&\quad - Zg (\cos\theta \cos\Phi \sin\psi + \sin\theta \sin\Phi) \\
Z &= Xg (\cos\theta \cos\Phi + \sin\theta \sin\psi \sin\Phi) + Yg \cos\psi \sin\Phi \\
&\quad + Zg (\cos\theta \sin\psi \sin\Phi - \sin\theta \cos\Phi)
\end{aligned}
\right\} \quad (4a, b, c)
$$

Equations 4a, 4b, and 4c represent the geometric resolution of body and earth-fixed axes. In matrix notation (Ref. 15), the transformation is

$$
\begin{pmatrix} X \\ Y \\ Z \end{pmatrix} = \begin{pmatrix} d_{11} & d_{12} & d_{13} \\ d_{21} & d_{22} & d_{23} \\ d_{31} & d_{32} & d_{33} \end{pmatrix} \begin{pmatrix} Xg \\ Yg \\ Zg \end{pmatrix} \qquad (5)
$$

where

$$d_{11} = \sin\theta \cos\psi$$

$$d_{12} = -\sin\psi$$

$$d_{13} = \cos\theta \cos\psi$$

$$d_{21} = \cos\theta \sin\Phi - \sin\theta \sin\psi \cos\Phi$$

$$d_{22} = -\cos\psi \cos\Phi$$

$$d_{23} = -(\cos\theta \cos\Phi \sin\psi + \sin\theta \sin\Phi)$$

$$d_{31} = \cos\theta \cos\Phi + \sin\theta \sin\psi \sin\Phi$$

$$d_{32} = \cos\psi \sin\Phi$$

$$d_{33} = \cos\theta \sin\psi \sin\Phi - \sin\theta \cos\Phi$$

These quantities are actually the direction cosines of angles between the earth-fixed and body axes expressed in terms of Euler angles. The methods for deriving the direction cosine relations by means of spherical trigonometry are outlined in Reference 7, but the approach used above presents fewer difficulties. Reference 7 also gives the orthogonality relations

$$\left.\begin{aligned} d_{11}^2 + d_{12}^2 + d_{13}^2 &= 1 \\ d_{21}^2 + d_{22}^2 + d_{23}^2 &= 1 \\ d_{31}^2 + d_{32}^2 + d_{33}^2 &= 1 \end{aligned}\right\} \qquad (6a, b, c)$$

These relations provide the means for a partial check of solutions of the equations of motion since the values determined for the Euler angles must satisfy the equations.

The matrix operation given in Equation 5 can be inverted to transform quantities from body to earth-fixed axes. Thus,

$$\begin{pmatrix} Xg \\ Yg \\ Zg \end{pmatrix} = \begin{pmatrix} d_{11} & d_{21} & d_{31} \\ d_{12} & d_{22} & d_{32} \\ d_{13} & d_{23} & d_{33} \end{pmatrix} \begin{pmatrix} X \\ Y \\ Z \end{pmatrix} \qquad (7)$$

The geometric transformation can only be used when transforming translational quantities such as distance, velocity, and acceleration. In the development of the equations of motion, the time rate of change of the Euler angles will be of interest. Another look at Figures 1 and 2 shows that the actual axes about which the rotations take place are Z_2, Yg, and X_1. The rotational resolution of this triad and the body axes is a necessity. The angular velocities about the X, Y, and Z axes are denoted by p, q, and r, respectively, and represent three rotational degrees-of-freedom of a rigid body. The relative orientation of the angular velocity vectors in the two systems is illustrated in Figure 2. From the figure, it is evident that

$$\left.\begin{aligned} p &= \dot{\Phi} - \dot{\theta} \sin \psi \\ q &= \dot{\psi} \sin \Phi - \dot{\theta} \cos \psi \cos \Phi \\ r &= \dot{\psi} \cos \Phi + \dot{\theta} \cos \psi \sin \Phi \end{aligned}\right\} \qquad (8a, b, c)$$

These equations represent the rotational resolution of the triad X, Yg, Z_1 to the body fixed axes. In matrix notation,

$$\begin{pmatrix} p \\ q \\ r \end{pmatrix} = \begin{pmatrix} 1 & -\sin \psi & 0 \\ 0 & -\cos \psi \cos \Phi & \sin \Phi \\ 0 & \cos \psi \sin \Phi & \cos \Phi \end{pmatrix} \begin{pmatrix} \dot{\Phi} \\ \dot{\theta} \\ \dot{\psi} \end{pmatrix} \qquad (9)$$

Inverting this matrix gives

$$\left.\begin{aligned} \dot{\theta} &= \frac{1}{\cos\psi}\,(r\sin\phi - q\cos\phi) \\ \dot{\psi} &= r\cos\phi + q\sin\phi \\ \dot{\phi} &= p + (r\sin\phi - q\cos\phi)\tan\psi \end{aligned}\right\} \qquad (10a, b, c)$$

or

$$\begin{pmatrix} \dot{\phi} \\ \dot{\theta} \\ \dot{\psi} \end{pmatrix} = \begin{pmatrix} 1 & -\cos\phi\tan\psi & \sin\phi\tan\psi \\ 0 & -\dfrac{\cos\phi}{\cos\psi} & \dfrac{\sin\phi}{\cos\psi} \\ 0 & \sin\phi & \cos\phi \end{pmatrix} \begin{pmatrix} p \\ q \\ r \end{pmatrix} \qquad (11)$$

Equation 10a has a singularity point at $\psi = \pm 90°$. This substantiates the earlier discussion pointing out that every Euler sequence has a singularity when the second rotation is exactly $\pm 90°$. No further transformations are necessary for this study.

SECTION III. EQUATIONS OF MOTION

A. BASIC EQUATIONS

The approach used in establishing the equations of motion is first to formulate the general case under certain restrictions, and consider simplifications later. For this study, the vehicle is considered a rigid body in space. Gravity is assumed to be constant in both magnitude and direction. The earth's rotation and orbital motion are neglected, making the earth-fixed axes an inertial system.

The assumption that the earth is fixed in an inertial reference frame ignores the existence of the Coriolis and centripetal accelerations due to angular velocity of the earth. Actually these two components of acceleration usually comprise only a small portion of the total acceleration experienced by the vehicle. Since the inertial frame is attached to the earth, additional errors result as flight progresses over the surface of the earth. Since the assumed gravitational field is in error by the inclination of the gravity force vector, neglecting the curvature of the earth's surface will introduce an altitude error. If the flight time is not excessive, and flight occurs over a small part of the earth's surface, all these errors may be neglected. These conditions are not met by either ballistic or complete orbital trajectories. For preliminary dynamic stability and control investigations of the boost phase of large vehicles, the area of interest is normally limited to atmospheric flight and the assumptions above appear justified.

The quantities u, v, and w are actually the speeds of the center of gravity. The shift of the center of gravity during flight, with respect to some fixed vehicle reference, will be accounted for in the equations of motion; however, the time rate of change of the center of gravity (the velocity of the center of gravity with respect to the vehicle) is small and can be neglected.

Newton's laws state that the sum of the external forces and moments acting on a rigid body can be equated to the time rate of change of linear and angular momentum, respectively. Accordingly, the force and moment equations are:

$$\frac{d\bar{L}_T}{dt} = \bar{i}\sum F_X + \bar{j}\sum F_Y + \bar{k}\sum F_Z \qquad (12)$$

$$\frac{d\bar{H}_T}{dt} = \bar{i}\sum L + \bar{j}\sum M + \bar{k}\sum N \qquad (13)$$

where L_T and H_T are the linear and angular momentum, respectively, F_X, F_Y, F_Z, and L, M, N are the force and moment components along and about the X, Y, and Z axes, respectively.

The subscript T in the equation above refers to the total system and indicates the inclusion of gases in the nozzle generated by burning of propellant. To take into account the dynamic effect of the jet on the vehicle, the rate of change of linear momentum must include the rate of linear momentum leaving the nozzle exit in the jet. Likewise, the rate of change of angular momentum must include the rate of change due to gases leaving the nozzle.

The rigid body equations of motion for flight mechanics applications under all the assumptions made earlier, but with the additional restriction of constant mass, are derived in References 10 and 13. Vehicle mass is variable during the boost phase of any vehicle. The effect of mass loss has been considered by many investigators in analyses concerning such problems as the performance of high altitude sounding rockets and escape from the earth by a rocket (Refs. 14 and 15). In these analyses, however, dynamic stability was not included in the area of investigation.

It has been determined, however, that the variation in mass causes so-called jet damping forces and moments. A restricted two-dimensional analysis has been made in Reference 15 to determine the effect of mass variation on the dynamic stability of rocket-propelled vehicles. The vehicle involved in that study was a small, low-thrust, single-engine rocket. The results show that a disturbance of the variable mass vehicle damps out more rapidly than it does with the mass assumed constant, indicating that the variable mass vehicle is more stable. The effect of jet-damping is dependent on the ratio of the

time rate of change of mass to the gross mass of the vehicle. Since large multi-engine vehicles are generally aerodynamically unstable, any stabilizing effect should certainly be considered as a means of alleviating the control problem; therefore, mass was assumed variable in this study.

The basic three-dimensional six-degree-of-freedom equations are derived in Reference 16 for a single-engine missile. It is shown that Equations 12 and 13 can be expanded into the form

$$\frac{d\bar{L}_T}{dt} = \frac{d\bar{L}}{dt} + \dot{m}\,(\bar{V} - \bar{V}_e + \bar{\Omega} \times \bar{r}_e) \qquad (14)$$

and

$$\frac{d\bar{H}_T}{dt} = \frac{d\bar{H}}{dt} + \dot{m}\,\bar{r}_e \times (\bar{V}_e + \bar{\Omega} \times \bar{r}_e) \qquad (15)$$

where $\bar{V}_e$ is the velocity of the exhaust gases relative to the vehicle, $\bar{V}$ is the translational velocity of the vehicle, $\bar{\Omega}$ is the rotational velocity of the vehicle, and $\bar{r}_e$ is the vector distance from the instantaneous center of gravity to the center of the nozzle exit. The mass flow rate, $\dot{m}$, is defined as

$$\dot{m} = -\frac{dm}{dt} \qquad (16)$$

Furthermore, L and H are the linear and angular momentum neglecting the exhaust gases.

Following the methods of Reference 17, remembering that $\bar{L}$ and $\bar{H}$ are referred to the body axes system which is rotating with an angular velocity $\bar{\Omega}$ with respect to the earth-fixed or inertial system, the scalar components of Equations 14 and 15 for the case of a multi-engine vehicle can be shown to be

$$\sum F_X = m(\dot{u} + wq - vr) + \sum_1^n \dot{m}_n\,(q\,r_{ez_n} - r\,r_{ey_n}) \qquad (17)$$

$$\sum F_Y = m(\dot{v} + ur - wp) + \sum_1^n \dot{m}_n\,(r\,r_{ex_n} - p\,r_{ez_n}) \qquad (18)$$

$$\sum F_Z = m(\dot{w} + vp - up) + \sum_1^n \dot{m}_n \, (p \, r_{ey_n} - q \, r_{ex_n}) \tag{19}$$

$$\sum L = \dot{p} \, I_X + qr(I_Z - I_Y) + (pr - \dot{q}) \, I_{XY} - (pq + \dot{r}) \, I_{XZ} - (r^2 - q^2) \, I_{YZ} - \dot{p} I_X + \dot{q} I_{XY} + \dot{r} I_{XZ} + \sum_1^n \dot{m}_n \left[p(r_{ey_n}^2 + r_{ez_n}^2) + r_{ez_n} \, (q \, r_{ey_n} + r \, r_{ez_n}) \right] \tag{20}$$

$$\sum M = \dot{q} I_Y + pr(I_X - I_Z) + (pq - \dot{r}) I_{YZ} - (\dot{p} + qr) \, I_{XY} + (p^2 - r^2) \, I_{XZ} - \dot{q} I_Y + \dot{r} I_{YZ} + \dot{p} I_{XZ} + \sum_1^n \dot{m}_n \left[q(r_{ez_n}^2 + r_{ex_n}^2) + r_{ey_n} \, (r \, r_{ez_n} + p \, r_{ex_n}) \right] \tag{21}$$

$$\sum N = \dot{r} I_Z + pq(I_Y - I_X) + (qr - \dot{p}) \, I_{XZ} + (pr + \dot{q}) \, I_{YZ} + (q^2 + p^2) \, I_{XY} - \dot{r} I_Z + \dot{p} I_{XZ} + \dot{q} I_{YZ} + \sum_1^n \dot{m}_n \left[r(r_{ex_n}^2 + r_{ey_n}^2) + r_{ez_n} \, (p \, r_{ex_n} + q \, r_{ey_n}) \right] \tag{22}$$

where the subscript n refers to a particular engine.

These equations represent the motion along and about the X, Y, and Z axes. The equations are complete, within the assumptions made to date, except for the external forces and moments which appear on the left side of each equation.

One immediate simplifying assumption can be made concerning $\bar{r}_{e_n}$ where, as defined above,

$$\bar{r}_{e_n} = \bar{i} \, r_{ex_n} + \bar{j} \, r_{ey_n} + \bar{k} \, r_{ez_n}$$

For single engine boosters where the nozzle center line coincides with the longitudinal axis, r_{ey} and r_{ez} are identically zero. For multi-engine vehicles with the engines mounted symmetrically about the longitudinal axis,

$$\sum_1^n r_{ey_n} = \sum_1^n r_{ez_n} = 0 \tag{23}$$

Actually Equation 23 is true only when the engines are not gimbaled. Neglecting the small bias resulting from gimbaling or engine-out conditions, and assuming that the engines always lie to the rear of the center of gravity, then

$$\bar{r}_{e_n} = -\bar{i}\, r_{ex_n}$$

If it is further assumed that all nozzle exits lie in a plane approximately parallel to the Y-Z plane, then r_{ex} is the same for all engines and the subscript n can be dropped. Under these assumptions, the basic equations reduce to

$$\sum F_X = m(\dot{u} + wq - vr) \tag{24}$$

$$\sum F_Y = m(\dot{v} + ur - wp) - \sum_1^n \dot{m}_n\, r\, r_{ex} \tag{25}$$

$$\sum F_Z = m(\dot{w} + vp - uq) + \sum_1^n \dot{m}_n\, q\, r_{ex} \tag{26}$$

$$\sum L = \dot{p} I_X + qr(I_Z - I_Y) + (pr - \dot{q})\, I_{XY} - (pq + \dot{r})\, I_{XZ} + (r^2 - q^2)\, I_{YZ} - p\dot{I}_X + q\dot{I}_{XY} + r\dot{I}_{XZ} \tag{27}$$

$$\sum M = \dot{q}\, I_Y + pr(I_X - I_Z) + (pq - \dot{r})I_{YZ} - (\dot{p} + qr)I_{XY} + (p^2 - r^2)I_{XZ} - q\dot{I}_Y + r\dot{I}_{YZ} + p\dot{I}_{XY} + \sum_1^n \dot{m} q\, r_{ex}^2 \tag{28}$$

$$\sum N = \dot{r}I_Z + pq(I_Y - I_X) + (qr - \dot{p})\, I_{XZ} + (pr + \dot{q})\, I_{YZ}$$

$$+ (p^2 + q^2)\, I_{XY} - rI_Z + pI_{XZ} + qI_{YZ} + \sum_1^n r\, r_{ex}^2 \qquad (29)$$

Further simplifying assumptions could be made at this point. For example, it could be assumed that the X - Z plane is a plane of symmetry so that $I_{YZ} = I_{XY} = 0$. This condition is normally a basic design criteria; however, in some cases, it may be desirable to determine the effect of certain symmetries. In studies where analytical or closed-form solutions are a desired result, it is necessary to linearize the equations (Ref. 18). Such situations are restricted to a solution for a particular type of problem and are not readily adaptable to a variety of unexpected problems which typically arise in the preliminary design phase. Where large highspeed electronic computers are available, the best approach is to hold simplification to a minimum; then if simplications are desired, certain parameters are simply set equal to zero. In cases where the simplified equations cannot handle a particular problem, the zeros are easily removed and no major modifications are necessary. Consequently, no further simplifying assumptions are made concerning Equations 24 through 29. The purpose of this study is not to establish any particular stability criteria (Ref. 19), but to establish a flexible simulation applicable to the variety of problems encountered in preliminary design.

The complete equations of motion assumed in this study are established by formulating the various forces and moments represented by the left-hand side of Equations 24 through 29. For this purpose, it is assumed that

$$\bar{i}\sum F_X + \bar{j}\sum F_Y + \bar{k}\sum F_Z = \bar{F}_A + \bar{F}_T + \bar{F}_G + \bar{F}_M \qquad (30)$$

$$\bar{i}\sum L + \bar{j}\sum M + \bar{k}\sum N = \bar{M}_M + \bar{M}_A + \bar{M}_T \qquad (31)$$

where

$\bar{F}_M$, $\bar{M}_M$ = miscellaneous forces and moments such as those resulting from thrust misalignment or retro-rockets

$\bar{F}_G$ = gravitational force

$\bar{F}_A$, $\bar{M}_A$ = aerodynamic forces and moments

$\bar{F}_T$, $\bar{M}_T$ = forces and moments caused by thrusting action.

It should be noted that there are no gravitational moments since the origin of the body axes is at the instantaneous center of gravity of the vehicle. Each of the forces and moments will now be developed separately according to their source.

B. GRAVITY FORCES

The gravitational vector is referenced to the earth-fixed system and is directed along the negative Zg axis. The transformation given in Equation 5 can be used to resolve the vehicle weight into body-axes components as follows:

$$\begin{aligned} F_{G_X} &= - mg \cos\theta \cos\psi \\ F_{G_Y} &= mg (\cos\theta \sin\psi \cos\Phi + \sin\theta \sin\Phi) \\ F_{G_Z} &= mg (\sin\theta \cos\Phi - \cos\theta \sin\psi \sin\Phi) \end{aligned} \qquad (32)$$

where g is the magnitude of the acceleration of gravity.

The introduction of θ, ψ, and Φ into the equations of motion adds three unknowns to the six basic unknowns defined earlier in Equations 24 through 29. The situation is such that these are six equations with nine unknowns. Consequently, auxiliary equations are needed to determine θ, ψ, and Φ in terms of the basic unknowns. In Equation 10 it was shown that the time rate of change of the Euler angles can be expressed in terms of the rotational velocity components p, q, and r. The Euler angles can thus be calculated from the relations

$$\left.\begin{aligned} \theta &= \int \dot{\theta}\, dt + \theta_o \\ \psi &= \int \dot{\psi}\, dt + \psi_o \\ \Phi &= \int \dot{\Phi}\, dt + \Phi_o \end{aligned}\right\} \qquad (33a, b, c)$$

where θ_o, ψ_o, and Φ_o are initial values and $\dot{\theta}$, $\dot{\psi}$, and $\dot{\Phi}$ are given in Equations 10a, b, c.

C. AERODYNAMIC FORCES AND MOMENTS

The aerodynamic forces and moments can be formulated in terms of the normal and axial force coefficients and the so-called stability derivatives. The aerodynamic forces and stability derivatives are usually referenced to either body or experimental axis system, depending on model instrumentation or methods of calculation (Refs. 9 and 13). In this study, it is assumed that all aerodynamic data are referenced to the body axis system since the basic equations of motion have been established in that system. Following the approach of References 7, 12, and 13, it is further assumed that all stability derivatives for large missiles, with or without non-symmetrical payloads, are either zero or negligible except

Axial Force - $C_{X_{\alpha_P}}$

Side Force - $C_{Y_{\alpha_Y}}$

Normal Force - $C_{Z_{\alpha_P}}$

Rolling Moment - $C_{\ell_{\alpha_Y}}$, C_{ℓ_P}, C_{ℓ_r}

Pitching Moment - $C_{m_{\dot{\alpha}_P}}$, C_{m_q}

Yawing Moment - $C_{n_{\dot{\alpha}_Y}}$, C_{n_r}

where α_P and α_Y are the pitch angle of attack and yaw angle of attack (commonly referred to as the angle of sideslip) as illustrated in Figure 4. These angles will be discussed later.

The stability derivatives and the experimental and analytical methods for determining them are discussed thoroughly in the literature, particularly in many reports published by the National Advisory Committee for Aeronautics (NACA) and later by the National Aeronautics and Space Administration (NASA). The methods of calculating the stability derivatives will not be discussed here; however, in any stability investigation it is desirable to have specific analytical or empirical relations for calculating these when experimental data are not available.

In more detailed stability and control studies, or when an attempt is made to establish a general stability criteria (Ref. 19), it may be necessary to account for more of the numerous stability derivatives. For this study, those listed above are sufficient.

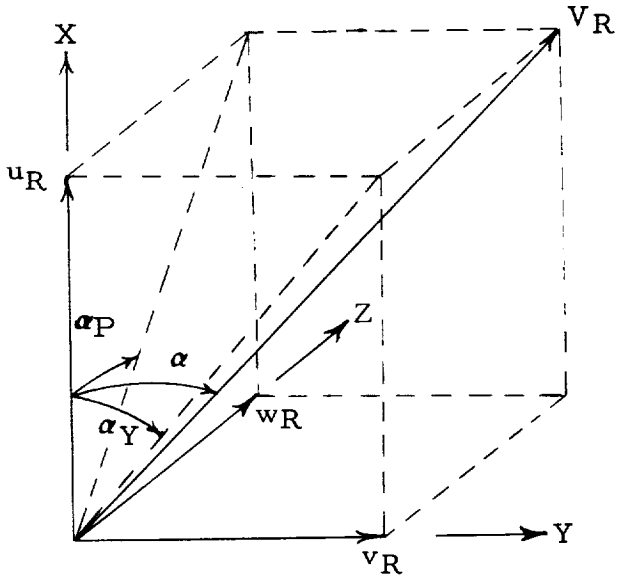

FIGURE 4. ILLUSTRATION OF AERODYNAMIC ANGLES

Standard NASA notation is employed (see List of Symbols) in defining the stability derivatives. The so-called static derivatives are simply partial derivatives with respect to a particular variable. For example

$$C_{Z_{\alpha_P}} = \frac{\partial C_Z}{\partial \alpha_P} .$$

where C_Z is the normal force coefficient.

The dynamic stability derivatives, in which the variable in the denominator of the derivative is associated with motion, and nondimensionalized by multiplying the partial derivative by the parameter $2V_R/D$ where V_R is the resultant flow velocity. Thus

$$C_{m_q} = \left(\frac{2V_R}{D}\right)\left(\frac{\partial C_m}{\partial q}\right) = \frac{\partial C_m}{\partial \left(\frac{qD}{2V_R}\right)}$$

where C_m is the pitching moment coefficient.

The convention is adopted that drag, side, and normal forces are positive along the negative X, Y, and Z axes. Thus the aerodynamic equations are

$$F_{A_X} = - (C_{X_0} + C_{X_{\alpha_P}} \alpha_P)\ q'S \tag{34a}$$

$$F_{A_Y} = - C_{Y_{\alpha_Y}} \alpha_Y\ q'S \tag{34b}$$

$$F_{A_Z} = - C_{Z_{\alpha_P}} \alpha_P\ q'S \tag{34c}$$

$$M_{A_Y} = \left[C_{Z_{\alpha_P}} \alpha_P \left(\frac{CP-CG}{D}\right) + C_{m_{\dot{\alpha}_P}} \left(\frac{\dot{\alpha}_P D}{2V_R}\right) + C_{m_q} \left(\frac{qD}{2V_R}\right) \right] q'S\ D \tag{34d}$$

$$M_{A_X} = \left[C_{\ell_{\alpha_Y}} \alpha_Y + C_{\ell_P} \left(\frac{pD}{2V_R}\right) + C_{\ell_r} \left(\frac{rD}{2V_R}\right) \right] q'S\ D \tag{34e}$$

$$M_{A_Z} = \left[C_{n_{\dot{\alpha}_Y}} \left(\frac{\dot{\alpha}_Y D}{2V_R} \right) - C_{Y_{\alpha_Y}} \left(\frac{CP-CG}{D} \right) + C_{n_r} \left(\frac{rD}{2V_R} \right) \right] q'S\,D \qquad (34f)$$

where CP and CG denote the distance from a reference plane passing through the engine gimbal points to the center of pressure and center of gravity, respectively. Furthermore S and D are the reference area and diameter, respectively, and the dynamic pressure, q', is calculated from

$$q' = \frac{1}{2} \rho_\infty \; V_R^2$$

where ρ_∞ is the free-stream density and V_R is the resultant flow velocity.

The aerodynamic forces and moments are seen to be dependent upon the resultant air-flow velocity. In the absence of wind the velocity of the vehicle relative to the earth-fixed system, $\overline{V}$, and its velocity relative to the flow, $\overline{V}_R$, are equal in magnitude. Since the basic equations of motion are derived in terms of the components of $\overline{V}$, it is necessary to calculate $\overline{V}_R$ to account for the possibility of wind.

Wind data are usually referenced to the earth-fixed coordinate system. The wind velocity can be broken into components $\dot{X}_{wg}$, $\dot{Y}_{wg}$, and $\dot{Z}_{wg}$ along the X_g, Y_g, and Z_g axes, respectively. These components can be resolved into the body axes system, using Equation 5, and combined algebraically with u, v, and w to yield the respective components of $\overline{V}_R$ as follows:

$$\left.\begin{aligned}
u_R &= u - \dot{X}_{wg} \sin\theta \cos\psi + \dot{Y}_{wg} \sin\psi - \dot{Z}_{wg} \cos\theta \cos\psi \\
v_R &= v - \dot{X}_{wg} (\cos\theta \sin\Phi - \sin\theta \cos\Phi \sin\psi) + \dot{Y}_{wg} \cos\Phi \cos\psi \\
&\quad + \dot{Z}_{wg} (\cos\theta \cos\Phi \sin\psi + \sin\theta \sin\Phi) \\
w_R &= w - \dot{X}_{wg} (\cos\theta \cos\Phi + \sin\theta \sin\Phi \sin\psi) - \dot{Y}_{wg} \sin\Phi \cos\psi \\
&\quad - \dot{Z}_{wg} (\cos\theta \sin\psi \sin\Phi - \sin\theta \cos\Phi)
\end{aligned}\right\} (35a, b, c)$$

In the presentation of wind data it is customary to list vertical gusts, $\dot{Z}_{wg}$, and the resultant wind parallel to the Xg - Yg plane, necessitating the calculation of $\dot{X}_{wg}$ and $\dot{Y}_{wg}$. A scheme similar to that presented in Reference 12 is convenient for wind resolution in the Xg - Yg plane. The resultant wind parallel to this plane is denoted

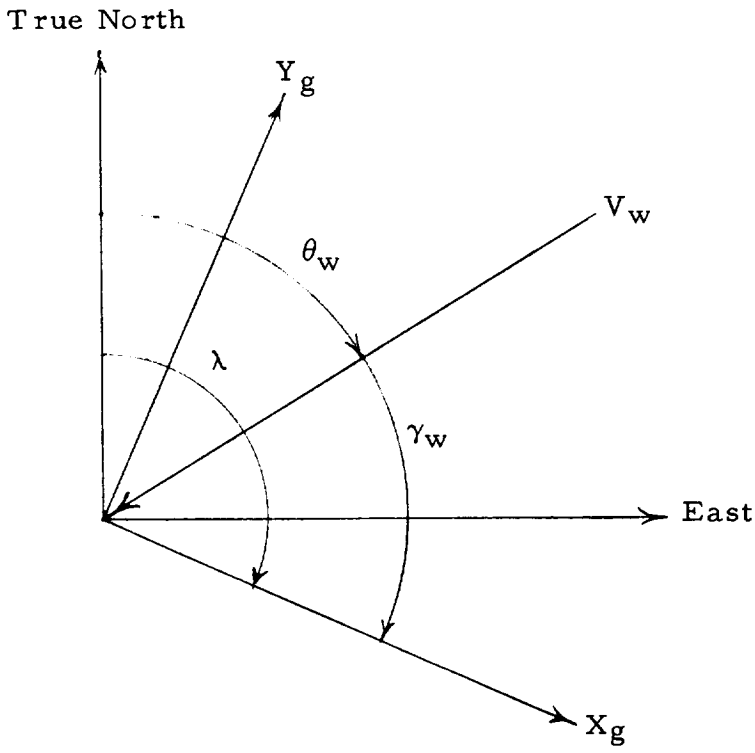

FIGURE 5. WIND RESOLUTION IN THE X_g - Y_g PLANE

by V_W, whichis referenced to true north by the direction angle θ_W (Fig. 5). The Xg axis, corresponding to the desired launch azimuth, is referenced to north by the azimuth angle, λ.

From Figure 5 it is obvious that

$$\gamma_W = \lambda - \theta_W$$

where γ_W is introduced as a means of referencing V_W to the Xg axis. Now it follows that

$$\left.\begin{aligned} \dot{X}_{wg} &= - V_W \cos \gamma_W \\ \dot{Y}_{wg} &= - V_W \sin \gamma_W \end{aligned}\right\} \qquad (36a, b)$$

The introduction of winds during launch creates large angles of attack ($\pm 90°$ for vertically launched vehicles) which are beyond the range of linear aerodynamics. Nonlinear aerodynamic characteristics with respect to angle of attack are assumed to simulate the launch motion under wind conditions. Furthermore, since Mach number varies considerably during the flight of a vehicle, it is also necessary to consider the variation of the aerodynamic characteristics with Mach number. Mach number is determined by the usual relation

$$M = \frac{V_R}{V_S} \qquad (37)$$

where V_S is the speed of sound.

Referring again to Figure 4, the pitch and yaw angles of attack are seen to be defined by

$$\left.\begin{aligned} \alpha_P &= \tan^{-1}\left(\frac{w_R}{u_R}\right) \\ \alpha_Y &= \tan^{-1}\left(\frac{v_R}{u_R}\right) \end{aligned}\right\} \qquad (38a, b)$$

The resultant angle of attack is determined from

$$\alpha = \tan^{-1}\left(\frac{v_R^2 + w_R^2}{u_R}\right) \tag{39}$$

where u_R, v_R, and w_R are components of the resultant flow vector.

The time derivatives of the pitch and yaw angles of attack are needed in the calculation of the aerodynamic forces and moments. From Equations 38a, b:

$$\dot{\alpha}_P = \left(\frac{\dot{w}_R\, u_R - \dot{u}_R\, w_R}{u_R^2}\right) \cos^2 \alpha_P \tag{40a}$$

$$\dot{\alpha}_Y = \left(\frac{\dot{v}_R\, u_R - \dot{u}_R\, v_R}{u_R^2}\right) \cos^2 \alpha_Y \tag{40b}$$

D. THRUST FORCES AND MOMENTS

Before deriving the equations for thrust forces and moments, it is necessary to adopt a sign convention and define several angles associated with the engine. For a multi-engine booster, a number system must also be adopted to facilitate references to a particular engine. For this purpose consider the typical engine arrangement for an eight-engine booster shown in Figure 6.

In such an arrangement, the outer engines are usually the control engines while the inner ones are held fixed. No restriction has been placed on the relative locations of the control and fixed engines. For reference purposes, the control engines were assigned odd numbers (1, 3, 5, 7, - - -) and the fixed engines were assigned even numbers (2, 4, 6, 8, - - -). The only other restriction is that the complete arrangement will be symmetrical with respect to the center line of the vehicle.

The angles associated with the engines, in both the initial and gimbaled positions, are defined in the list of symbols. Using engine one in Figure 6 as an example, the angles are illustrated in Figure 7. Note that the initial position illustrated is typical for all engines, whereas the gimbaled position is applicable only to the control engines.

The sign convention adopted is such that positive β_{Y_T} and β_{P_T} produce force components in the positive Y and Z directions, respectively.

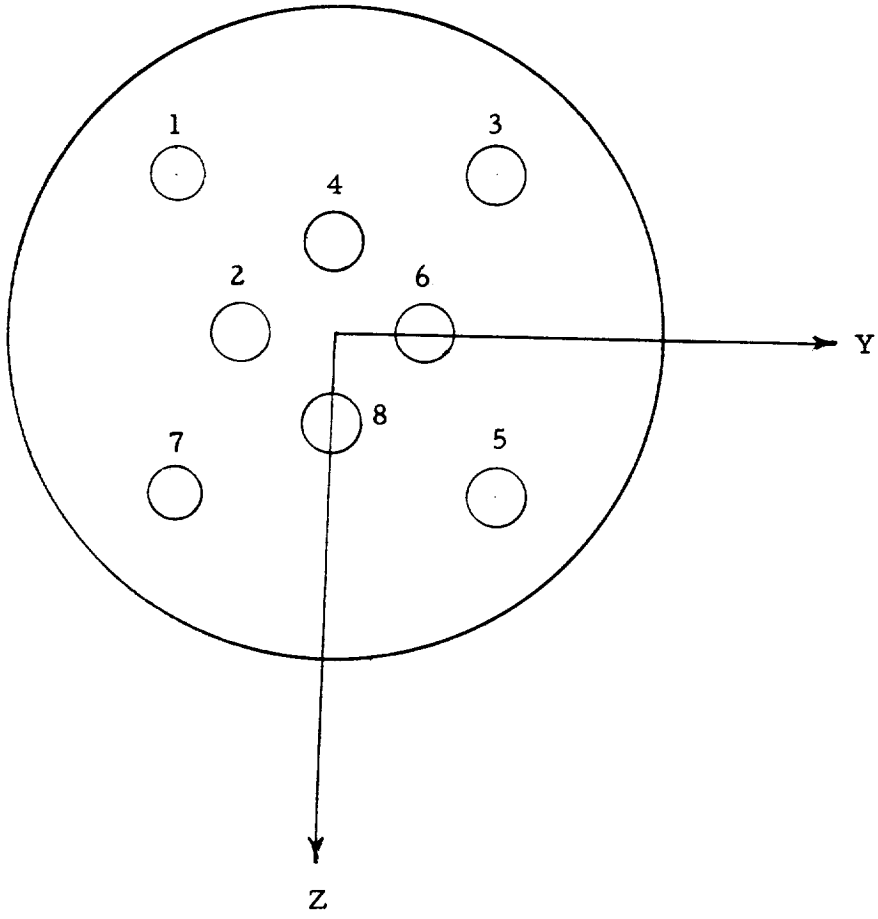

FIGURE 6. TYPICAL ARRANGEMENT OF EIGHT-ENGINE BOOSTER AS SEEN FROM REAR

The thrust force and moment equations can be derived by using engine one of Figure 7 as an example, then amplifying to obtain the general equations for a multi-engine vehicle.

From Figure 7 note that

$$\beta_{Y_{T_1}} = \beta_{Y_{01}} + \beta_{Y_1} \tag{41}$$

$$\beta_{P_{T_1}} = \beta_{P_{01}} + \beta_{P_1} \tag{42}$$

where β_{Y_1} and β_{P_1} are the yaw and pitch gimbal angles measured from the original canted axis of the engine. Note that an initial cant angle is not a restriction, but is considered as the general case since rocket engines are quite often canted. The main purpose of this is to direct the thrust of the engine toward the center of gravity at liftoff, thus reducing moments that could occur in the event of engine failure in a multi-engine vehicle.

Further relations which are either obvious from Figure 7 or easily derived are

$$\tan \beta_{P_{01}} = \tan \beta_{01} \cos \beta_{\rho_{01}} \tag{43}$$

$$\tan \beta_{Y_{01}} = \tan \beta_{01} \sin \beta_{\rho_{01}} \tag{44}$$

$$\tan \beta_1 = \left(\tan^2 \beta_{Y_{T_1}} + \tan^2 \beta_{P_{T_1}} \right)^{1/2} \tag{45}$$

$$\tan \beta_{01} = \left(\tan^2 \beta_{Y_{01}} + \tan^2 \beta_{P_{01}} \right)^{1/2} \tag{46}$$

$$\cos \beta_{01} = \frac{1}{\left(1 + \tan^2 \beta_{01}\right)^{1/2}} = \frac{1}{\left(1 + \tan^2 \beta_{Y_{01}} + \tan^2 \beta_{P_{01}}\right)^{1/2}} \tag{47}$$

$$\cos \beta_1 = \frac{1}{\left(1 + \tan^2 \beta_{Y_{T_1}} + \tan^2 \beta_{P_{T_1}}\right)^{1/2}} \tag{48}$$

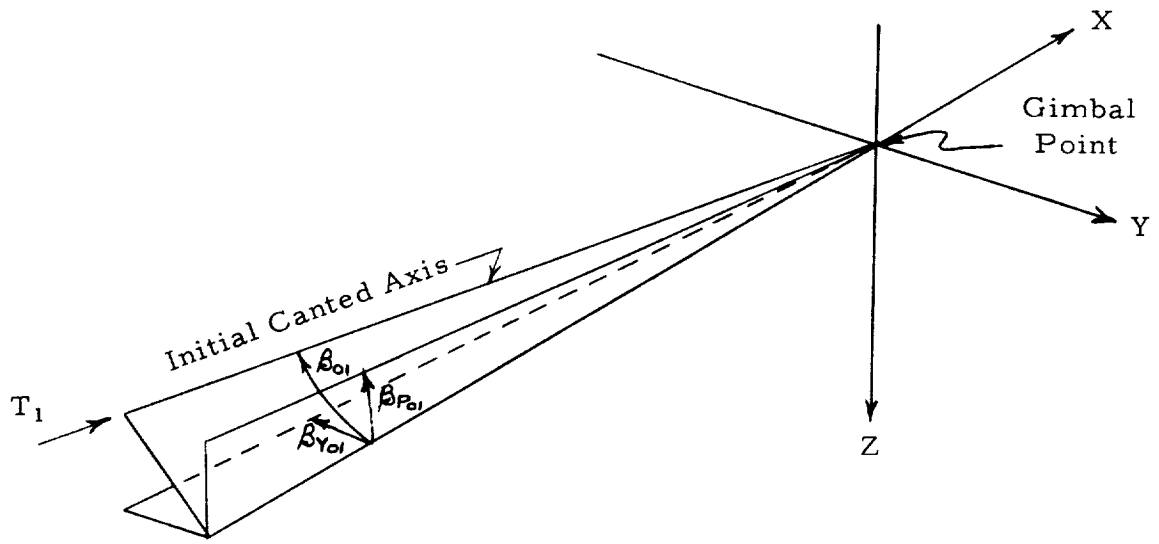

Initial Canted Position

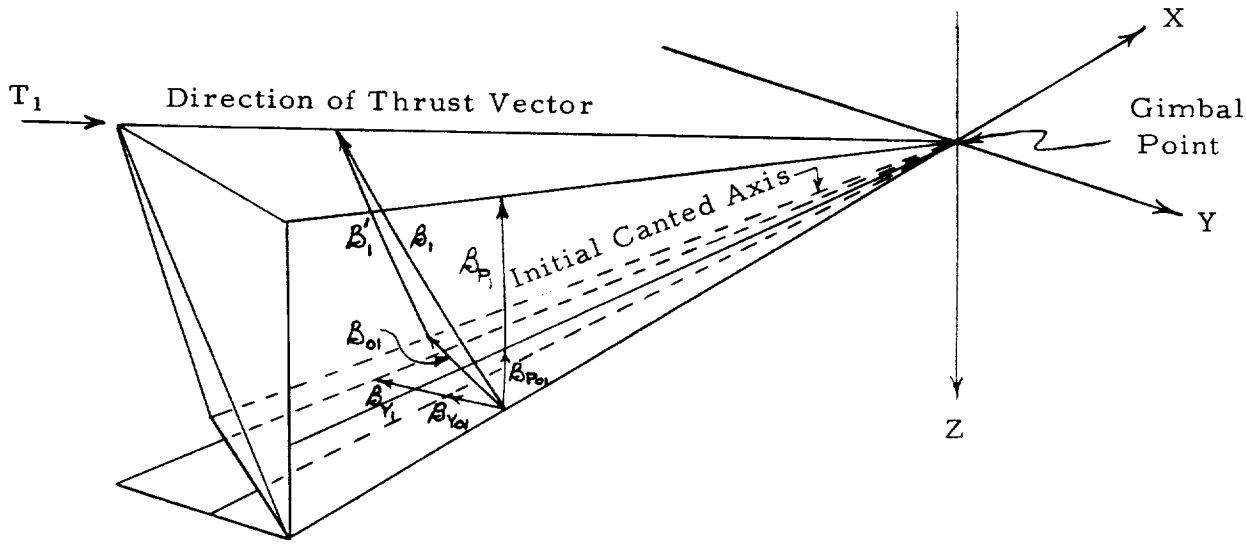

Gimbaled Position

FIGURE 7. ILLUSTRATION OF ANGLES ASSOCIATED WITH INITIAL AND GIMBALED POSITIONS OF ENGINE NUMBER ONE

The angle β_{ρ_1} is introduced as a means of quickly locating the thrust direction with respect to the center line of the vehicle. Looking along the X axis in Figure 7b, β_{ρ_1} is the angle between the X-Z plane and the plane containing the thrust vector and the X axis. From this figure it is seen that

$$\tan \beta_{\rho_1} = \frac{\tan \beta_{Y_{T_1}}}{\tan \beta_{P_{T_1}}} \tag{49}$$

and

$$\tan \beta_{\rho_{01}} = \frac{\tan \beta_{Y_{01}}}{\tan \beta_{P_{01}}} \tag{50}$$

The component thrust forces are easily developed for the engine in its initial position, being simply

$$F_{T_{X_1}} = T_1 \cos \beta_{01} \tag{51}$$

$$F_{T_{Y_1}} = T_1 \cos \beta_{01} \tan \beta_{Y_{01}} = T_1 \sin \beta_{01} \sin \beta_{\rho_{01}} \tag{52}$$

$$F_{T_{Z_1}} = T_1 \cos \beta_{01} \tan \beta_{P_{01}} = T_1 \sin \beta_{01} \cos \beta_{\rho_{01}} \tag{53}$$

where T_1 is the thrust of the example engine.

The development of the forces for the engine in a gimbaled position is more difficult. If the forces are formulated in their exact form, it is difficult to study the resulting motion independently in pitch and yaw because of the dependency of β_1 on β_{P_1} and β_{Y_1}. For example, the exact form of the $F_{T_{Z_1}}$ in a gimbaled position is

$$F_{T_{Z_1}} = \frac{T_1 \tan\left(\beta_{P_{01}} + \beta_{P_1}\right)}{\left[1 + \tan^2\left(\beta_{Y_{01}} + \beta_{Y_1}\right) + \tan^2\left(\beta_{P_{01}} + \beta_{P_1}\right)\right]^{1/2}} \quad (54)$$

The dependency of $F_{T_{Z_1}}$ on β_{Y_1} and β_{P_1} is obvious. As will be seen later in the development of the control equations, it is desirable to have the engine pitch force dependent only on the pitch gimbal angle β_{P_1}, and known initial values. The same applies for having the yaw force component dependent only on known initial values and the yaw gimbal angle, β_{Y_1}. The desired relationship for $F_{T_{Z_1}}$ can be obtained by assuming that its dependency on β_{Y_1} is negligible for reasonably small angles. For this first approximation, Equation 54 becomes

$$F_{T_{Z_1}} = \frac{T_1 \tan\left(\beta_{P_{01}} + \beta_{P_1}\right)}{\left[1 + \tan^2 \beta_{Y_{01}} + \tan^2\left(\beta_{P_{01}} + \beta_{P_1}\right)\right]^{1/2}} \quad (55)$$

The desired result has been obtained since $F_{T_{Z_1}}$ is now dependent only upon the initial values and β_{P_1}. The dependency is of a trigonometric form, however, making it difficult to see readily the change in $F_{T_{Z_1}}$ because of a change in β_{P_1}.

Suppose then, as a second approximation, it can be assumed that $F_{T_{Z_1}}$ can be represented by its value in the engine's undeflected position, given by Equation 55, plus a linear gradient through $\beta_{Y_1} = \beta_{P_1} = 0$. In other words, it is assumed that

$$F_{T_{Z_1}} = \left(F_{T_{Z_1}} \right)_{\beta_{Y_1} = \beta_{P_1} = 0} + \frac{\partial F_{T_{Z_1}}}{\partial \beta_{P_1}} \beta_{P_1} + \frac{\partial F_{T_{Z_1}}}{\partial \beta_{Y_1}} \beta_{Y_1}$$

and then shown that the last term can be neglected within certain limits so that finally

$$F_{T_{Z_1}} = \left(F_{T_{Z_1}} \right)_{\beta_{Y_1} = \beta_{P_1} = 0} + \frac{\partial F_{T_{Z_1}}}{\partial \beta_{P_1}} \beta_{P_1} \qquad (56)$$

The gradient of $F_{T_{Z_1}}$ with respect to β_{P_1} is obtained by partial differentiation of Equation 54 with the result

$$\frac{\partial F_{T_{Z_1}}}{\partial \beta_{P_1}} = \frac{\left[1 - \frac{\tan^2 \left(\beta_{P_{O1}} + \beta_{P_1} \right)}{1 + \tan^2 \left(\beta_{P_{O1}} + \beta_{P_1} \right) + \tan^2 \left(\beta_{Y_{O1}} + \beta_{Y_1} \right)} \right] T_1}{\cos^2 \left(\beta_{P_{O1}} + \beta_{P_1} \right) \left[1 + \tan^2 \left(\beta_{P_{O1}} + \beta_{Y_1} \right) + \tan^2 \left(\beta_{Y_{O1}} + \beta_{Y_1} \right) \right]^{1/2}}$$

For reasonably small values of the angles, this gradient can be assumed linear. At the initial point of $\beta_{Y_1} = \beta_{P_1} = 0$ the value is

$$\frac{\partial F_{T_{Z_1}}}{\partial \beta_{P_1}} = \frac{\left[1 - \frac{\tan^2 \beta_{P_{O1}}}{\left(1 + \tan^2 \beta_{Y_{O1}} + \tan^2 \beta_{P_{O1}} \right)} \right] T_1}{\cos^2 \beta_{P_{O1}} \left(1 + \tan^2 \beta_{P_{O1}} + \tan^2 \beta_{Y_{O1}} \right)^{1/2}}$$

Making use of Equations 44 and 47, this is further reduced to

$$\frac{\partial F_{T_{Z_1}}}{\partial \beta_{P_1}} = \frac{\cos \beta_{O1}}{\cos^2 \beta_{P_{O1}}} \left(1 - \sin^2 \beta_{O1} \cos^2 \beta_{P_{O1}}\right) T_1 \qquad (57)$$

Similarly the gradient of $F_{T_{Z_1}}$ with respect to β_{Y_1}, evaluated at $\beta_{Y_1} = \beta_{P_1} = 0$, is

$$\frac{\partial F_{T_{Z_1}}}{\partial \beta_{Y_1}} = \frac{-\sin^2 \beta_{O1} \cos \beta_{O1} \sin \beta_{\rho_{O1}} \cos \beta_{\rho_{O1}}}{\cos^2 \beta_{Y_{O1}}} T_1 \quad . \qquad (58)$$

For small initial angles, the cross coupling term represented by Equation 58 can be ignored in comparison with the related term given by Equation 57. As a result, Equation 56 can be applied so that

$$F_{T_{Z_1}} = \left[\sin \beta_{01} \cos \beta_{\rho_{01}} + \frac{\cos \beta_{01}}{\cos^2 \beta_{P_{01}}} \left(1 - \sin^2 \beta_{01} \cos^2 \beta_{\rho_{01}}\right) \beta_{P_1}\right] T_1 \qquad (59)$$

This expression of $F_{T_{Z_1}}$ is also dependent only upon initial values and the pitch gimbal angle, β_{P_1}. In this case, as opposed to Equation 55, the dependency of $F_{T_{Z_1}}$ on β_{P_1} is a simple linear relationship since the initial values are known and the coefficient of β_{P_1} is a constant. The relative accuracies of both approximations must be compared with the exact value given by Equation 54. To make this comparison, typical values for the initial cant angle must be assumed. Consider the case $\beta_{Y_{01}} = \beta_{P_{01}} = 3°$. Knowing these two values, the remaining initial values can be computed. Figure 8 shows the comparison of the approximate and exact values over a wide spread of values for β_{Y_1}. As indicated in the figure, β_{P_1} values of five and ten degrees are assumed which correspond to the lower and upper set of curves, respectively. The difference between the first and second approximations, representing Equations 55 and 59, is seen to be

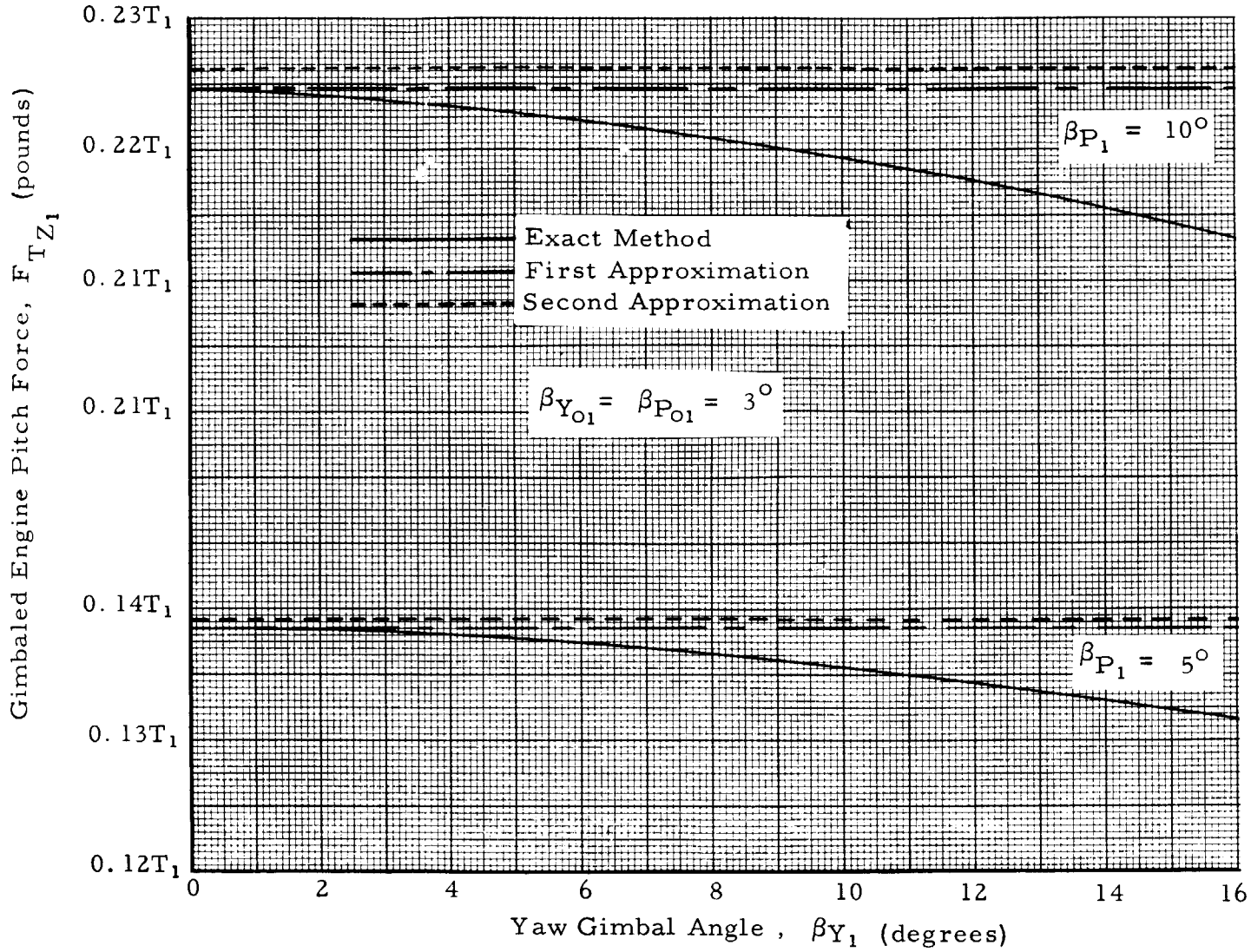

FIGURE 8. COMPARISION OF EXACT AND APPROXIMATE METHODS FOR CALCULATING F_{TZ_1}

less than one per cent for $\beta_{P_1} = 10°$, with the first approximation being closer to the exact value. Because of this small difference, the second approximation is used to take advantage of the straightforward expression.

Referring again to Figure 8, it can be seen that for values of β_{Y_1} up to ten degrees, the error involved in using the second approximation amounts to only three per cent for $\beta_{P_1} = 10°$, and less than three per cent for $\beta_{P_1} = 5°$. For values of β_{Y_1} exceeding ten degrees, the error increases at a moderate rate. A gimbal angle of ten degrees is conservative for most vehicles and use of the second approximation is justified.

The remaining forces and moments caused by thrust are developed under the same assumptions. Following the procedure applied previously to the pitch force, the yaw force is found to be

$$F_{T_{Y_1}} = \left[\sin \beta_{01} \sin \beta_{\rho_{01}} + \frac{\cos \beta_{01}}{\cos^2 \beta_{Y_{01}}} \left(1 - \sin^2 \beta_{01} \sin^2 \beta_{\rho_{01}}\right) \beta_{Y_1}\right] T_1 \qquad (60)$$

The exact form for the axial component of thrust is

$$F_{T_{X_1}} = T_1 \cos \beta_1 = \frac{T_1}{\left[1 + \tan^2 \left(\beta_{Y_{01}} + \beta_{Y_1}\right) + \tan^2 \left(\beta_{P_{01}} + \beta_{P_1}\right)\right]^{1/2}}$$

For this component, the pitch and yaw gimbal angles share equal importance so that the one cannot be neglected in favor of the other. To avoid this double dependency, both β_{Y_1} and β_{P_1} can be neglected for the angular magnitudes normally encountered. The axial component thus becomes

$$F_{T_{X_1}} = \frac{T_1}{\left(1 + \tan^2 \beta_{Y_{01}} + \tan^2 \beta_{P_{01}}\right)^{1/2}}$$

which, by use of Equation 45, reduces to

$$F_{T_{X_1}} = T_1 \cos \beta_{01} \tag{61}$$

Equation 61 is identical with Equation 51 which expressed the value of $F_{T_{X_1}}$ in the engine undeflected position. Ignoring the effect of β_{Y_1} and β_{P_1} upon $F_{T_{X_1}}$ is thus tantamount to assuming that the change is negligible in the axial component of thrust because of gimbaling.

The development of the thrust force component for the example engine has been completed. It should be emphasized that, although a particular engine is used in the development, the results are applicable to any engine no matter what its location relative to the vehicel center line may be, so long as the sign convention specified is used. Thus for the general case Equations 59, 60, and 61 can be written as

$$F_{T_{X_n}} = T_n \cos \beta_{on}$$

$$F_{T_{Y_n}} = \left[\sin \beta_{on} \sin \beta_{\rho_{on}} + \frac{\cos \beta_{on}}{\cos^2 \beta_{Y_{on}}} \left(1 - \sin^2 \beta_{on} \sin^2 \beta_{\rho_{on}} \right) \beta_{Y_n} \right] T_n$$

$$F_{T_{Z_n}} = \left[\sin \beta_{on} \cos \beta_{\rho_{on}} + \frac{\cos \beta_{on}}{\cos^2 \beta_{Y_{on}}} \left(1 - \sin^2 \beta_{on} \cos^2 \beta_{\rho_{on}} \right) \beta_{P_n} \right] T_n$$

where the subscript n refers to a particular engine (n = 1, 2, 3, 4, - - -). Earlier it was specified that all fixed engines would be identified by even numbers. Therefore for n, an even number, the gimbal angles β_{Y_n} and β_{P_n} are zero and terms involving these variables have no meaning. The summation of components for all engines of a multi-engine vehicle can be written

$$F_{T_X} = \sum_{1}^{n} T_n \cos \beta_{on} \tag{62}$$

$$F_{T_Y} = \sum_{1}^{n} T_n \sin \beta_{on} \sin \beta_{\rho_{on}}$$

$$+ \sum_{1}^{n_c} \frac{\cos \beta_{on_c}}{\cos^2 \beta_{Y_{on_c}}} \left(1 - \sin^2 \beta_{on_c} \sin^2 \beta_{\rho_{on_c}} \right) T_{n_c} \beta_{Y_{n_c}} \tag{63}$$

$$F_{T_Z} = \sum_{1}^{n} T_n \sin \beta_{on} \cos \beta_{\rho_{on}}$$

$$+ \sum_{1}^{n_c} \frac{\cos \beta_{on_c}}{\cos^2 \beta_{P_{on_c}}} \left(1 - \sin^2 \beta_{on_c} \cos^2 \beta_{\rho_{on_c}} \right) T_{n_c} \beta_{P_{n_c}} \tag{64}$$

where n again refers to any particular engine, control or fixed, and n_c ($n_c = 1, 3, 5, - - -$) refers to control engines only. Note that the first summation term in both Equations 63 and 64 will be zero if the engine arrangement is symmetrical with respect to the center line and all engines perform as expected. In case of engine failure or thrust misalignment, however, biases are created which result in an unbalance of forces and moments. Thrust misalignments are not considered in the development of the thrust equations but a term is included in the general equations of motion to account for such misalignments.

Since all the initial values are known in Equations 62 through 64, the equations can be expressed in a simpler notation by grouping certain constants. For this purpose, let:

$$K_{X_{1n}} = \cos \beta_{on}$$

$$K_{Y_{1n}} = \sin \beta_{on} \sin \beta_{\rho_{on}}$$

$$K_{Y_{2n_c}} = \frac{\cos \beta_{on_c}}{\cos^2 \beta_{Y_{on_c}}} \left(1 - \sin^2 \beta_{on_c} \sin^2 \beta_{\rho_{on_c}} \right)$$

$$K_{Z_{1n}} = \sin \beta_{on} \cos \beta_{\rho_{on}}$$

$$K_{Z_{2n_c}} = \frac{\cos \beta_{on_c}}{\cos^2 \beta_{P_{on_c}}} \left(1 - \sin^2 \beta_{on_c} \cos^2 \beta_{\rho_{on_c}} \right)$$

Then Equations 62 through 64 can be written in the simplified form

$$F_{T_X} = \sum_{1}^{n} K_{X_{1n}} T_n \tag{65}$$

$$F_{T_Y} = \sum_{1}^{n} K_{Y_{1n}} T_n + \sum_{1}^{n_c} K_{Y_{2n_c}} T_{n_c} \beta_{Y_{n_c}} \tag{66}$$

$$F_{T_Z} = \sum_{1}^{n} K_{Z_{1n}} T_n + \sum_{1}^{n_c} K_{Z_{2n_c}} T_{n_c} \beta_{P_{n_c}} \tag{67}$$

The components of the moment caused by thrust are developed in a manner similar to that used above for the force components. In the development of the pitching moment, for example, it is assumed that

$$M_1 = (M_1)_{\beta_{Y_1} = \beta_{P_1} = 0} + \frac{\partial M_1}{\partial \beta_{P_1}} \beta_{P_1}$$

where engine number one is again used for illustration. The gradient term is again assumed linear and evaluated at the initial condition $\beta_{Y_1} = \beta_{P_1} = 0$. Furthermore, cross-coupling terms are found to be small for the gimbal angle range of interest and consequently are neglected. Thus pitching moments caused by thrust are assumed to be dependent only on pitch gimbal angles and yaw moments dependent only on yaw gimbal angles. It is also assumed that, except for an engine malfunction, the summation of thrust moments are zero when none of the engines are in a gimbaled position. Under these assumptions, the pitch and yaw components are found to be

$$M_{T_Y} = \sum_{1}^{n} T_n \left(CGK_{M_{2n}} - R_n K_{M_{1n}} \right) + \sum_{1}^{n_c} T_{n_c} \left(R_{n_c} K_{M_{4n_c}} + CGK_{M_{3n_c}} \right) \beta_{P_{n_c}} \quad (68)$$

$$M_{T_Z} = \sum_{1}^{n} T_n \left(R_n K_{N_{1n}} - CGK_{N_{2n}} \right) + \sum_{1}^{n_c} T_{n_c} \left(R_{n_c} K_{N_{4n_c}} - CGK_{3n_c} \right) \beta_{Y_{n_c}} \quad (69)$$

where R_n is the perpendicular distance from the vehicle center line to the gimbal point of a particular engine, and

$$K_{M_{1n}} = \cos \beta_{on} \cos \beta_{\rho_{on}}$$

$$K_{M_{2n}} = \cos \beta_{on} \tan \beta_{P_{on}}$$

$$K_{M_{3n_c}} = \frac{\cos \beta_{on_c}}{\cos^2 \beta_{P_{on_c}}} \left(1 - \frac{\sin 2\beta_{on_c}}{2} \cos^2 \beta_{\rho_{on_c}} \tan \beta_{on_c} \right)$$

$$K_{M_{4n_c}} = \frac{\cos \beta_{on_c} \sin 2\beta_{on_c}}{2 \cos^2 \beta_{P_{on_c}}} \cos^2 \beta_{\rho_{on_c}}$$

$$K_{N_{1n}} = \cos \beta_{on} \sin \beta_{\rho_{on}}$$

$$K_{N_{2n}} = \cos \beta_{on} \tan \beta_{Y_{on}}$$

$$K_{N_{3n_c}} = \frac{\cos \beta_{on_c}}{\cos^2 \beta_{Y_{on_c}}} \left(1 + \frac{\sin 2\beta_{on_c}}{2} \sin^2 \beta_{\rho_{on_c}} \tan \beta_{on_c} \right)$$

$$K_{N_{4n_c}} = \frac{\cos \beta_{on_c} \sin 2\beta_{on_c} \sin^2 \beta_{\rho on_c}}{2 \cos^2 \beta_{Y_{on_c}}}$$

The production of rolling moments with thrust vector control is also necessary for asymmetric configurations to counteract induced aerodynamic rolling moments. In a later development of the control equations, it is assumed that when only pitch forces and moments are produced by thrust gimbaling, all of the pitch gimbal angles of all control engines are equal. The same applies to yaw forces and moments produced by yaw gimbal angles. If this restriction is maintained in the overall control of the vehicle, it is impossible to produce rolling moments, except in the case of a malfunction, because of the earlier restriction concerning the symmetry of the engines. Therefore to produce coordinated rolling moments, certain pairs of engines must gimbal with equal magnitudes but in opposite directions. This will be taken into account in the control equations. For practical multi-engine configurations, roll rates should not be severe so that large rolling moment corrections are not needed. Thus it can be assumed that roll control can be accomplished by either pitch or yaw gimbaling independently.

Following previous procedures, the general expression for thrust rolling moment was found to be

$$M_{T_X} = C_1 \sum_{1}^{n} T_n R_n K_{L_{3n}} + \sum_{1}^{n_c} T_{n_c} R_{n_c} K_{L_{4n_c}} \beta_{Y_{n_c}} \qquad (70)$$

$$- C_2 \sum_{1}^{n} T_n R_n K_{L_{1n}} + \sum_{1}^{n_c} T_{n_c} R_{n_c} K_{L_{2n_c}} \beta_{P_{n_c}}$$

where C_1 and C_2 are so-called "go-or-no-go" constants. For pitch gimbal roll control, $C_1 = 0$ and $C_2 = 1$ and vice-versa for yaw gimbal roll control. Also

$$K_{L_{1n}} = \cos \beta_{on} \tan \beta_{P_{on}} \sin \beta_{\rho on}$$

$$K_{L_{2n_c}} = \frac{\cos \beta_{on_c} \sin \beta_{\rho_{on_c}}}{\cos^2 \beta_{P_{on_c}}} \left(1 - \sin^2 \beta_{on_c} \cos^2 \beta_{\rho_{on_c}} \right)$$

$$K_{L_{3n}} = \cos \beta_{on} \tan \beta_{Y_{on}} \cos \beta_{\rho_{on}}$$

$$K_{L_{4n_c}} = \frac{\cos \beta_{on_c} \cos \beta_{\rho_{on_c}}}{\cos^2 \beta_{Y_{on_c}}} \left(1 - \sin^2 \beta_{on_c} \sin^2 \beta_{\rho_{on_c}} \right)$$

The thrust in all previous equations is assumed to be a function of time to simulate thrust build-up and decay with altitude. The altitude correction is given by the usual relation

$$T_n = T_{on} + (P_o - P_\infty) A_{en}$$

where T_{on} is the thrust of a particular engine at some reference pressure P_o, A_{en} is the nozzle exit area, and P_∞ is the trajectory free stream static pressure. It is assumed that the thrust of all engines is measured at the same reference pressure, and that each functions ideally or not at all.

E. MISCELLANEOUS FORCES AND MOMENTS

In the formulation of the general equations of motion, it is virtually impossible to account for all possible sources of external forces and moments. Forces and moments caused by thrust misalignments, fin deflections, or retro-rockets, as a few examples, are not considered in detail. Consequently, as a means of making the equations as general as possible, a miscellaneous term is added to each equation. Thus,

$$\left.\begin{aligned} \bar{F}_M &= \bar{i} F_{X_M} + \bar{j} F_{Y_M} + \bar{k} F_{Z_M} \\ \bar{M}_M &= \bar{i} L_M + \bar{j} M_M + \bar{k} N_M \end{aligned}\right\} \qquad (71a, b)$$

The miscellaneous terms can be either constant or time variant. Actually the term F_{X_M} is needed in the axial force equation to balance the gravitational force at time zero. At this point, as will be seen later, the axial force equation reduces to

$$F_{X_M} = mg \tag{72}$$

F. GENERAL EQUATIONS OF MOTION

The general equations of motion are obtained by summing the X, Y, and Z components of the various forces and moments, and substituting on the left-hand side of Equations 24 through 30. The general equations are

$$F_{X_M} - \left(C_{X_o} + C_{X_{\alpha_P}}\right) q'S - mg \cos\theta \cos\psi + \sum_1^n T_n K_{X_{1n}} = m(\dot{u} + wq - vr) \tag{73}$$

$$F_{Y_M} - C_{Y_{\alpha_Y}} \alpha_Y q'S + mg(\cos\theta \cos\Phi \sin\psi + \sin\theta \sin\Phi) + \sum_1^n T_n K_{Y_{1n}} + \sum_1^{n_c} T_{n_c} K_{Y_{2n_c}} \beta_{Y_{n_c}} = m(\dot{v} + ur - wp) - \dot{m} r r_{ex} \tag{74}$$

$$F_{Z_M} - C_{Z_{\alpha_P}} \alpha_P q'S + mg(\cos\Phi \sin\theta - \sin\Phi \sin\psi \cos\theta) + \sum_1^n T_n K_{Z_{1n}} + \sum_1^{n_c} T_{n_c} K_{Z_{2n_c}} \beta_{P_{n_c}} = m(\dot{w} + vp - uq) + \dot{m} q r_{ex} \tag{75}$$

$$L_M + \left[C_{\ell_{\alpha_Y}} \alpha_Y + C_{\ell_P}\left(\frac{pD}{2V_R}\right) + C_{\ell_r}\left(\frac{rD}{2V_R}\right)\right] q'SD + C_1 \left[\sum_1^n T_n R_n K_{L_{3n}} + \sum_1^{n_c} T_{n_c} R_{n_c} K_{L_{4n}} \beta_{Y_{n_c}}\right] - C_2 \left[\sum_1^n T_n R_n K_{L_{1n}} + \sum_1^{n_c} T_{n_c} R_{n_c} K_{L_{2n_c}} \beta_{P_{n_c}}\right]$$

$$= \dot{p}I_X + qr\,(I_Z - I_Y) + (pr - \dot{q})\,I_{XY} - (pq + \dot{r})\,I_{XZ} + (r^2 - q^2)\,I_{YZ}$$
$$- \dot{p}I_X + \dot{q}I_{XY} + \dot{r}I_{XZ} \qquad (76)$$

$$M_M + \left[C_{Z_{\alpha_P}}\,\alpha_P\left(\frac{CP-CG}{d}\right) + C_{\dot{m}_{\alpha_P}}\left(\frac{\dot{\alpha}_P D}{2V_R}\right) + C_{m_q}\left(\frac{qD}{2V_R}\right)\right] q'SD$$
$$+ \sum_1^n T_n\left(K_{M_{2n}}\,CG - R_n\,K_{M_{1n}}\right) + \sum_1^{n_c}\left(R_{n_c}\,K_{M_{4n_c}} + CG\,K_{M_{3n_c}}\right)T_{n_c}\,\beta_{P_{n_c}}$$

$$= \dot{q}\,I_Y + pr\,(I_X - I_Z) + (pq - \dot{r})\,I_{YZ} - (\dot{p} + qr)\,I_{XY}$$
$$+ (p^2 - r^2)\,I_{XZ} - \dot{q}I_Y + \dot{r}I_{YZ} + \dot{p}I_{XY} + \dot{m}q\,r_{ex}^2 \qquad (77)$$

$$N_M + \left[C_{n_{\dot{\alpha}_Y}}\left(\frac{\dot{\alpha}_Y D}{2V_R}\right) + C_{n_r}\left(\frac{rD}{2V_R}\right) - C_{Y_{\alpha_Y}}\,\alpha_Y\left(\frac{CP-CG}{d}\right)\right] q'SD$$
$$+ \sum_1^n T_n\left(R_n\,K_{N_{1n}} - CG\,K_{N_{2n}}\right) + \sum_1^{n_c}\left(R_{n_c}\,K_{N_{4n_c}}\right)T_{n_c}\,\beta_{Y_{n_c}} = \dot{r}I_Z$$
$$+ pq\,(I_Y - I_X) + (qr - \dot{p})\,I_{XZ} + (q^2 + p^2)\,I_{XY} - \dot{r}I_{XZ} + \dot{p}I_{XZ}$$
$$+ \dot{q}I_{YZ} + \dot{m}r\,r_{ex}^2 \qquad (78)$$

Table 1 is included as a convenient reference, listing all inputs to the equations according to the independent variables of which they are a function.

TABLE 1

PROGRAM INPUTS

Inputs which are a function of time only are

F_{X_M}, F_{Y_M}, F_{Z_M}, L_M, M_M, N_M, m, $\dot{m}$, I_X, I_Y, I_Z, $\dot{I}_X$, $\dot{I}_Y$, $\dot{I}_Z$

I_{XY}, I_{YZ}, I_{XZ}, $\dot{I}_{XY}$, $\dot{I}_{YZ}$, $\dot{I}_{XZ}$, T_{on}, A_{en}, CG, r_{ex}, a_{OY}

a_{OP}, a_{1Y}, a_{1P}, b_{OY}, b_{OP}, h_{OY}, h_{OP}, θ_c, θ_c, Φ_c

Inputs which are a function of Mach number only are

C_{X_0}

Inputs which are a function of altitude only are

V_s, V_w, Z_{wg}

Inputs which are a function of Mach number and pitch angle of attack, or its derivative, are

C_{m_q}, $C_{m_{\alpha_P}}$, $C_{X_{\alpha_P}}$, $C_{Z_{\alpha_P}}$, $C_{m_{\dot{\alpha}_P}}$

Inputs which are a function of Mach number and yaw angle of attack, or its derivative, are

C_{ℓ_q}, C_{ℓ_r}, C_{n_r}, $C_{\ell_{\alpha_Y}}$, $C_{Y_{\alpha_Y}}$, $C_{n_{\alpha_Y}}$

Inputs which are a function of total angle of attack are

CP

Constant inputs are

C_1, C_2, P_0, $K_{L_{1n}}$, $K_{L_{2n_c}}$, $K_{L_{3n}}$, $K_{L_{4n_c}}$, $K_{M_{1n}}$, $K_{M_{2n}}$

TABLE 1 (CONCLUDED)

$K_{M_{3n_c}}$, $K_{M_{4n_c}}$, $K_{N_{1n}}$, $K_{N_{2n}}$, $K_{N_{3n_c}}$, $K_{N_{4n_c}}$, $K_{X_{1n}}$, $K_{Y_{1n}}$,

$K_{Y_{2n_c}}$, $K_{Z_{1n}}$, $K_{Z_{2n_c}}$, $K_{R_{n_c}}$, D, S, g, R_n, λ

Initial values of the basic variables are

t_o, u_o, v_o, p_o, q_o, r_o, Xg_o, Yg_o, Zg_o, ψ_o, Φ_o, w_o

θ_o, $\beta_{Y_{on}}$, $\beta_{P_{on}}$

SECTION IV. CONTROL EQUATIONS

The six general equations of motion representing the six degrees of freedom of a rigid body given by Equations 73 through 78 contain 11 unknown variables, namely the linear velocities (u, v, w), the rotational velocities (p, q, r), the orientation angles (θ, ψ, ϕ) and the gimbal angles ($\beta_{Y_{n_c}}$, $\beta_{P_{n_c}}$) . The auxiliary relations, given by Equations 33 a, b, and c, determine the orientation angles. Two additional equations are needed to match the number of equations with the number of unknowns. These additional relations are the control equations which can be employed for the determination of the gimbal angles.

The control equations have a tremendous influence on the eventual motion of the vehicle. The physical behavior of a vehicle without control varies considerably during its flight because of variation in the vehicle's mass and its aerodynamic characteristics. The control system has to be adapted to these variations which are often not accurately known. Control requirements for a given configuration are dependent on the mode of operation of the control system. This will be discussed in more detail later.

One of the basic assumptions of this study is that the vehicle is considered a rigid body. However, deformation of the vehicle under the influence of aerodynamic and maneuver loads, together with propellant sloshing, creates interactions between the associated modes of motion which require more complex analysis. Interaction between motions around the three body axes is usually small since the control system keeps angular velocities and deviations small. For preliminary design purposes the control equations can be assumed to contain only linear functions of certain control variables, with coupling in the control system ignored. Consequently, it was assumed that yawing motions are controlled by yaw gimbaling and pitching motion of pitch gimbaling. As mentioned earlier, it is assumed that roll control can be accomplished by either pitch or yaw gimbaling. In this study, it is further assumed that the vehicle is equipped with an attitude reference system and an angle-of-attack meter so that the control variables are the attitude angles and angle of attack. Under these assumptions, the general control equations are

$$---+ A_2\ddot{\beta}_{Y_{n_c}} + A_1\dot{\beta}_{Y_{n_c}} + \beta_{Y_{n_c}} = f(\psi, \alpha_Y, \Phi, \dot{\psi}, \dot{\alpha}_Y, \dot{\Phi} \text{ ---})$$

$$---+ B_2\ddot{\beta}_{P_{n_c}} + B_1\dot{\beta}_{P_{n_c}} + \beta_{P_{n_c}} = f(\theta, \alpha_P, \Phi, \dot{\theta}, \dot{\alpha}_P, \dot{\Phi} \text{ ---})$$

Path control, in which displacement variables and their derivatives are included among the control variables, usually has little or no effect on the gimbal angle requirements and can be neglected in initial studies (Ref. 4).

The control equations are idealized by neglecting derivatives of the gimbal angles on the left side which produce phase lags but are not important for basic studies (Ref. 2). Furthermore, all derivatives of the control variables are neglected in this study except the first derivatives of ψ and θ. The control equations can now be written in this form

$$\left.\begin{aligned} \beta_{Y_{n_c}} &= a_{OY}\,\psi + a_{1_Y}\,\dot{\psi} + b_{OY}\,\alpha_Y + h_{OY}\,(\Phi-\Phi_c) \\ \beta_{P_{n_c}} &= a_{OP}\,(\theta-\theta_c) + a_{1_P}\,(\dot{\theta}-\dot{\theta}_c) + b_{OY}\,\alpha_P + h_{OP}\,(\Phi-\Phi_c) \end{aligned}\right\} \quad (79a,\ b)$$

where the coefficients of the control variables are the so-called control gains and the variables with the subscript c indicate the desired value of that variable when the desired value is not zero. If the desired value of a variable is assumed to be zero at all times, no such term is necessary. As an illustration, consider the yaw control equation. If a solution of the general equations of motion indicates the vehicle is yawing, the yaw angle ψ is amplified by the gain factor a_{OY} and a yaw gimbal angle is created to correct the yawing motion. In the pitch plane, however, the trajectory is normally tilted so that the desired value of the pitch angle, θ_c, is not zero at all times. Thus if a solution of the equations of motion should indicate that the actual pitch angle θ is not equal to θ_c, then a pitch gimbal angle is initiated and the trajectory will be corrected. The desired value of the roll angle, Φ_c, is normally zero except in cases where launch equipment restricts the alignment of the vehicle so that a programmed roll is necessary. All the control gains and the desired trajectory parameters are time variables.

Using Equations 79 a and b for control, the simulation established in this study can be used for two specific types of problems. In the first case, completely arbitrary control gains can be assumed and the resulting dynamics of the vehicle determined. In the second case, which is the one encountered more often, the control gains are established according to some preset relation determined by the desired motion of the vehicle during flight. The establishment of a control program by which an otherwise unstable vehicle is stabilized is commonly referred to as artificial stabilization. As indicated earlier, the control modes capturing the most interest at present are the drift-minimum principle (DMP) and the load-minimum principle (LMP). Both principles are discussed in detail in References 3 and 6.

The DMP is simply a control program which minimizes the dispersion of the vehicle, in both the pitch and yaw planes, in response to a wind shear. This is accomplished by forcing the vehicle to assume an attitude which leads to the approximate cancellation of

forces perpendicular to the undisturbed flight path. The wind induced oscillations and accelerations approach zero and a component of thrust against the wind cancels the lift and side forces. Although a detailed derivation of the DMP is given in References 3 and 6, a short derivation is included here because of differences in sign convention and basic definitions. In the development of the DMP, it is assumed that the vehicle is not rolling and that control in the pitch and yaw planes can be analyzed independently. Considering then the motion in the pitch plane with a wind shear imposed on the vehicle, it is assumed that the wind is horizontal so that the resultant wind in the pitch plane, for small values of ψ, is $\dot{X}_{wg}$ (Fig. 9).

Referring to Figure 9, let

$$\left.\begin{aligned} \theta - \theta_c &= \Delta\theta \\ \dot{X}g - \dot{X}g_c &= \Delta\dot{X}g \end{aligned}\right\} \qquad (80a, b)$$

where θ_c and $\dot{X}g_c$ are the desired pitch angle and the desired rate of change of range, respectively. Also from the figure, for small angles

$$\alpha_{w_P} + \alpha_P = \frac{\Delta\dot{X}g}{V} - \Delta\theta \qquad (81)$$

where α_{w_p} is the wind angle, having the approximate value

$$\alpha_{w_P} \approx \frac{\dot{X}_{wg}}{V}$$

Consequently Equation 81 can be approximated by

$$\alpha_P = \frac{\Delta\dot{X}g - \dot{X}_{wg}}{V} - \Delta\theta \qquad (82)$$

The incremental motion in the Xg direction can be approximated by

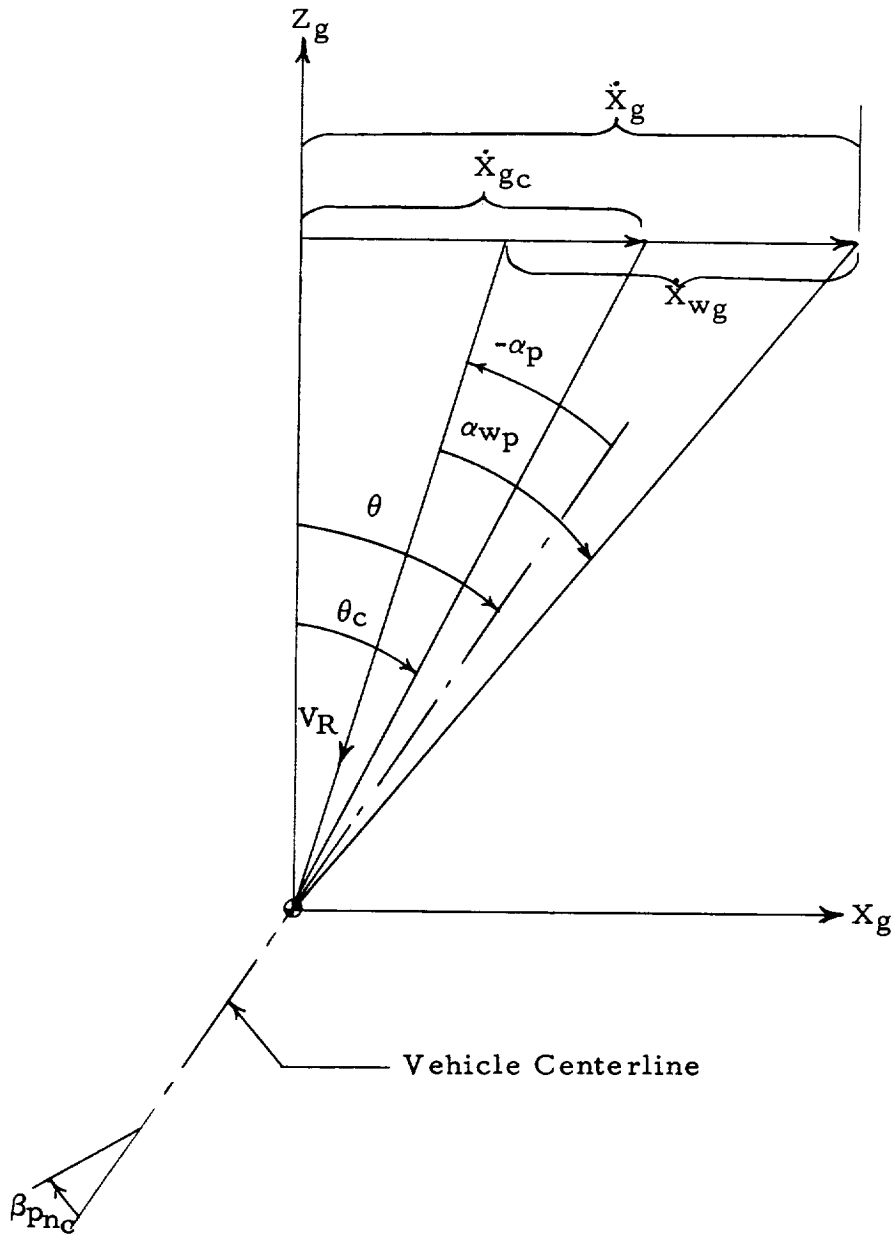

FIGURE 9. ATTITUDES OF AERODYNAMICALLY UNSTABLE VEHICLE IN RESPONSE TO WIND WITH ATTITUDE AND ANGLE OF ATTACK CONTROL

$$\Delta\ddot{X}_g = \frac{-C_{Z_{\alpha_P}} \alpha_P \, q'S}{m} + \frac{1}{m}\left(\sum_1^n T_n \cos\beta_{o_n} - C_{X_o} q'S\right) \Delta\theta$$

$$+ \frac{1}{m} \sum_1^{n_c} K_{Z_{2n_c}} T_{n_c} \beta_{P_{n_c}} \qquad (83)$$

In the derivation of the DMP, it is assumed that rolling motion is small and can be neglected; hence β_Y and β_P are the same for all engines.

The incremental pitching motion can be approximated by

$$\ddot{\theta} = \frac{1}{I_Y}\left[C_{Z_{\alpha_P}} q'S\,(CG-CP)\,\alpha_P - \sum_1^{n_c} CG\, K_{Z_{2n_c}} T_{n_c} \beta_{P_{n_c}}\right] \qquad (84)$$

let,

$$k_{1P} = \frac{1}{m}\left(\sum_1^n T_n \cos\beta_{on} - C_{Xo} q'S\right)$$

$$k_{2P} = \frac{C_{Z_{\alpha_P}} q'S}{m}$$

$$k_{3P} = \frac{1}{m} \sum_1^{n_c} T_{n_c} K_{Z_{2n_c}}$$

$$C_{1P} = \frac{C_{Z_{\alpha_P}} q'S\,(CG-CP)}{I_Y}$$

$$C_{2Y} = \frac{\sum_{1}^{n_c} T_{n_c} K_{Z_{2n_c}}}{I_Y}$$

so that Equations 83 and 84 can be written in the form

$$\ddot{\Delta Xg} = k_{1P} \Delta\theta - k_{2P} \alpha_P + k_{3P} \beta_{P_{n_c}} \tag{85}$$

$$\ddot{\Delta\theta} = C_{1P} \alpha_P - C_{2P} \beta_{P_{n_c}} \tag{86}$$

From Equation 79 b

$$\beta_{P_{n_c}} = a_{0P} \Delta\theta + a_{1P} \dot{\Delta\theta} + b_{0P} \alpha_P \tag{87}$$

where rolling motion is again neglected.

Substituting Equations 82 and 87 into Equation 86 gives

$$\ddot{\Delta\theta} + C_{2P}\, a_{1P}\, \dot{\Delta\theta} + \left[C_{2P}\, (a_{0P} - b_{0p}) + C_{1P}\right] \Delta\theta = \frac{\dot{\Delta Xg} - \dot{X}_{wg}}{V} (C_{1P} - C_{2P}\, b_{0P})$$

or

$$\frac{\dot{\Delta Xg} - \dot{X}_{wg}}{V} = \frac{\ddot{\Delta\theta} + C_{2P}\, a_{1P}\, \dot{\Delta\theta} + \left[C_{2P}\, (a_{0P} - b_{0P}) + C_{1P}\right] \Delta\theta}{C_{1P} - C_{2P}\, b_{0P}} \tag{88}$$

Substitution of Equations 82, 87, and 88 into Equation 85 gives

$$\ddot{\Delta X_g} = \frac{1}{C_{1P} - C_{2P}\, b_{OP}} \left\{ (k_{3P} b_{OP} - k_{2P})\, \ddot{\Delta\theta} + a_{1P}\, (k_{3P}\, C_{1P} - k_{2P}\, c_{2P})\, \Delta\theta \right.$$

$$\left. + \left[a_{OP}\, (C_{1P}\, k_{3P} - C_{2P}\, k_{2P}) + k_{1P}\, (C_{1P} - C_{2P}\, b_{OP}) \right] \Delta\theta \right\} \qquad (89)$$

For DMP it is assumed that

$$\ddot{X_g} = \ddot{\Delta\theta} = \dot{\Delta\theta} \approx 0$$

so that Equation 89 becomes

$$\frac{1}{C_{1P} - C_{2P}\, b_{OP}} \left[a_{OP}\, (C_{1P}\, k_{3P} - C_{2P}\, k_{2P}) + k_{1P}\, (C_{1P} - C_{2P}\, b_{OP}) \right] \Delta\theta = 0$$

Since

$$\frac{1}{C_{1P} - C_{2P}\, b_{OP}} \neq 0$$

then

$$a_{OP}\, (C_{1P}\, k_{3P} - C_{2P}\, k_{2P}) + k_{1P}\, (C_{1P} - C_{2P}\, b_{OP}) = 0$$

which can be expressed in the form

$$\frac{b_{OP} - \frac{C_{1P}}{C_{2P}}}{a_{OP}} = \frac{\frac{C_{1P}}{C_{2P}}\, k_{3P} - k_{2P}}{k_{1P}} \qquad (90)$$

Equation 90 represents the drift minimum condition and is identical with that derived in References 3, 4, and 6 except for certain differences in signs. These sign differences are solely caused by the sign conventions used here and do not detract from the basic principle involved. Equation 90 can also be derived as shown in Reference 6 by establishing the characteristic equation of Equations 86, 87, and 88, and examining the roots in detail as a check on the validity of the assumptions made. Such detail is not necessary here, since the basic principles are well known.

The DMP condition, represented by Equation 90, is not sufficient for determining the magnitude of the gains a_{OP} and b_{OP} but only indicates the linear relationship between them. Consequently another relation is needed to determine their values. By virtue of the DMP condition the translational path dispersion is practically eliminated (Refs. 3 and 6) so that the rotary motion of the vehicle about its center of gravity is predominant. Equation 89 is a linear differential equation describing the rotary motion in response to wind disturbances. From this equation, the undamped natural frequency of the rotary motion is found to be

$$f_{nP} = \frac{C_{1P} + C_{2P} (a_{OP} - b_{OP})}{2\pi}^{1/2} \tag{91}$$

so that

$$a_{OP} - b_{OP} = \frac{(2 f_{nP})^2 - C_{1P}}{C_{2P}} \tag{92}$$

The frequency has a definite influence on the control requirements. Care must be taken to insure that the frequency is not so low that it corresponds to the bending frequencies of the vehicle to give resonance effects. The high values of frequency are bounded by the limitations of the control system hardware. Frequencies currently being used range from about 0.2 to 0.9 cycles - per - second. As is pointed out in Reference 2 the optimum control frequency for a particular vehicle depends on the characteristics of the wind disturbances encountered. Once the frequency is established, or assumed, Equations 90 and 92 can be combined to determine the values of a_{OP} and b_{OP}. Adding the two equations gives

$$a_{OP} = \frac{(2\pi f_{nP})^2}{C_{2P} \left(1 + \frac{k_{2P}}{k_{1P}}\right) - \frac{k_{3P}}{k_{1P}} C_{1P}} \tag{93}$$

Once a_{OP} is determined Equation 92 can be used to calculate b_{OP}.

The value of a_{1P} for the DMP is determined by the damping of the rotary motion about the center of gravity. The ratio of damping to critical damping is found from Equation 88 to be

$$\zeta_P = \frac{C_{2P} a_{1P}}{4\pi f_{nP}} \tag{94}$$

so that if the frequency and damping are known a_{1P} is readily determined. A typical value of ζ is 0.75.

The lateral control gains for the DMP are established by identical procedures with those employed above. Thus analagous to Equations 91, 92, 93, and 94, it was found that

$$\frac{b_{OY} - \frac{C_{1Y}}{C_{2Y}}}{a_{OY}} = \frac{\frac{C_{1Y}}{C_{2Y}} k_{3Y} - k_{2Y}}{k_{1Y}} \tag{95}$$

$$f_{nY} = \frac{C_{1Y} + C_{2Y}(a_{OY} - b_{OY})}{2\pi} \tag{96}$$

$$a_{OY} = \frac{(2\pi f_{nY})^2}{C_{2Y}\left(1 + \frac{k_{2Y}}{k_{1Y}}\right) - \frac{k_{3Y}}{k_{1Y}} C_{1Y}} \tag{97}$$

$$\zeta_Y = \frac{C_{2Y} a_{1Y}}{4\pi f_{nY}} \tag{98}$$

When the DMP is applied, attitude deviations are small and the resultant angle of attack does not approach zero when wind disturbances are encountered. As a result, normal loads are imposed on the vehicle. In some cases these loads may be beyond the design limit of the vehicle and the DMP cannot be employed. The angle of attack can be reduced by reducing a_{OY} and a_{OP} since this allows greater path instability. The extreme is reached when a_{OY} and a_{OP} are equal to zero (Ref. 3). In this situation, the vehicle turns its nose in the resultant flow direction like a weathercock stable vehicle without special attitude control so that attitude deviations of the vehicle may be large. Since the angle of attack, and thus the aerodynamic loads, approaches zero in this extreme case, this is commonly referred to as the load-minimum principle (LMP). This approach may be indicated for large, highly unstable vehicle configurations where tremendous control torques and structural loads are involved (Ref. 2). If proper guidance equipment is available, the deviation of the flight path in the presence of wind is of little concern since it can be compensated for by guidance induced maneuvers during the latter part of propelled flight when the vehicle is relatively insensitive to aerodynamic effects.

If a_{OP} and a_{OY} are set equal to zero in Equations 92 and 96, it is found that

$$b_{OP} = \frac{C_{1P} - (2\pi f_{nP})^2}{C_{2P}} \tag{99}$$

$$b_{OY} = \frac{C_{1Y} - (2\pi f_{nY})^2}{C_{2Y}} \tag{100}$$

Note that the load-minimum principle is not a zero load condition but represents the least amount of load that can be associated with the DMP. For a given vehicle, however, there is a specific frequency at which the LMP does reduce to a zero-load condition.

The strong influence of C_{1P}, C_{2P}, C_{1Y}, and C_{2Y} on both the DMP and LMP is obvious. The parameters C_{1P} and C_{2P} are the specific aerodynamic restoring torque and the specific control torque (pitch plane), respectively, while C_{1Y} and C_{2Y} are identical parameters for the yaw plane. The fact that all four parameters are determined solely by the characteristics of the vehicle and its trajectory is illustrative of the interplay between design and control.

Since it is assumed in the development of the DMP that roll can be neglected, the roll control gains h_{OY} and h_{OP} remain undefined. Also no guarantee has been made that the DMP or LMP gains satisfy the stability conditions of the servomechanisms employed in the control system (Refs. 20 and 21). This requires a more detailed analysis. In view of this uncertainty it is assumed that arbitrary values for the roll gains can be chosen in any particular investigation, with the actual values being determined by the limitations of the control system hardware.

The general equations of motion are formulated so that roll can be controlled by either pitch or yaw gimbaling. In some cases it may not be necessary to use all engines for roll control. For this reason the control equations are now written in the form

$$\beta_{Y_{n_c}} = a_{OY}\psi + a_{1Y}\dot{\psi} + b_{OY}\alpha_Y + K_{R_{n_c}} h_{OY} (\Phi - \Phi_c) \tag{101}$$

$$\beta_{P_{n_c}} = a_{OP} (\theta - \theta_c) + a_{1P} (\dot{\theta} - \dot{\theta}_c) + b_{OP}\alpha_P + K_{R_{n_c}} h_{OP} (\Phi - \Phi_c) \tag{102}$$

where the constants $K_{R_{n_c}}$ are roll proportionality constants taking on values of zero, or plus or minus one. If the value is zero then the engine to which it is assigned does not participate in the roll control. Once it is established which engines will be used for roll

control, the engine arrangement must be analyzed to determine which will be assigned a plus or a minus one value. The plus or minus one value simply causes certain engine pairs to deflect with equal incremental magnitude but in opposite directions so that roll restoring moments are initiated.

SECTION V. SOLUTION OF THE EQUATIONS

Once the vehicle data is established and the initial conditions are specified, the general Equations 73 through 78 can be solved for $\dot{u}$, $\dot{v}$, $\dot{w}$, $\dot{p}$, $\dot{q}$, and $\dot{r}$. These, in turn, are integrated to obtain u, v, w, p, q, and r. The earth-fixed acceleration components can then be calculated by applying the transformation given by Equation 7. The body axis components should include both linear and rotational accelerations. Thus,

$$\begin{pmatrix} \ddot{X}_g \\ \ddot{Y}_g \\ \ddot{Z}_g \end{pmatrix} = \begin{pmatrix} d_{11} & d_{21} & d_{31} \\ d_{12} & d_{22} & d_{32} \\ d_{13} & d_{23} & d_{33} \end{pmatrix} \begin{pmatrix} \dot{u} + wq - vr \\ \dot{v} + ur - wp \\ \dot{w} + vp - uq \end{pmatrix} \tag{103}$$

The earth-fixed velocity and trajectory geometry components are obtained by singic and double integration of the respective acceleration components. Once this much ot the basic information has been obtained, the remaining variables, such as angle of attack, Mach number, gimbal angles, and Euler angles, can be calculated from the various auxiliary equations.

One point of importance should be made concerning the gimbal angles. The initial cant angles, β_{on}, and the resultant gimbal angles, β_{n_c}, used in the general equations are referenced to a line parallel to the vehicle center line. The engine gimbal angle measured from the initial canted axis (Fig. 7) may be of more physical interest since this angle is limited by auxiliary engine hardware or vehicle performance. Defining β'_{n_c} as the gimbal angle relative to the canted axis, Figure 7 determines that

$$\cos \beta'_{n_c} = \sin \beta_{on_c} \sin \beta_{n_c} \cos(\beta_{\rho_{n_c}} - \beta_{\rho_{on_c}}) + \cos \beta_{on_c} \cos \beta_{n_c} \tag{104}$$

SECTION VI. NUMERICAL EXAMPLE

A ficticious vehicle is now formulated as a means of illustrating how the simulation developed in this study may be used in making a stability and control investigation. A brief analysis is made to determine the gimbal angle requirements, and related performance

parameters, for the drift-minimum and load-minimum control modes. Typical results are shown and compared, where possible, with two-dimensional results for the same vehicle characteristics. Past experience has shown (Refs. 4 and 5) that the maximum gimbal angle requirements occur when a vehicle is disturbed by a high velocity wind shear in the region of maximum dynamic pressure. Consequently the numerical example will be restricted to the maximum dynamic pressure region of the assumed vehicle trajectory.

A vehicle having eight engines arranged and numbered as shown in Figure 6 is assumed, with the four outboard engines having gimbal capability. The thrust and nozzle exit area of all engines are the same, and the gimbal points are in a plane perpendicular to the vehicle center line . The total sea-level thrust of the vehicle is 1,500,000 pounds corresponding to a liftoff weight of 1,000,000 pounds. An instantaneous thrust build-up is assumed for simplicity so that T_{on} is constant with time. A thrust duration of 120 seconds is also assumed. The initial cant angle β_{on}, are 4° and 6° for the inboard and outboard engines, respectively. From Figure 6, the following angles defining the initial thrust direction of each engine are obvious.

$\beta_{\rho_{01}} = 45°$

$\beta_{\rho_{02}} = 90°$

$\beta_{\rho_{03}} = 315°$

$\beta_{\rho_{04}} = 0$

$\beta_{\rho_{05}} = 225°$

$\beta_{\rho_{06}} = 270°$

$\beta_{\rho_{07}} = 135°$

$\beta_{\rho_{08}} = 180°$

The outboard engines lie on a circle about the vehicle center line such that

$R_1 = R_3 = R_5 = R_7 = 8.5$ feet

Similarly,

$R_2 = R_4 = R_6 = R_8 = 3.5$ feet

Roll control will be provided by yaw deflections of the control engines so that (Eq. 72):

$C_1 = 1$

$C_2 = 0$

From Figure 6 note that a yaw deflection of engines one and three in the negative direction would tend to correct a positive roll, while a positive yaw deflection would be needed for engines five and seven. Thus, assuming that all of the control engines share in roll control, the roll proportionality constants are (Eqs. 102 and 103):

$$K_{R_1} = K_{R_3} = -1$$

$$K_{R_5} = K_{R_7} = 1$$

The mass, center of gravity, inertia, and thrust moment arm characteristics of the assumed vehicle are shown in Figures 10 and 11. It is assumed that all the miscellaneous forces, such as F_{Y_M}, are zero. The assumed aerodynamic characteristics of the ficticious vehicle are shown in Figures 12 through 15. Since the current example is limited to the region of maximum dynamic pressure, the angles of attack will not be large and most of the curves shown do not consider the variation of the aerodynamic parameters with angle of attack. Figure 13 illustrates the more general case, although the curves shown for large angles of attack are not needed for this example. A double iteration procedure is employed in the simulation when both the Mach number and angle-of-attack variation of the aerodynamic parameters are considered (Ref. 9).

The desired (no wind) trajectory parameters in the region of maximum dynamic pressure are given in Table 2. The desired roll angle, ϕ_c, is zero for the entire flight. The desired flight path angle, θ_c, and its first time derivative are the only parameters shown in Table 2 that are required inputs to the control equations.

The desired launch azimuth is due east from Cape Canaveral, Florida so that

$$\lambda = 90°$$

Typical wind profiles and wind shear data for Cape Canaveral are given in Reference 22. A typical wind profile is shown in Figure 16. It is assumed that the vehicle formulated in the present example must be designed to fly through the wind shear represented by this profile. The assumed wind profile is designed so that the maximum wind velocity corresponds to the same altitude at which the vehicle encounters maximum dynamic pressure (Table 2). The wind shear is assumed to have an 8.5 second build-up; consequently, the vehicle enters the shear at t = 51.5 seconds, which is assumed to be the starting time for calculations made in this example. The initial conditions of the desired trajectory are thus

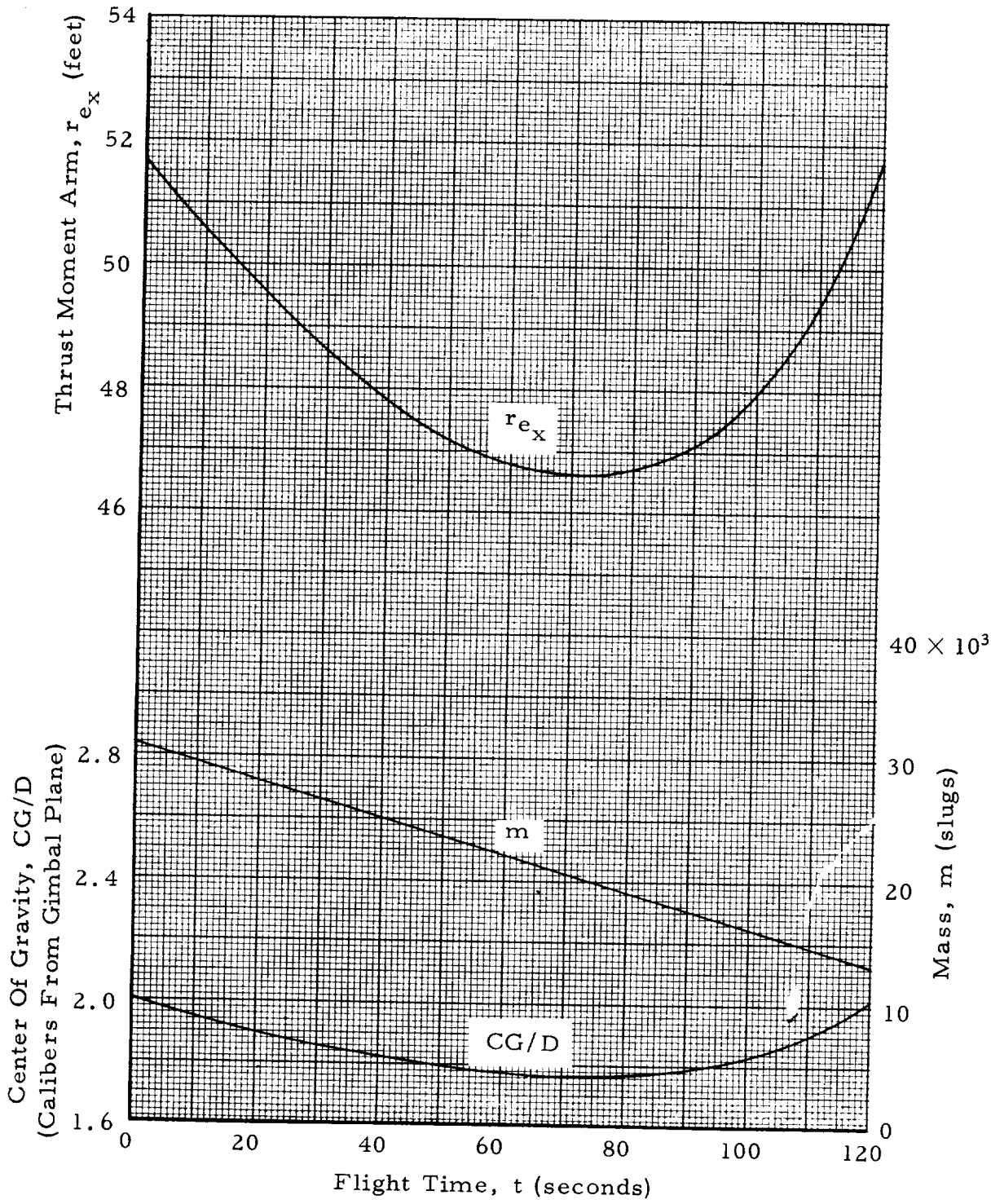

FIGURE 10. MASS, CENTER OF GRAVITY AND THRUST MOMENT ARM DATA

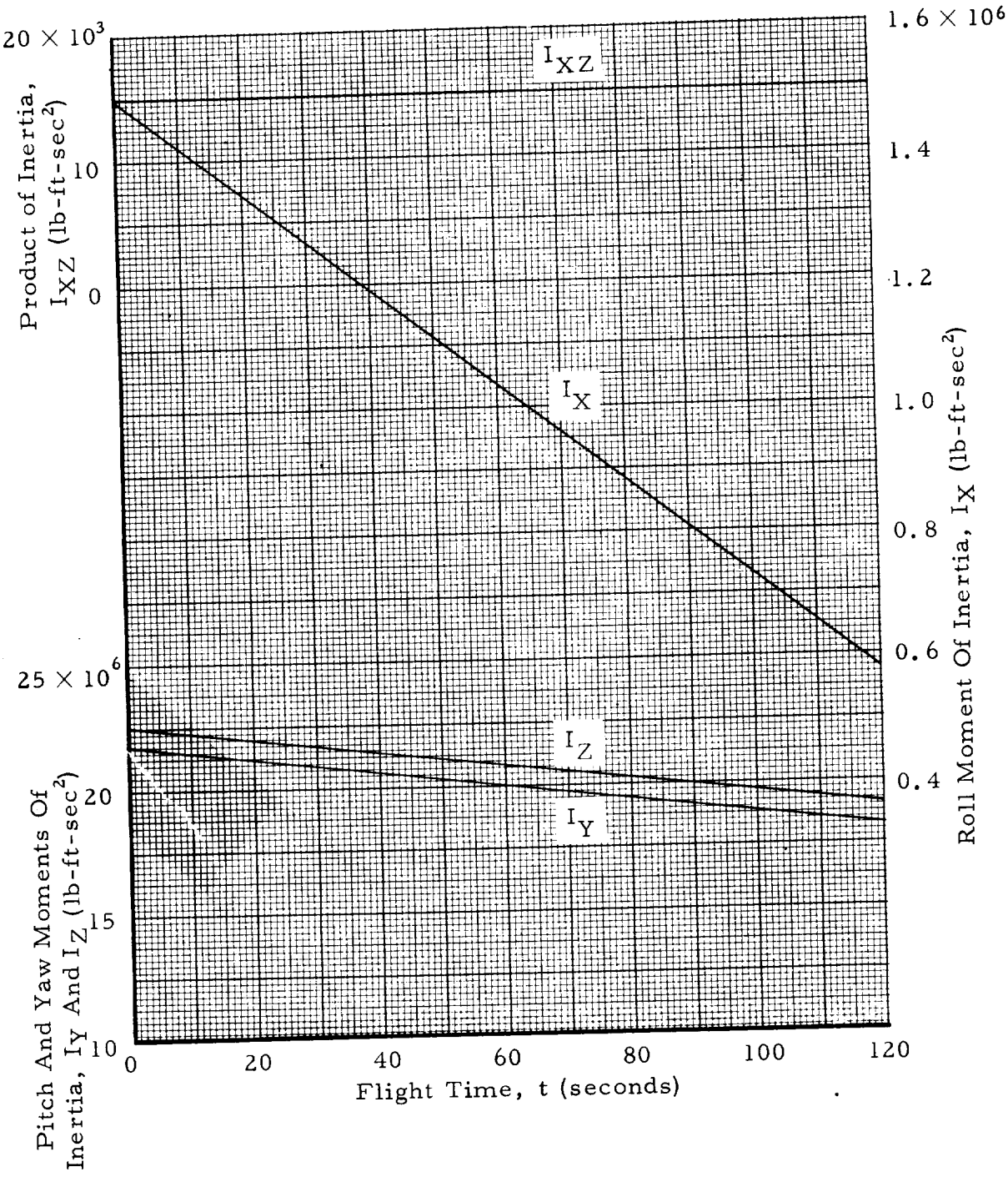

FIGURE 11. MASS MOMENTS AND PRODUCT OF INERTIA CHARACTERISTICS

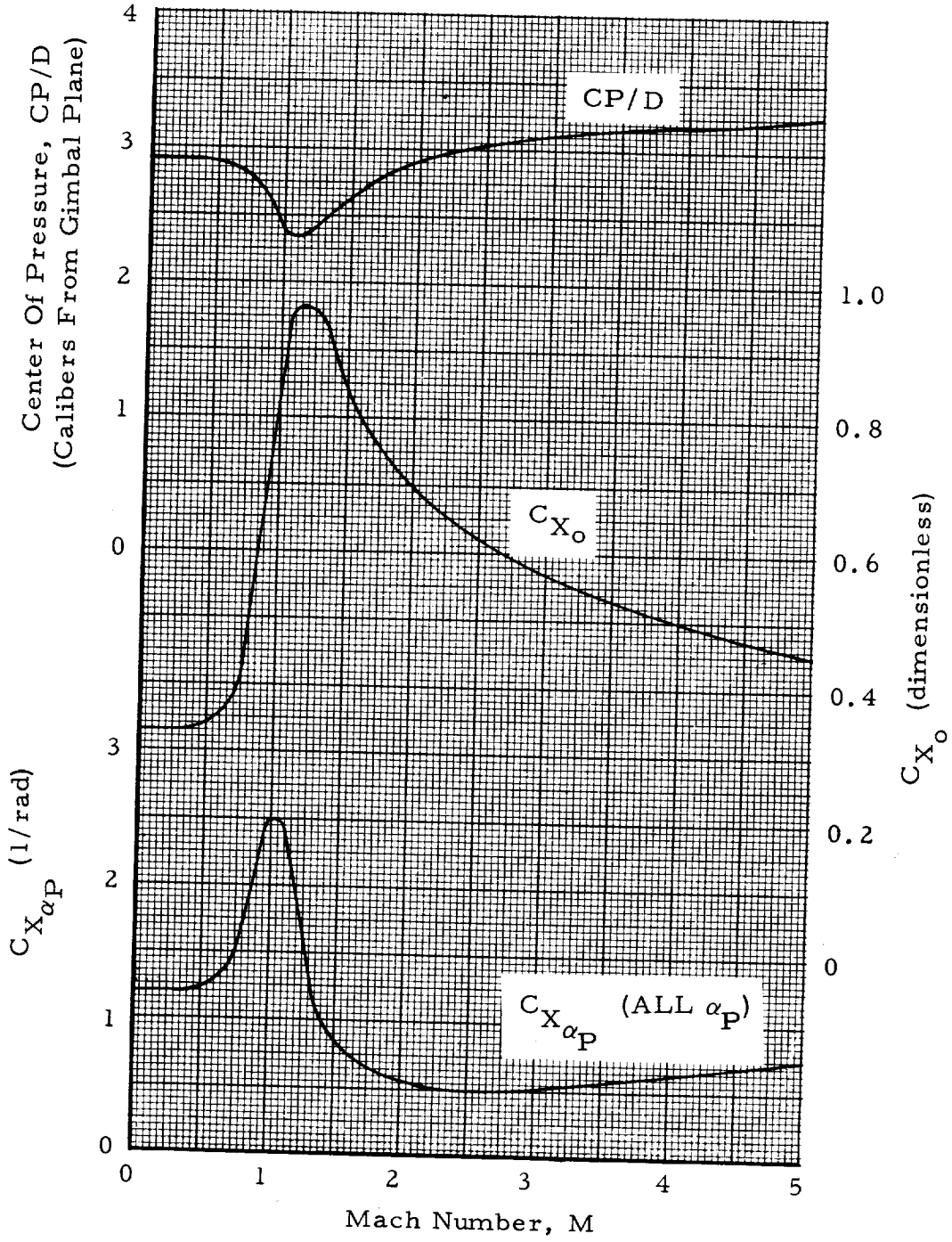

FIGURE 12. CENTER OF PRESSURE AND AXIAL FORCE COEFFICIENT

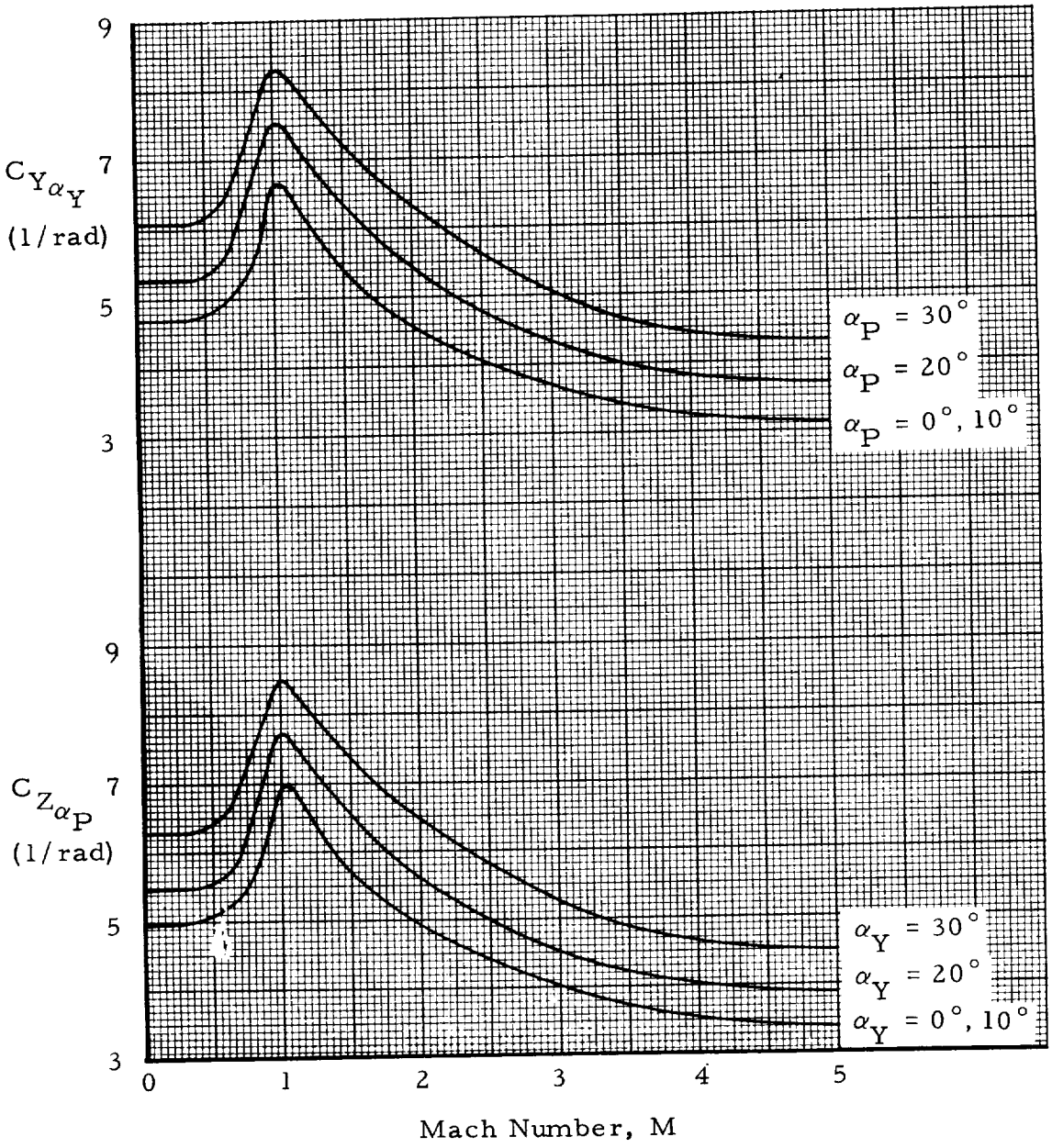

FIGURE 13. RATE OF CHANGE OF NORMAL FORCE COEFFICIENTS WITH ANGLE OF ATTACK

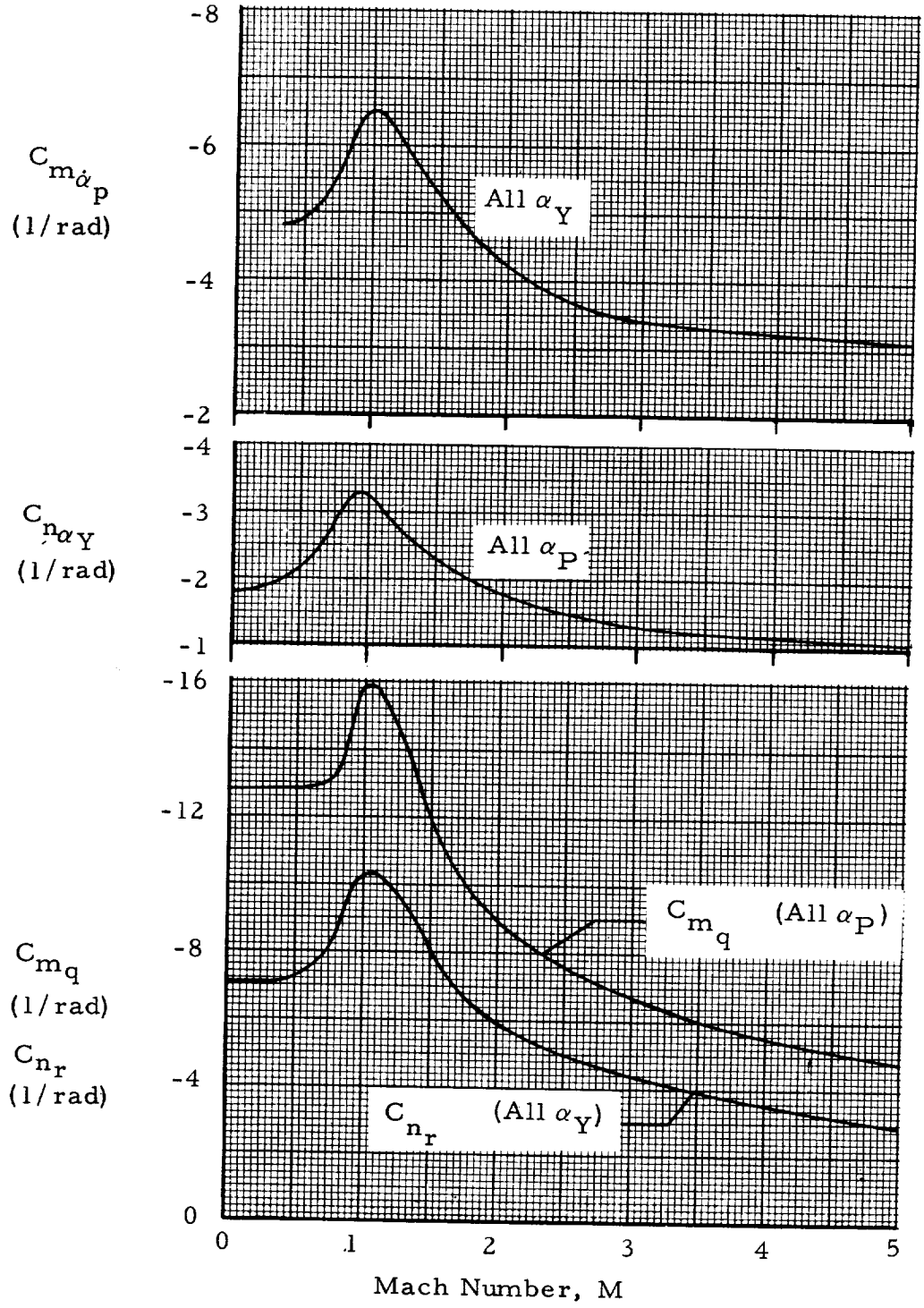

FIGURE 14. PITCHING MOMENT AND YAWING MOMENT STABILITY DERIVATIVES

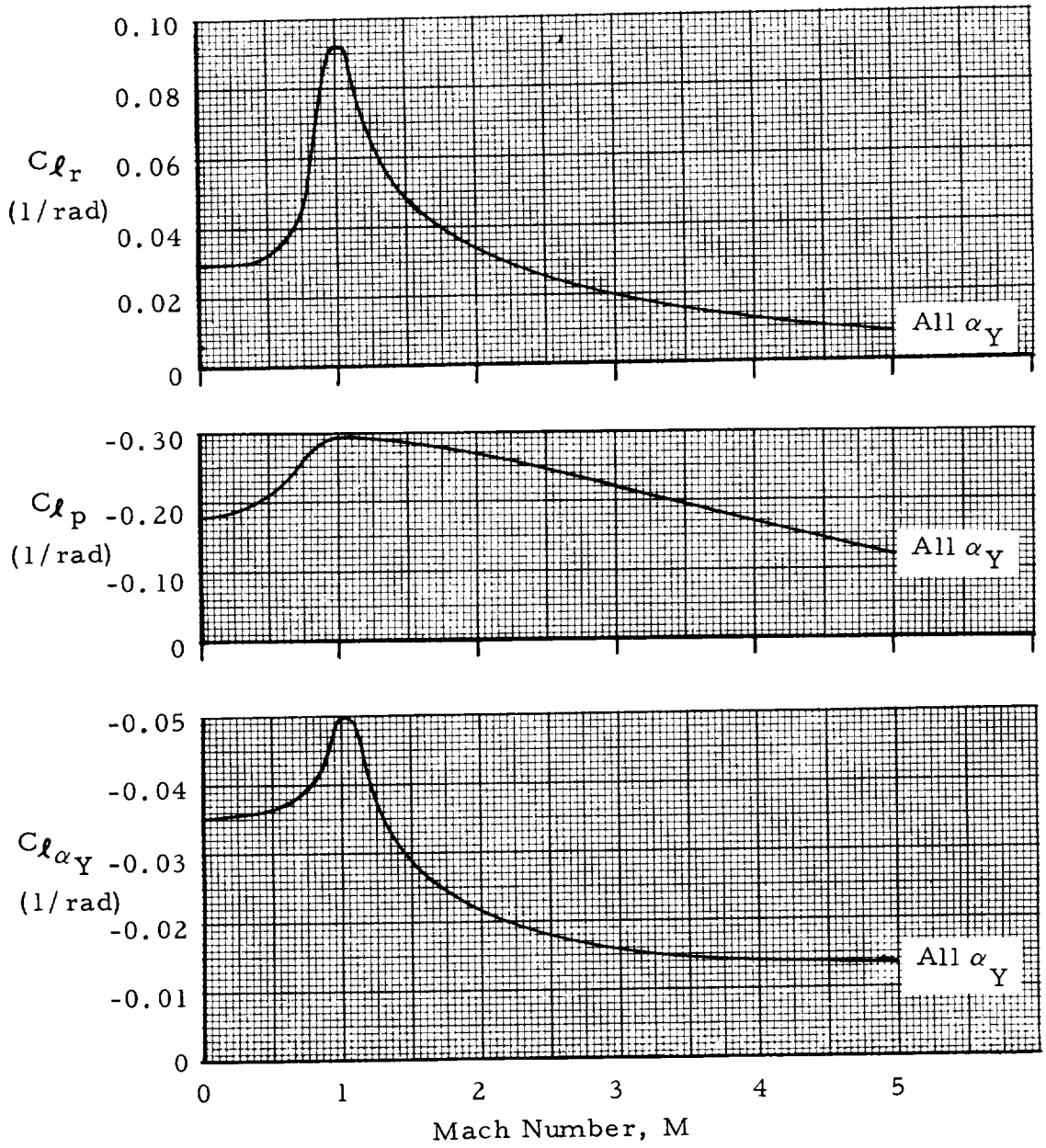

FIGURE 15. ROLLING MOMENT STABILITY DERIVATIVES

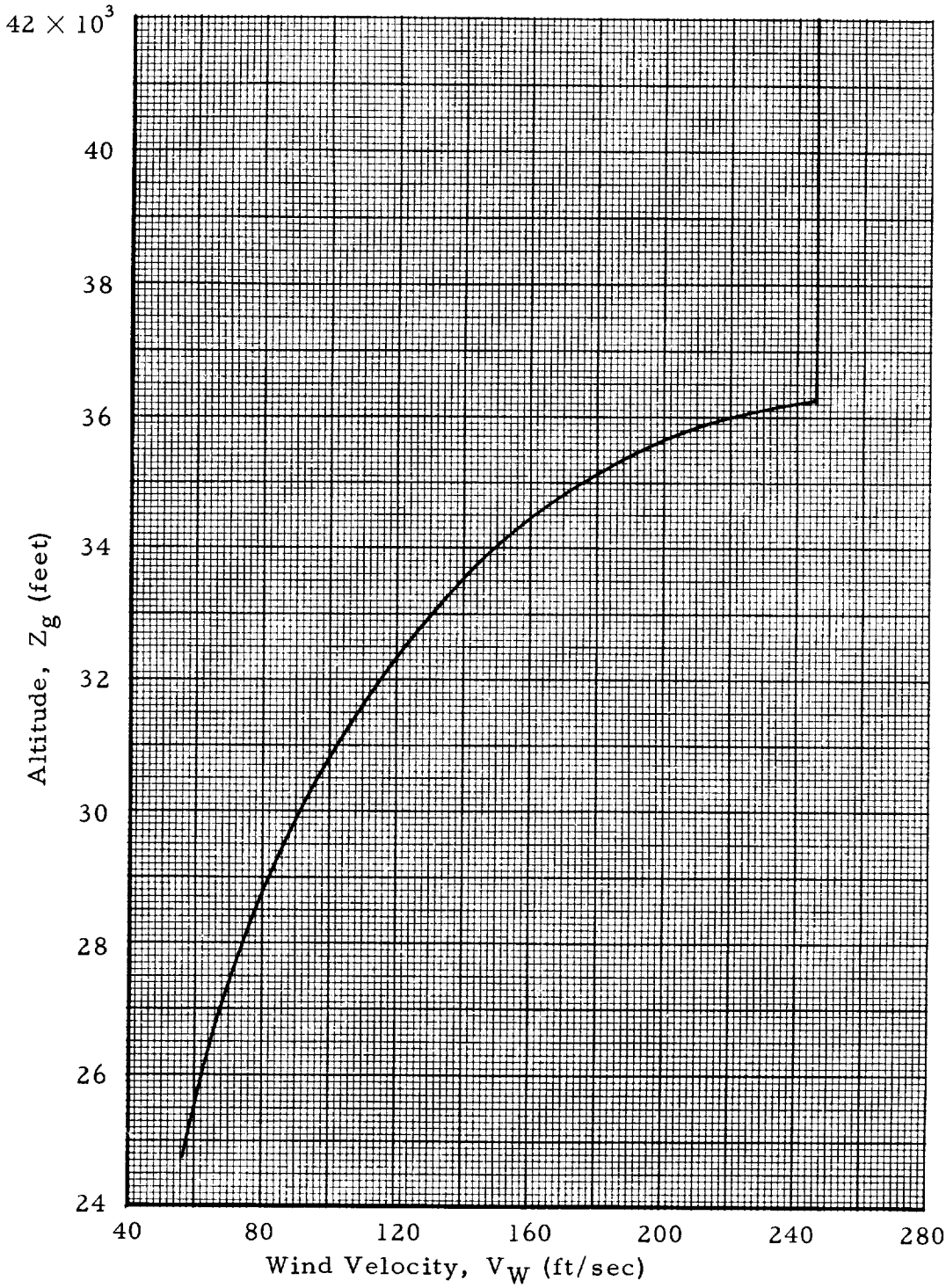

FIGURE 16. WIND VELOCITY PROFILE

TABLE 2

NOMINAL TRAJECTORY FOR NUMERICAL EXAMPLE

t (sec)	M	q' (lb/ft^2)	θ_c (deg)	$\dot{\theta}_c = -q$ (rad/sec)	u (ft/sec)	w (ft/sec)	$\dot{u}$ (ft/sec^2)	$\dot{w}$ (ft/sec^2)	X_g (feet)	Z_g (feet)
51.5	1.17	725.1	23.76	0.0091	1190.8	14.80	28.01	0.941	6920.6	26191.0
52.0	1.19	728.7	24.02	0.0091	1205.6	15.27	29.72	0.96	7170.0	26735.8
54.0	1.27	741.5	25.06	0.0091	1266.2	17.20	30.93	0.98	8505.1	29543.0
56.0	1.34	750.6	26.07	0.0088	1329.6	19.19	32.52	1.01	9379.1	31295.6
58.0	1.43	756.0	27.08	0.0087	1396.3	21.23	34.24	1.03	10634.7	33714.8
60.0	1.52	757.5	28.06	0.0086	1484.8	23.80	36.56	1.00	11999.2	36876.1
62.0	1.59	737.5	29.04	0.0085	1540.8	25.25	38.06	0.92	13479.2	38849.1
64.0	1.67	714.7	30.01	0.0085	1618.9	26.96	40.13	0.77	15081.8	41571.9
66.0	1.76	689.3	30.99	0.0085	1701.3	28.30	42.26	0.56	17268.9	45129.4
68.0	1.85	661.1	31.97	0.0086	1787.9	29.11	44.30	0.24	19175.5	48103.1
70.0	1.94	630.4	32.95	0.0087	1878.6	29.21	46.41	-0.16	20702.4	50410.3
72.0	2.04	597.6	33.96	0.0088	1973.6	28.43	48.55	-0.65	22874.2	53591.5
74.0	2.14	562.9	34.99	0.0090	2098.3	25.88	50.70	-1.25	25209.8	56895.3
76.0	2.25	526.7	36.03	0.0092	2176.4	23.37	52.89	-1.94	27718.5	60324.4
78.0	2.36	489.6	37.10	0.0095	2284.4	18.71	55.13	-2.73	30409.9	63881.0
80.0	2.48	451.9	38.20	0.0097	2396.9	12.40	57.40	-3.60	33294.1	67567.5

$t_o = 51.5$ sec

$u_o = 1190.8$ ft/sec $\qquad p_o = 0$

$v_o = 0$ $\qquad q_o = -0.0091$ rad/sec

$w_o = 14.8$ ft/sec $\qquad r_o = 0$

$X_{go} = 6920.6$ ft $\qquad \psi_o = 0$

$Y_{go} = 0$ $\qquad \theta_o = 23.76°$

$Z_{go} = 26191.0$ ft $\qquad \Phi_o = 0$

The drift-minimum attitude and angle-of-attack control gains can be calculated from Equations 92, 93, 96, and 97, and are shown in Figures 17 and 18 for several undamped natural frequencies of the control system. The attitude control gains are zero for the load-minimum principle. The load minimum angle-of-attack control gains can be calculated from Equations 99 and 100, and are shown in Figure 19. The attitude rate control gains are the same for the LMP and the DMP but are a function of the damping ratio. In this example, it is assumed that the pitch and yaw damping ratios are equal. The attitude rate control gains calculated from Equations 94 and 98 are shown in Figures 20a, b, and c for several assumed damping ratios.

Initial calculations are made for both drift-minimum and load-minimum control under the following assumptions:

$$f_{nY} = f_{nP} = 0.5 \text{ cps}$$

$$\zeta_Y = \zeta_P = 0.75$$

$$\theta_W = 180°$$

$$h_{OY} = \frac{a_{OY}}{2}$$

$$h_{OP} = \frac{a_{OP}}{2}$$

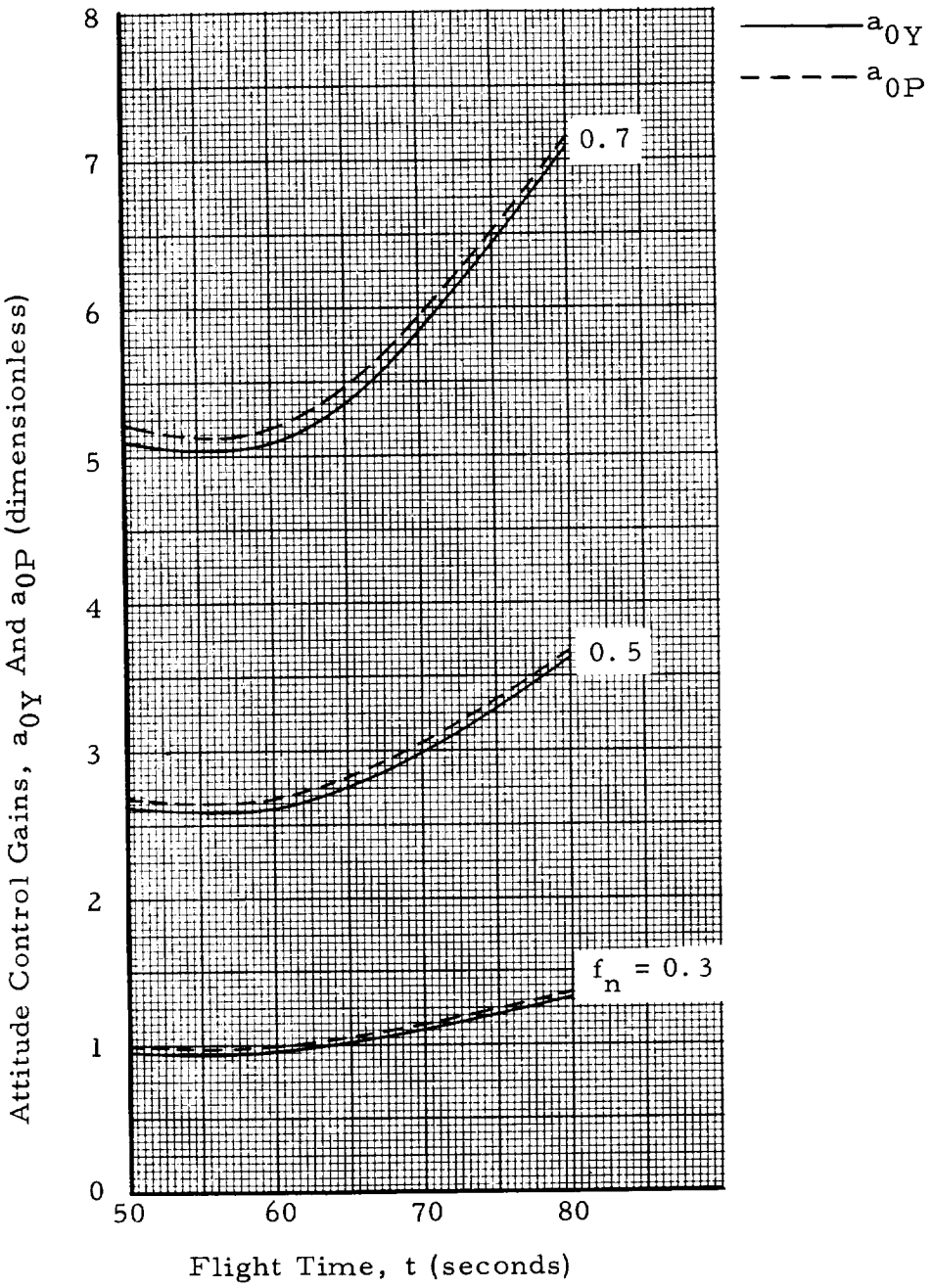

FIGURE 17. DRIFT MINIMUM YAW AND PITCH ATTITUDE CONTROL GAINS

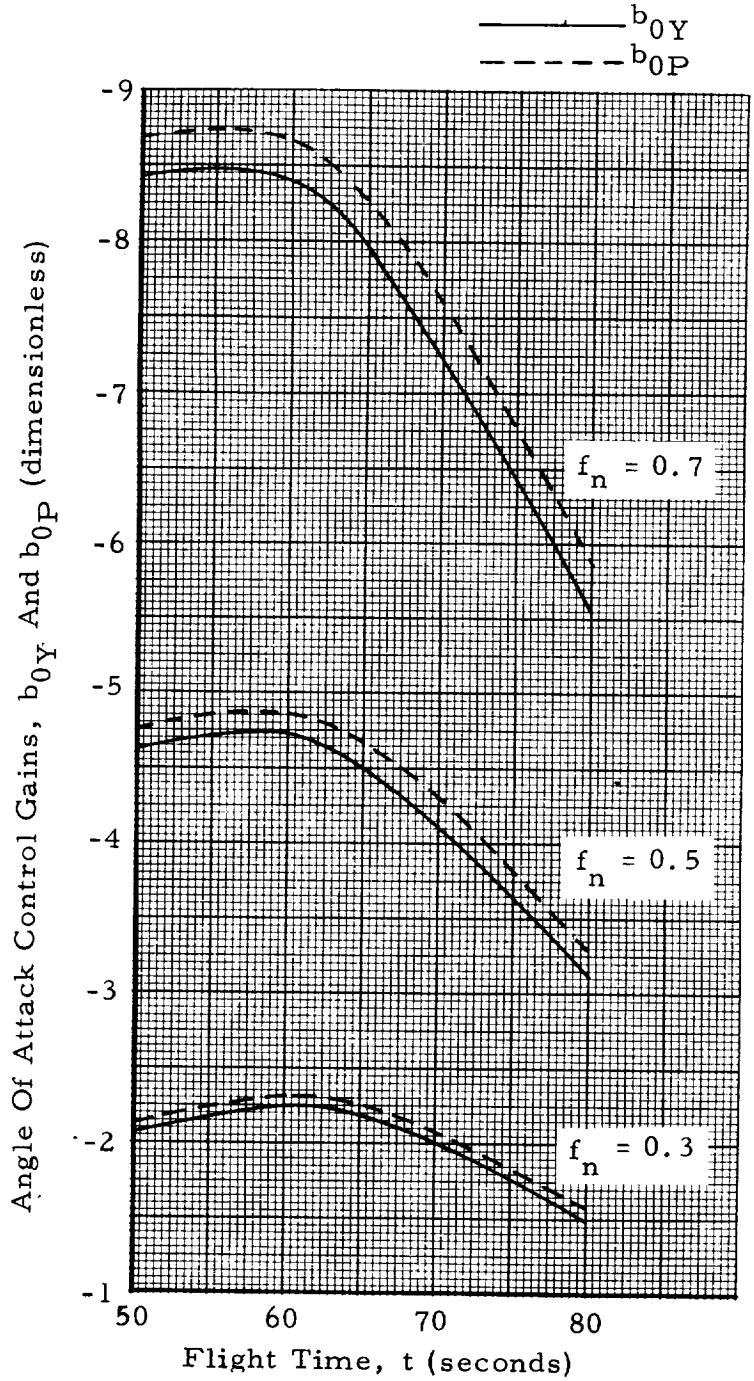

FIGURE 18. DRIFT-MINIMUM YAW AND PITCH ANGLE OF ATTACK CONTROL GAINS

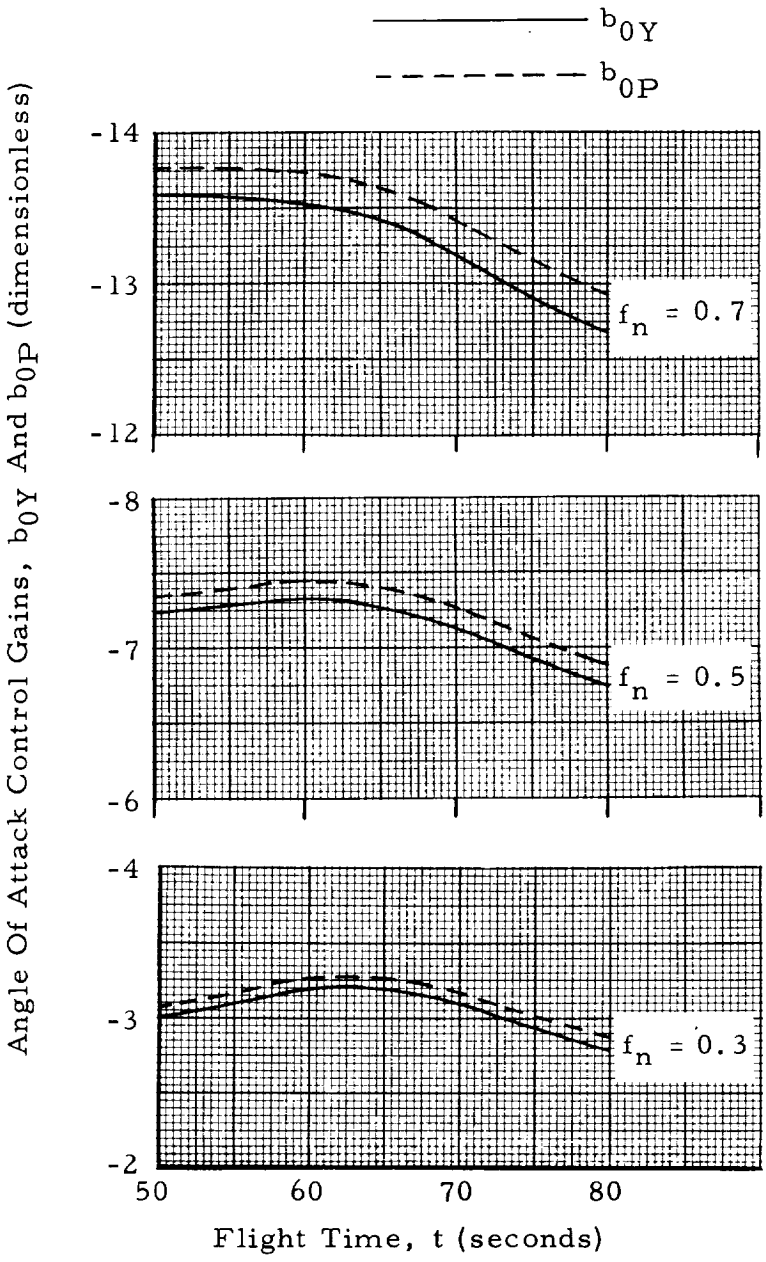

FIGURE 19. LOAD-MINIMUM YAW AND PITCH ANGLE OF ATTACK CONTROL GAINS

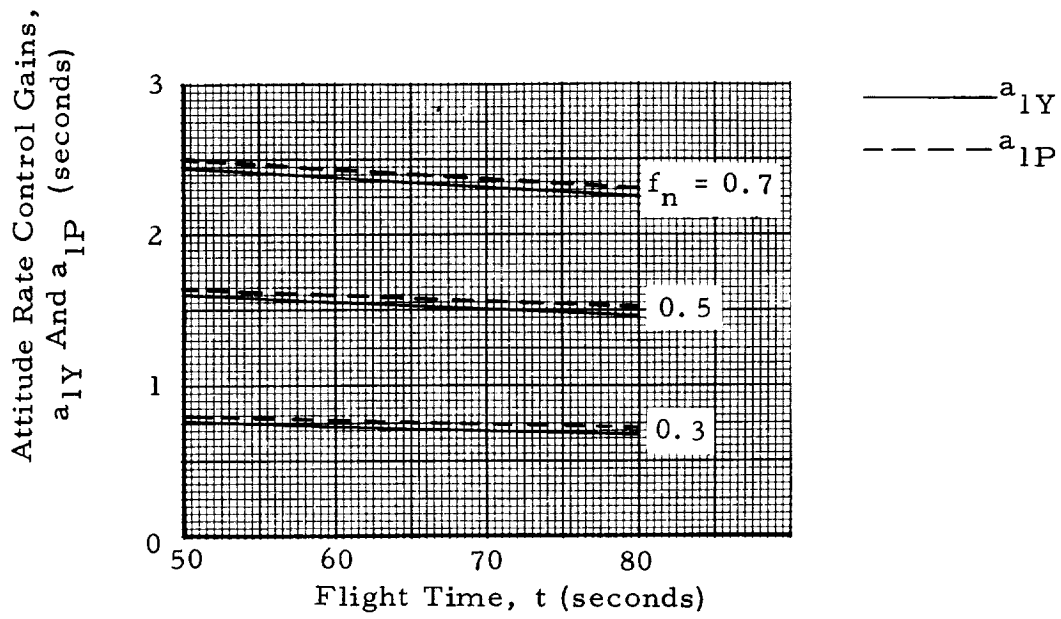

(a) Damping Ratios ζ_Y And ζ_P Equal 0.5

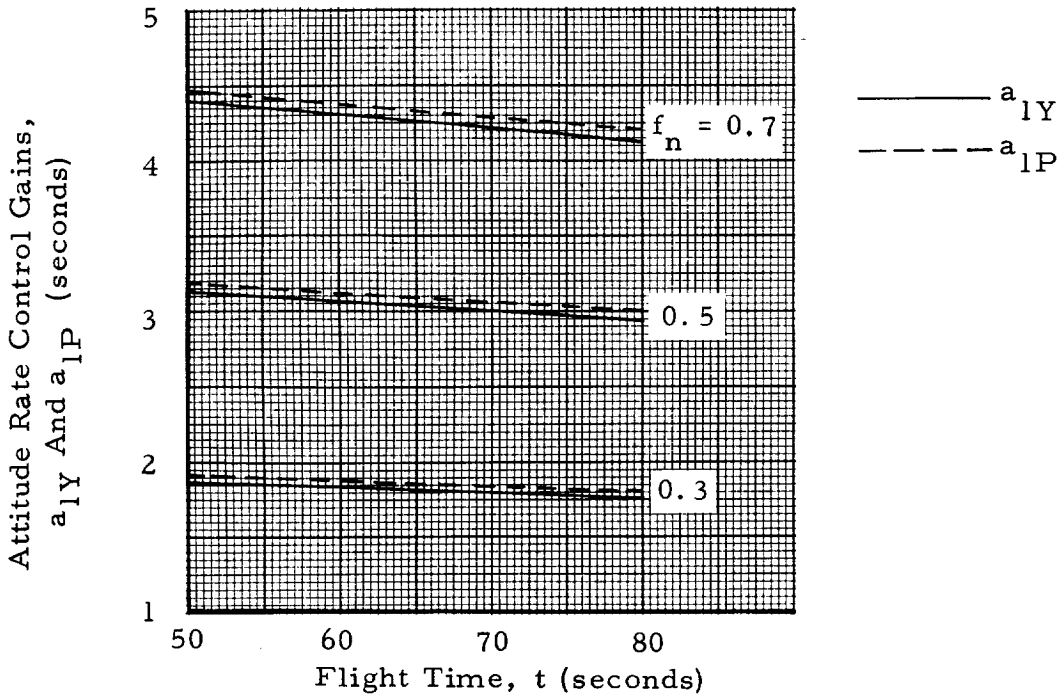

(b) Damping Ratios ζ_Y And ζ_P Equal 0.75

FIGURE 20. YAW AND PITCH ATTITUDE RATE CONTROL GAINS

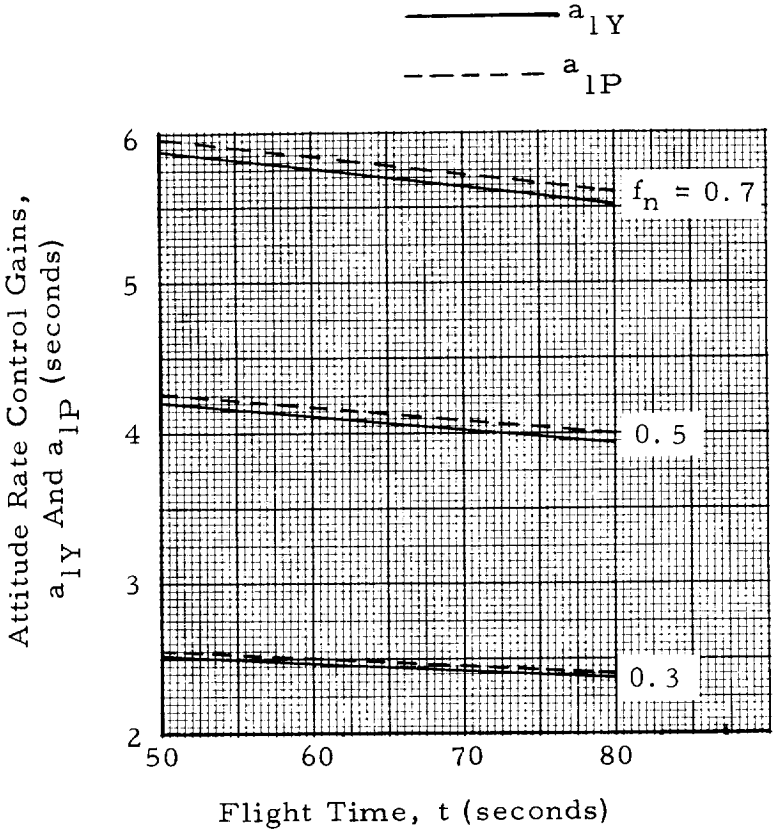

(c) Damping Ratios ζ_Y And ζ_P Equal 1.0

FIGURE 20. (CONCLUDED)

The assumptions concerning the roll control gains h_{OY} and h_{OP} are completely arbitrary. A direct side wind ($\theta_W = 180°$) is selected to facilitate the comparison of the current calculations with the results of a typical two-dimensional simulation. The two-dimensional analysis accounts only for normal and axial aerodynamic forces which are assumed constant.

The drift-minimum control requirements are examined first. Figure 21 shows the time history of the gimbal angle and lateral acceleration in response to the assumed wind disturbance. In this and succeeding figures, time is assumed to be zero at the instant the vehicle encounters the wind disturbance. In other words, zero time corresponds to the actual flight time of t = 51.5 seconds with maximum dynamic pressure occurring 8.5 seconds later. The finite gimbal angle shown in Figure 21 for the present simulation at zero time is the value required to fly the desired trajectory without wind conditions. Calculations are stopped when the variables approach steady-state conditions Time histories of the yaw angle and angle of attack, for drift-minimum control are shown in Figure 22.

Application of the load-minimum principle yields similar results as shown in Figures 23 and 24. Load-minimum control reduces the gimbal angle and angle of attack as compared with drift-minimum control. The yaw angle and lateral acceleration are larger and continue to increase rather than approaching a steady-state condition, thus indicating path instability.

The results of the present analysis are in general agreement with two-dimensional results for both control principles. This indicates that the two-dimensional analysis gives satisfactory results when the disturbed motion of the vehicle takes place primarily in one plane as it does in the case of a direct side wind.

The time histories of the gimbal angle calculated from the present simulation are not associated with any particular one of the four control engines of the assumed vehicles; rather the maximum value at each instant of time is used. However, since the gimbal angle relative to the initial canted axis is shown, the value is the same for all four engines except for small differences necessary for roll control.

The roll angle of the assumed vehicle is negligible with both load-minimum and drift-minimum control for the case of a direct side wind. The dispersions of the flight path angle and longitudinal acceleration are shown in Figure 25. For the case of a side-wind the two-dimensional analysis neglects motion in the pitch plane; hence no comparison can be made for the pitch plane variables.

All of the results shown thus far are for a frequency of 0.5 cycles per second. The effect of frequency on the maximum values of lateral acceleration, yaw angle, gimbal angle, and angle of attack are shown in Figure 26 for drift-minimum control. Similar results are shown in Figure 27 for load minimum control. Values for yaw angle and

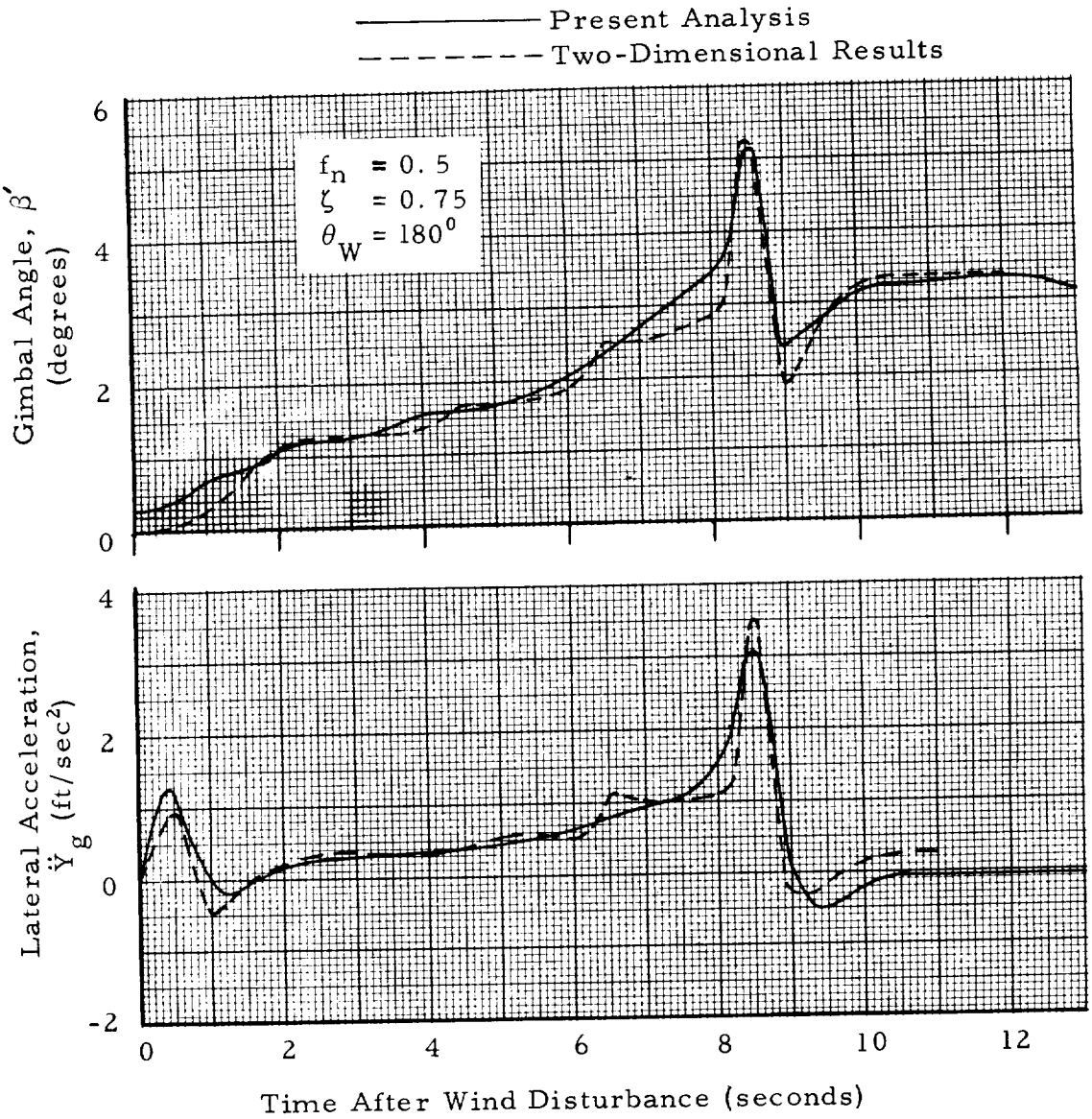

FIGURE 21. TIME HISTORY OF GIMBAL ANGLE AND LATERAL ACCELERATION IN RESPONSE TO WIND DISTURBANCE (DRIFT-MINIMUM PRINCIPLE)

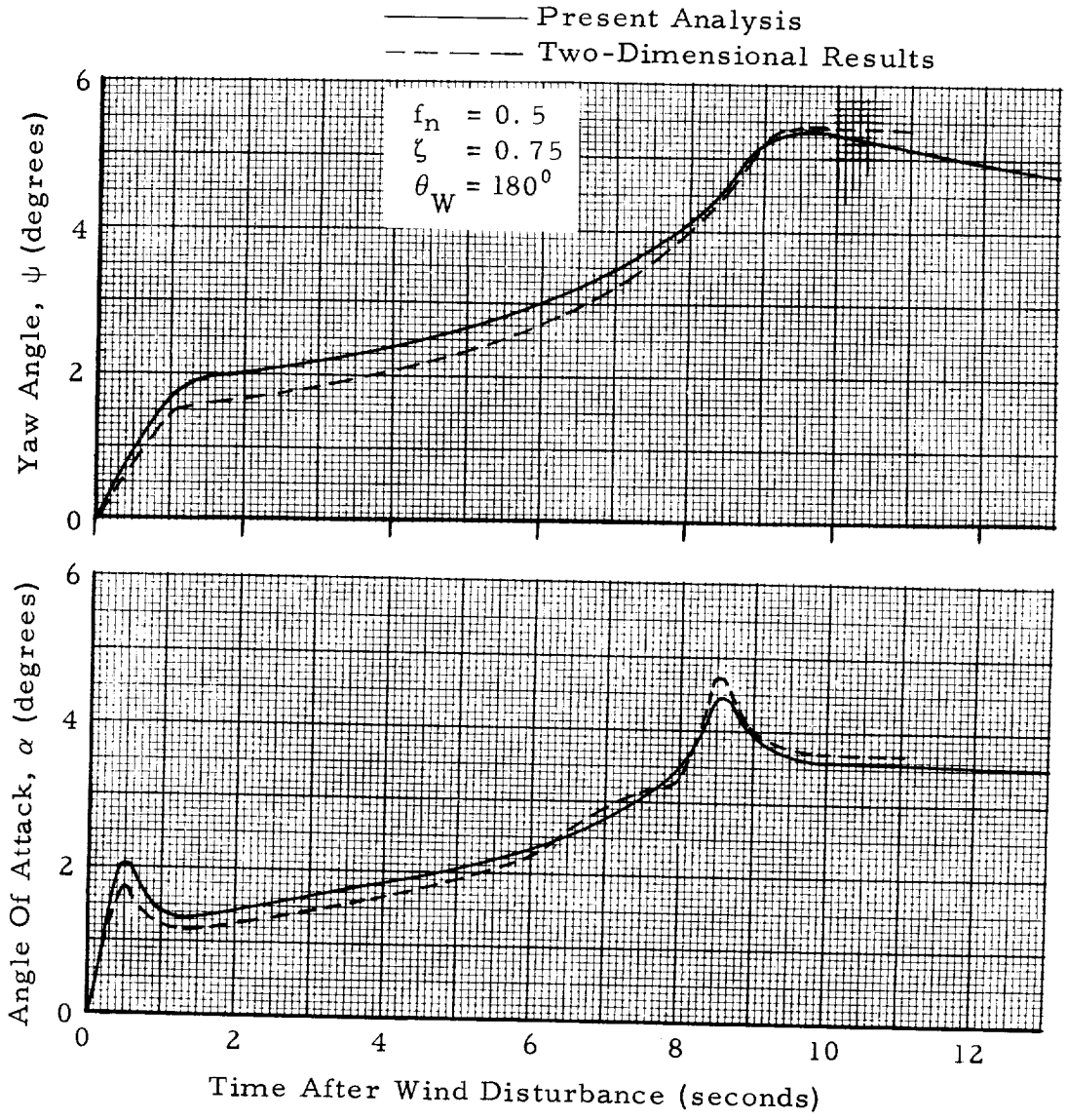

FIGURE 22. TIME HISTORY OF ANGLE OF ATTACK AND YAW ANGLE IN RESPONSE TO WIND DISTURBANCE (DRIFT-MINIMUM PRINCIPLE)

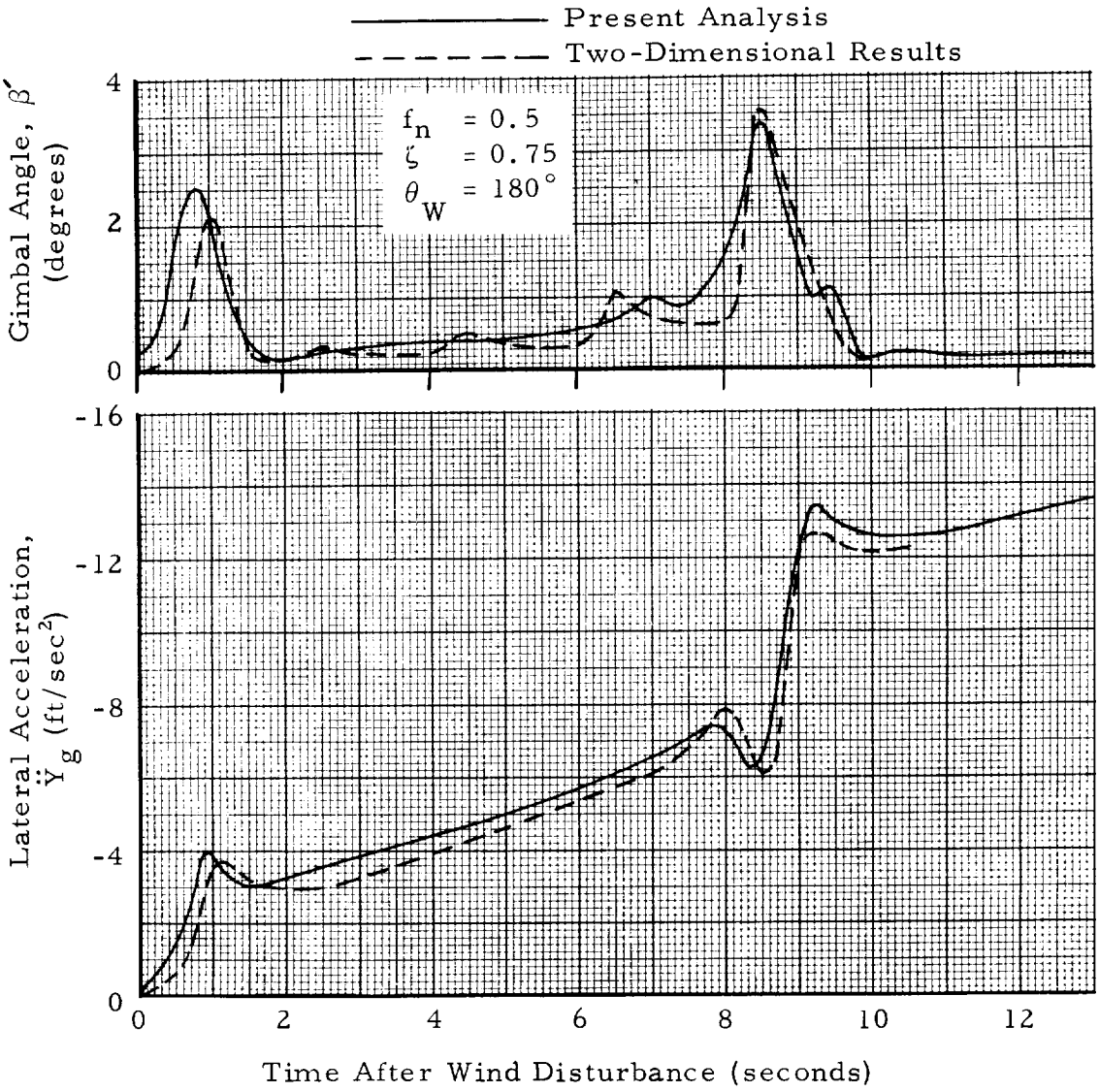

FIGURE 23. TIME HISTORY OF LATERAL ACCELERATION AND GIMBAL ANGLE IN RESPONSE TO WIND DISTURBANCE (LOAD-MINIMUM PRINCIPLE)

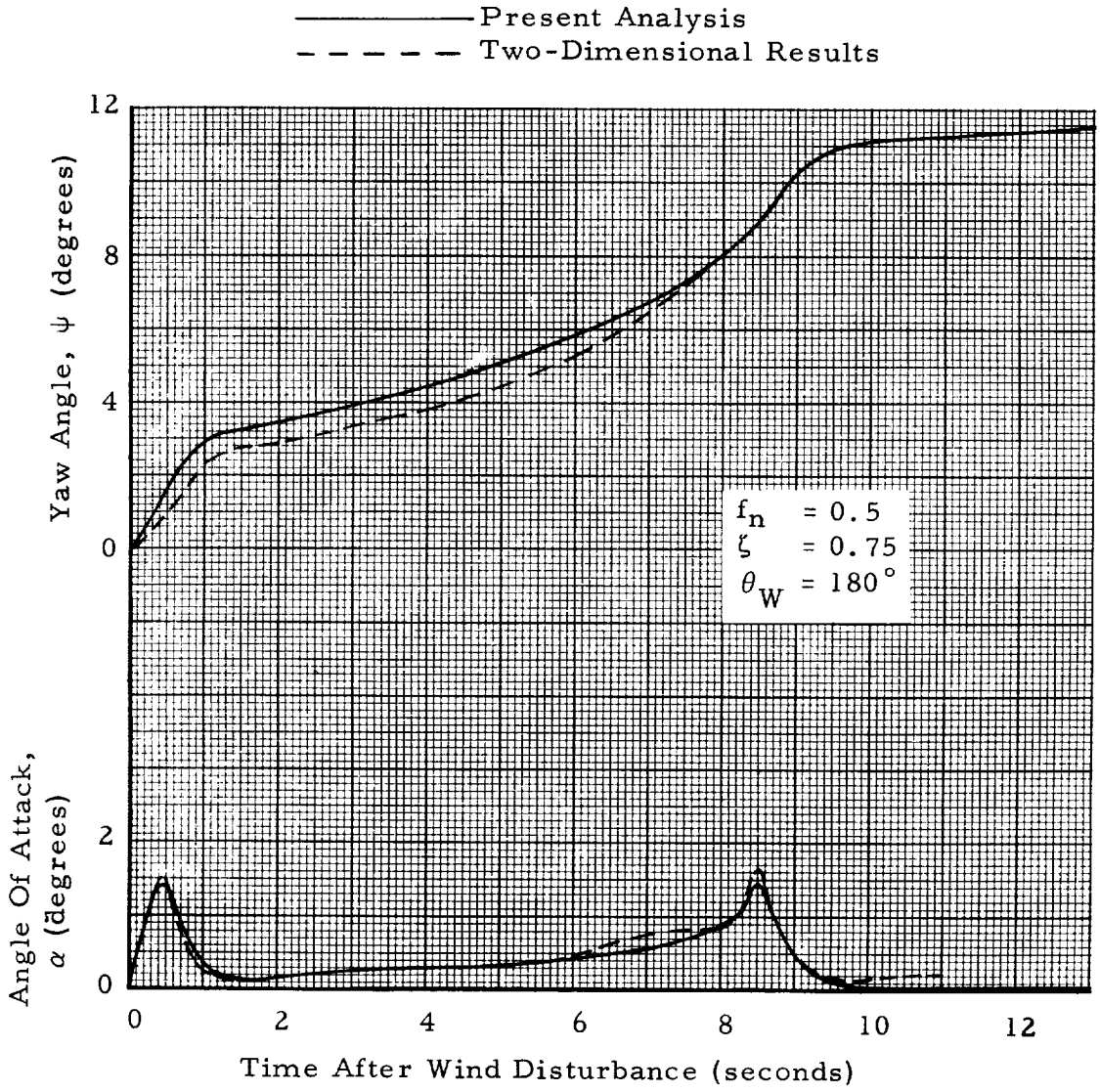

FIGURE 24. TIME HISTORY OF YAW ANGLE AND ANGLE OF ATTACK IN RESPONSE TO WIND DISTURBANCE (LOAD-MINIMUM PRINCIPLE)

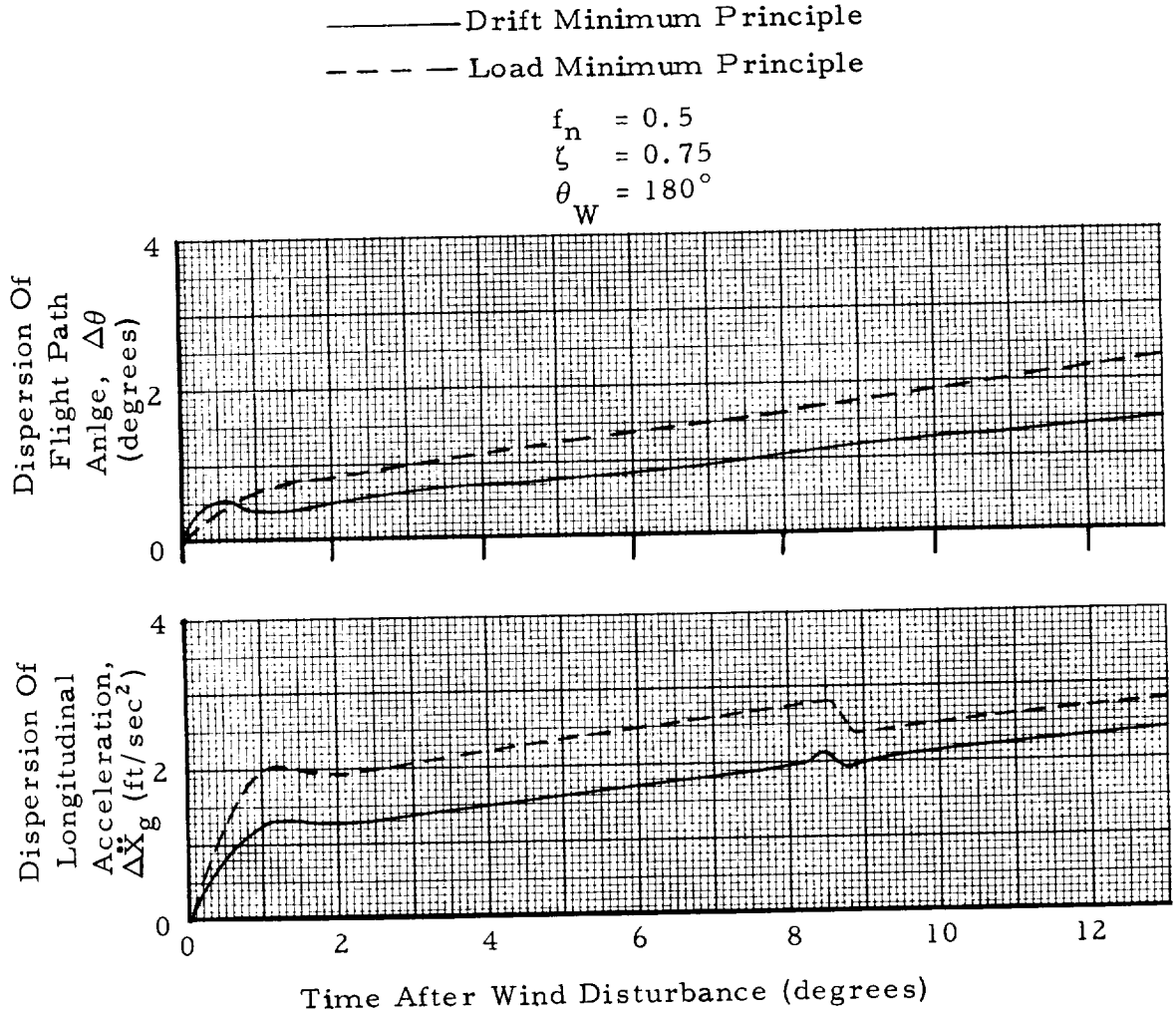

FIGURE 25. TIME HISTORY OF DISPERSION OF LONGITUDINAL ACCELERATION AND FLIGHT PATH ANGLE

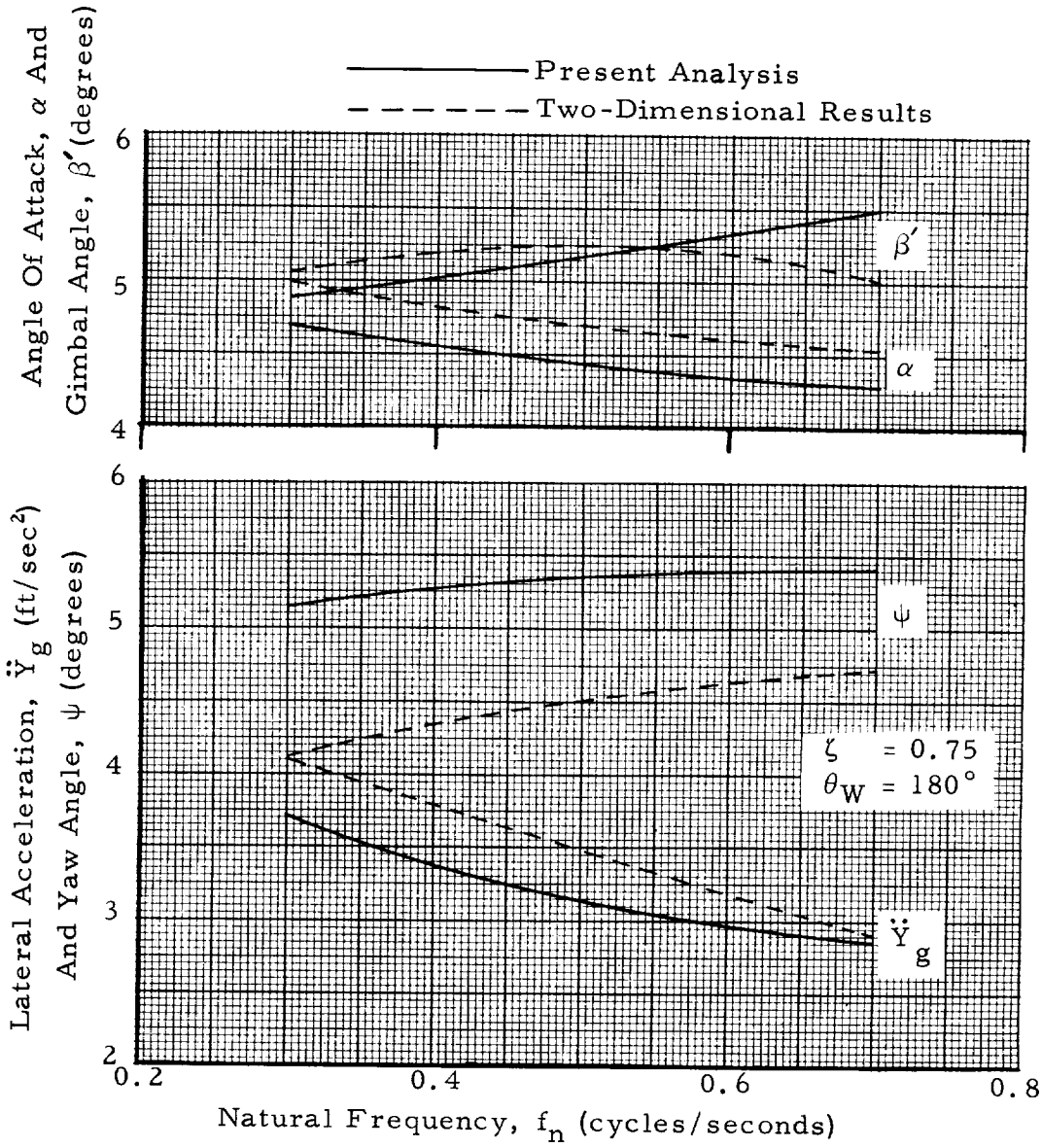

FIGURE 26. EFFECT OF NATURAL FREQUENCY ON MAXIMUM VALUES OF LATERAL ACCELERATION, YAW ANGLE, ANGLE OF ATTACK AND GIMBAL ANGLE (DRIFT-MINIMUM PRINCIPLE)

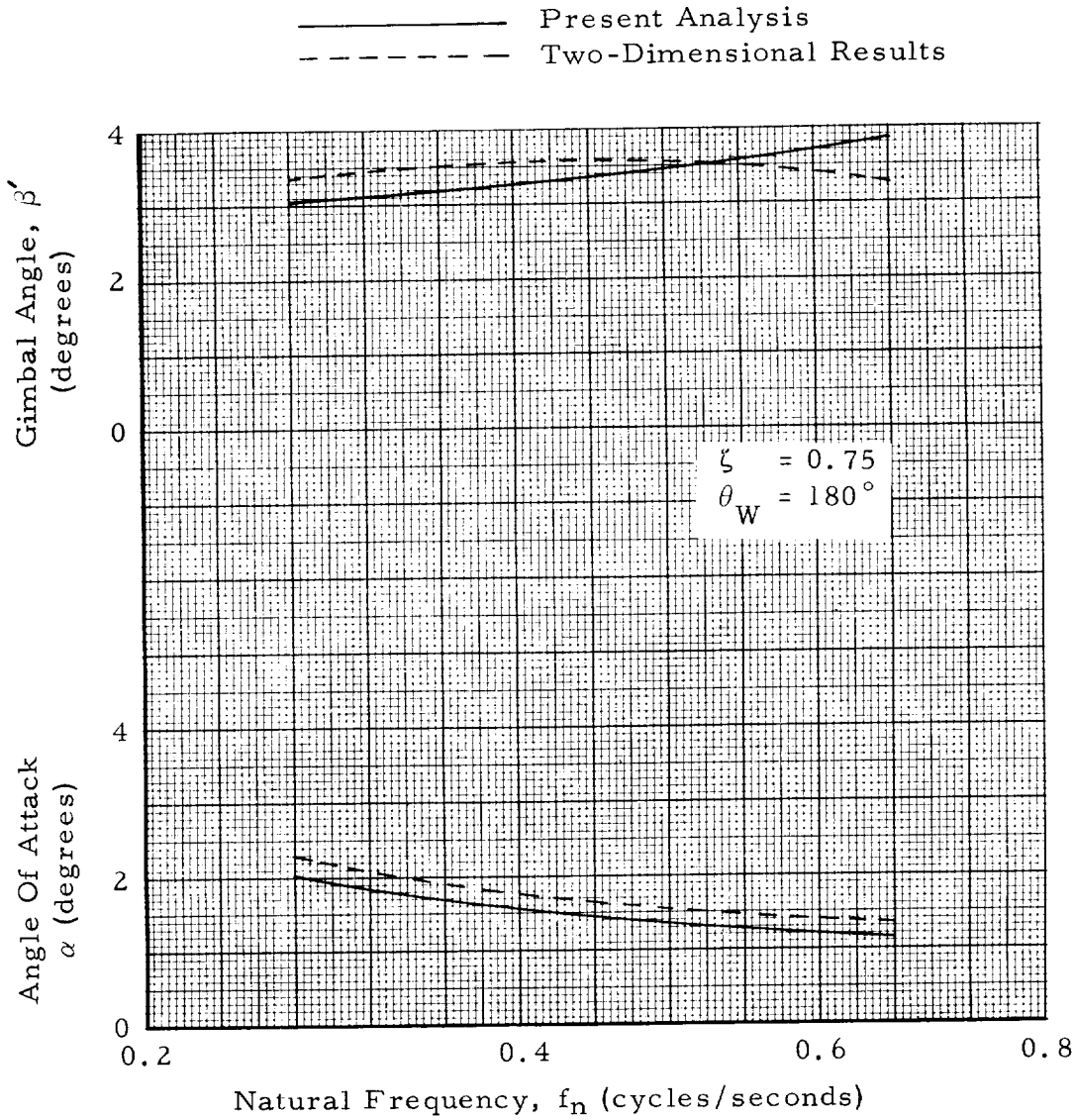

FIGURE 27. EFFECT OF NATURAL FREQUENCY ON MAXIMUM VALUES OF GIMBAL ANGLE AND ANGLE OF ATTACK (LOAD-MINIMUM PRINCIPLE)

lateral acceleration are not shown for load-minimum control since they increase continuously and consequently have no maximum value (Figs. 23 and 24). The two-dimensional results here are generally conservative as compared with the results of the present analysis. A notable exception is the yaw angle with drift-minimum control, the two-dimensional analysis predicting 20 per cent lower values (Fig. 23).

The effect of wind direction on the lateral acceleration is shown in Figure 28 for both control principles. Similar variations for gimbal angle and angle of attack are shown in Figure 29. The case of a failure of engine number one ($T_1 = 0$) is also considered in Figure 29. All of the curves shown in Figures 28 and 29 have mirror images for the other 180-degree range of wind direction except for the curves considering engine failure.

It is apparent from Figures 28 and 29 that the maximum points on the curves are not coincident with a direct side wind ($\theta_W = 180°$) as is sometimes assumed. For the present example, however, the maximum values are not significantly different from those corresponding to a side wind.

A significant roll angle results in the case of engine failure, for some wind directions. The range of the roll angle for θ_W between 90 degrees and 270 degrees for the assumed vehicle is as follows:

$$-1.20° \leq \Phi \leq -2.76°$$

It is beyond the scope of this example to consider all of the possible variations and combinations of the parameters involved. A complete stability and control investigation of any vehicle requires a tremendous volume of charts and calculations. While the results shown are brief, they illustrate the application and flexibility of the simulation developed in this report. The simulation should be restricted primarily to first stage flight because of the assumptions of a non-rotating, flat earth and a constant acceleration of gravity.

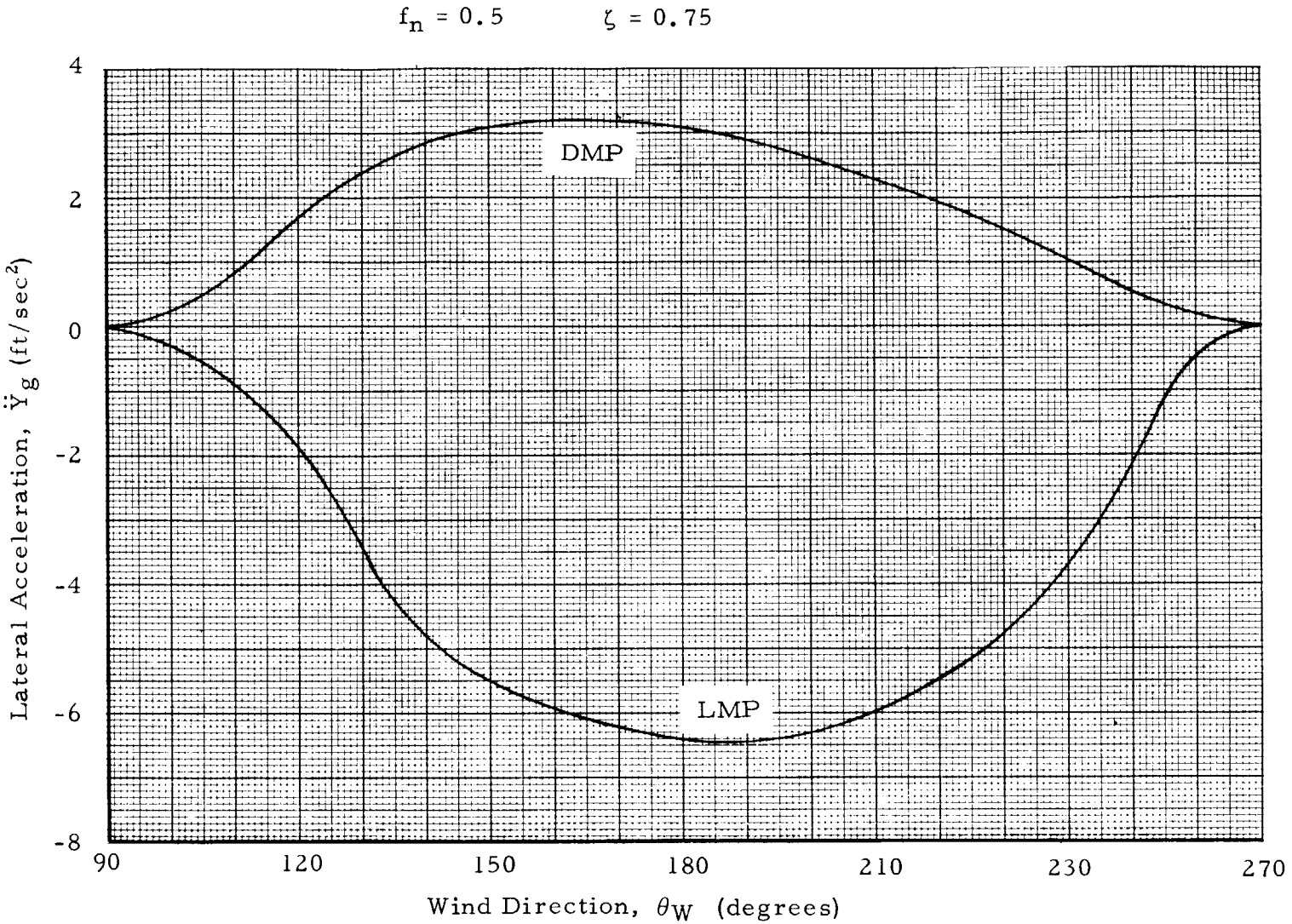

FIGURE 28. EFFECT OF WIND DIRECTION ON MAXIMUM ACCELERATION

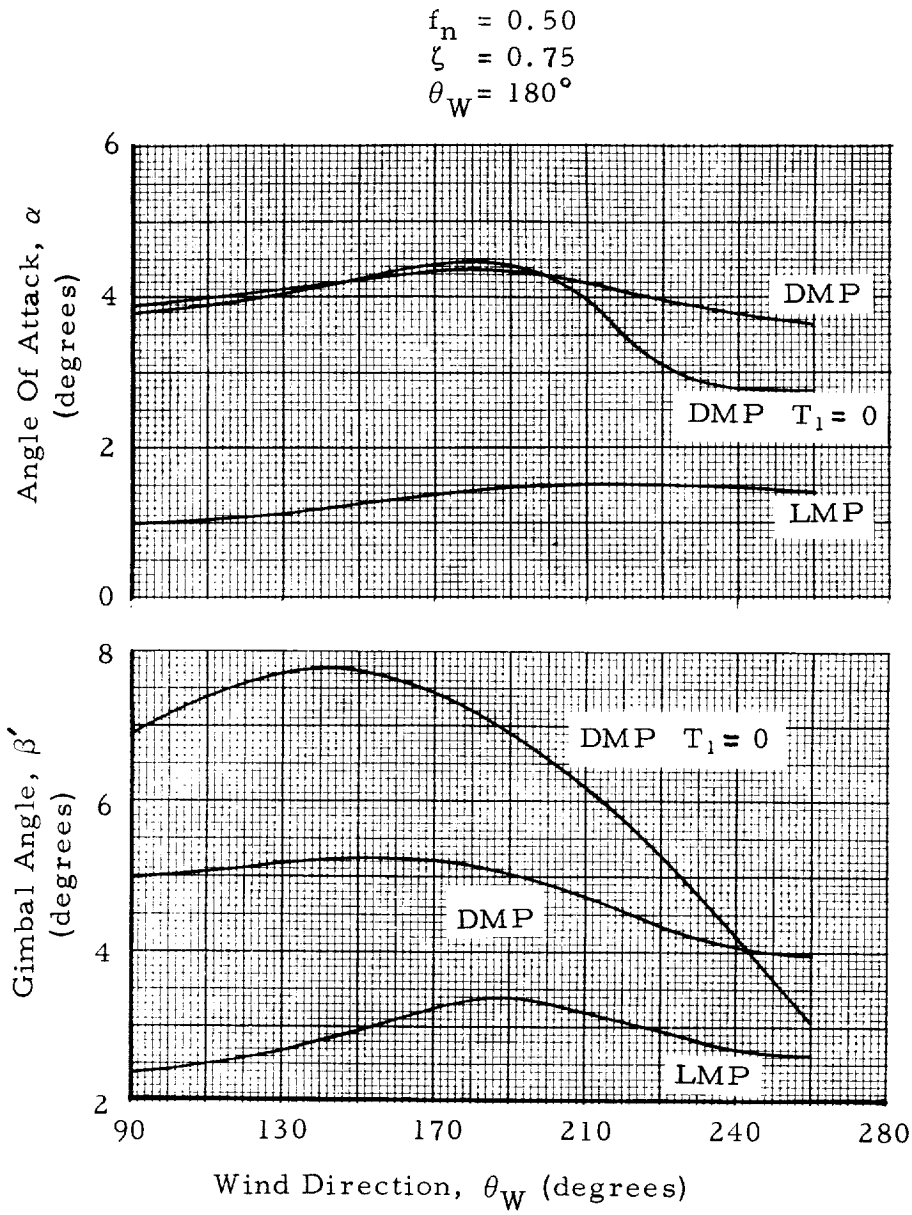

FIGURE 29. EFFECT OF WIND DIRECTION ON MAXIMUM VALUES OF GIMBAL ANGLE AND ANGLE OF ATTACK

REFERENCES

1. Phillips, William H., Effect of Steady Rolling on Longitudinal and Directional Stability. NACA TN-1627, July 1948.

2. Geissler, Ernst D., Problems in Attitude Stabilization of Large Guided Missiles. ABMA DA-TR-21-60, June 13, 1960.

3. Hoelker, R. F., The Principle of Artificial Stabilization of Aerodynamically Unstable Missiles, ABMA DA-TR-64-59, September 25, 1959. Confidential.

4. McNair, Lewis L., and Lisle, Ben J., Juno V Missile (Saturn); Preliminary First Stage Control Analysis for Missiles SA-3 and SA-4. ABMA DA-TM-32-59, March 10, 1959. Secret

5. Sullivan, E. L. and Jean, Otha C., Saturn C-1 Control Study for Three Control Motors Operative and Possible Improvement Measures. ABMA TM-51-60, June 8, 1960. Confidential.

6. Hoelker, R. F., Theory of Artificial Stabilization of Missiles and Space Vehicles with Exposition of Four Control Principles. NASA TN D-555, June 1961.

7. Kolk, W. Richard, Modern Flight Dynamics. Prentice Hall, Inc., Englewood Cliffs, New Jersey, 1961.

8. James, Robert L., Jr. and Harris, Ronald J., Calculation of Wind Compensation for Launching of Unguided Rockets. NASA TN D-645, April 1961.

9. James, Robert L., Jr., A Three Dimensional Trajectory Simulation Using Six-Degrees-of-Freedom with Arbitrary Winds, NASA TN D-641, March 1961.

10. Mann, Patricia, Equations of Motion of Ballistic Missiles in Six Degrees of Freedom. ABMA DA-M-44-58, April 25, 1958.

11. Howe, R. M., Coordinate Systems for Solving the Three-Dimensional Flight Equations. WADC TN 55-747, June 1956.

12. Etkin, Bernard, Dynamics of Flight. John Wiley and Sons, London, 1959.

13. Dynamics of the Airframe, Bu Aer Report AE-61-4-II, September 1952.

14. Malina, F. J. and Smith, O. M. A., Flight Analysis of Sounding Rockets. Journal of the Aeronautical Sciences, Volume 5, Number 3, March 1938, pp. 199-202.

15. Malina, F. J. and Summerfield, M., The Problem of Escape from the Earth by Rocket. Journal of the Aeronautical Sciences, Volume 14, Number 8, August 1947, pp. 471-480.

16. Barton, M. V., The Effect of Variation of Mass on the Dynamic Stability of Jet-Propelled Missiles. Journal of the Aeronautical Sciences, Volume 7, Number 4, April 1950, pp. 197-201.

17. Chang, T., General Equations of Motion of a Rigid Missile. Cornell Aeronautical Laboratory MR-43, July 15, 1952.

18. Charters, A. C., The Linearized Equations of Motion Underlying the Dynamic Stability of Aircraft, Spinning Projectiles and Symmetrical Missiles. NACA TN-3350, January 1955.

19. Laitone, E. V., Dynamic Stability Criteria for Arbitrary Rigid Bodies in Flight. STL Report GM-TR-71, August 30, 1956.

20. Blanton, J. E., Stability Regions for an Accelerometer Controlled Missile. ABMA DG-TM-50-59, December 1, 1959.

21. Haeussermann, Walter, Stability Areas of Missile Control Systems. ABMA Research Report IRII, February 27, 1956.

22. Vaughan, W. W., Wind Speed and Wind Shear Data, Cape Canaveral, Florida. MSFC-M-AERO-Office Memo, February 2, 1961. Confidential.

NASA-Langley, 1963 M307